NASA
CC-L-403

Copy 1

NATIONAL AERONAUTICS AND SPACE ADMINISTRATION

CC-L-403

CALCULATION OF THE FRICTIONLESS INCOMPRESSIBLE FLOW FOR A GIVEN TWO-DIMENSIONAL CASCADE (DIRECT PROBLEM)

By Hermann Schlichting

Translation of "Berechnung der reibungslosen inkompressiblen Strömung für ein vorgegebenes ebenes Schaufelgitter." VDI - Forschungsheft 447, Edition B, Vol. 21, 1955.

(1) TMX # 56364

LANGLEY RESEARCH CENTER

October 1958

CALCULATION OF THE FRICTIONLESS INCOMPRESSIBLE FLOW FOR A GIVEN TWO-DIMENSIONAL CASCADE (DIRECT PROBLEM)

By Hermann Schlichting

ABSTRACT

A simple method for calculating the frictionless incompressible flow through a two-dimensional cascade is described for the case where the blade and cascade geometries are prescribed and the aerodynamic coefficients and pressure distributions are desired. The calculation method which makes use of a continuous vortex and source-sink distributions is set up in such a manner that each geometric parameter can be varied independently. Measured values of pressure distributions agree well with those calculated by present theory.

INDEX HEADINGS

Flow, Incompressible	1.1.1
Cascades	1.4.5
Compressor Flow Theory and Experiment	3.6.1
Turbine Flow Theory and Experiment	3.7.1

NATIONAL AERONAUTICS AND SPACE ADMINISTRATION

CALCULATION OF THE FRICTIONLESS INCOMPRESSIBLE FLOW FOR A GIVEN TWO-DIMENSIONAL CASCADE (DIRECT PROBLEM)*

By Hermann Schlichting

1. INTRODUCTION[1]

For further developments in jet-engine design, a deeper understanding of the physical flow processes is indispensable today. For axial-flow machines, the flow problems are centered around the so-called cascade obtained by developing a coaxial cylinder section through the rotor and the stator. Necessarily, the starting point for all investigations on cascade flows must be the incompressible flow through a two-dimensional cascade. Only when this flow can be controlled, can one hope to do fundamental research regarding the remaining influences as, for instance, wall and clearance losses, compartmenting, compressibility, and centrifugal forces.

At the Institute for Flow Mechanics of the Technical Academy of Braunschweig, systematic cascade investigations, theoretical as well as experimental (ref. 1), have been under way for several years. Earlier theoretical investigations on cascade flows were based throughout on frictionless fluids; the above named investigations took into account, for the first time, the friction of the fluid also, by means of boundary-layer theory considerations (ref. 2). This makes it possible

---

*"Berechnung der reibungslosen inkompressiblen Strömung für ein vorgegebenes ebenes Schaufelgitter." VDI - Forschungsheft 447, Edition B, Vol. 21, 1955.

[1]The author has lectured on the method in excerpt at the flow conference of June 9-11, 1954 in Zürich, arranged jointly by the VDI - Branch Committee for Flow Research, the Swiss Engineers' and Architects' Association, and the Confederate Technical Academy Zürich. The investigations were supported by the German Research Association. L. Speidel tested the calculation method within the scope of the cascade research program of the Institute. The measurements used for comparison with the theory (section 6) have been taken from as yet unpublished voluminous experimental cascade investigations by N. Scholz. Contributions to these investigations in the form of theses and research memoranda of the Mechanical Engineering Department of the Technical Academy of Brauschweig were made by K. H. Grewe (1951), J. Vahlbruch (1950), W. Richter (1952), and H. Schäffer (1951).

L-403

to determine theoretically the loss coefficients of a cascade which govern the efficiency of the turbo-machine. The aim of the cascade investigations is to indicate, for a given application, cascades of optimum efficiency. For this purpose, the connection between the geometric and the aerodynamic parameters of a cascade must be known.

The geometric parameters of a two-dimensional cascade are, according to figures 1(a) to 1(c), the blade profile and the cascade geometry which is determined by the pitch ratio t/l (where t denotes the spacing, l the blade chord), and by the blade angle β_s. As aerodynamic parameters we designate the inflow and outflow velocities W_1 and W_2, the inflow and outflow angles β_1 and β_2, the pressure change $\Delta p = p_2 - p_1$ in the cascade where p_1 and p_2 denote the static pressures in front of and behind the cascade, the pressure distribution $p(x)$ on a cascade blade, and the energy loss in the cascade which, for incompressible flow, is best measured as total-pressure loss $\Delta p_g = p_{g1} - p_{g2}$, with p_{g1} and p_{g2} denoting the total pressures in front of and behind the cascade. From the pressure distribution on the cascade blade we may then determine the resultant blade force.

The connection between the geometric and aerodynamic parameters is found in two steps: (1) determination of the pressure distribution on the blade, according to potential theory, for frictionless flow and (2) calculation of the blade-boundary layer and the flow losses from this pressure distribution. Here we shall treat only the first step.[2] Two main problems must be distinguished: for the first main problem, β_1 and β_2 are thus given the velocity triangle; the cascade and blade geometry and the pressure distribution on the blade are the desired quantities (for instance, with the secondary condition that the distribution should be "as favorable as possible with regard to the flow losses"). For the second main problem the cascade and blade geometry are given and the pressure distribution on the blade, the blade force, and the outflow direction as a function of the inflow direction are desired. For the first main problem, therefore, the aerodynamic parameters of the cascade are given and the geometric parameters are desired; whereas the second main problem represents the inverse case. The first main problem is applied chiefly for practical design problems (for instance, selection of an optimum cascade for given operational conditions); the second main problem is applied in systematic cascade

---

[2]L. Speidel (ref. 3) reported recently on voluminous results regarding systematic calculations of the loss coefficients (second step) for unstaggered cascades. Communication of results for staggered cascades will follow.

investigations where, for instance, the geometric cascade parameters are varied in order to find the most favorable cascades. Also, the second main problem is applied for "checking" a cascade of predetermined geometry, which frequently occurs in practice.

For the first main problem (inverse problem), N. Scholz (ref. 4) indicated recently a convenient calculation method. In what follows, we shall treat the second main problem (direct problem) exclusively. Both methods are based on the interpretation of cascade flow according to lifting-surface theory where, in contrast to the tunnel flow, the individual blade is interpreted as an airfoil and where the mutual interference of the blades plays an important part. For the single airfoil, the connection between the geometric and the aerodynamic parameters has been largely clarified by theoretical and experimental investigations. For the cascade, however, we are still a long way from having deep insight, due to the larger number of geometric and aerodynamic parameters.

The potential flow of a two-dimensional cascade may be calculated with the aid of conformal mapping or according to the singularity method.

For the conformal mapping which is limited exclusively to the two-dimensional problem, the flow around the infinite row of congruent blades is reduced to the well-known circular-cylinder flow by means of a complex transformation function (cf. F. Weinig, ref. 5; I. E. Garrick, ref. 6; and W. Traupel, ref. 7). This method does give an exact solution of the flow problem but is so troublesome with respect to numerical performance, even for simple blade shapes, that the investigation of a larger number of cascades is, in practice, not possible. In particular, neither the first nor the second main problem can be solved directly by means of this method; nor can a row of cascades be investigated where only one geometric cascade parameter varies - for instance, the pitch ratio - but all others are to be fixed.

In the singularity method, the blade contour is replaced by singularities (vortices, sources, and sinks). This method is fundamentally suitable for the three-dimensional case also; it was used by N. Scholz (ref. 4) for the solution of the first main problem and will likewise be taken here as a basis for the solution of the second main problem. The singularity method offers the opportunity to make, in a simple manner, the transition from the single blade to the blade in cascade configuration and thus to express the influence of the cascade. For the single airfoil this method was first applied by W. Birnbaum (ref. 8) and H. Glauert (ref. 9); later, it was developed to great perfection by F. Riegels (ref. 10) and H. J. Allen (ref. 11). The first applications to a cascade stem from M. Schilhansl (ref. 12) and A. Betz (ref. 13). J. Ackeret (ref. 14), E. Pistolesi (ref. 15), V. Lieblein (ref. 16), and R. A. Spurr and H. J. Allen (ref. 17) contributed to the future improvement of this method for the cascade. S. Katzoff, R. S. Finn, and J. C. Laurence (ref. 18) work partly with the conformal mapping, partly with the singularity method which is rather troublesome numerically. In some cases, for simplification of the calculation, vortex and source-sink distributions are assumed along the length of the blade chord and are arranged on a straight blade chord line instead of on the mean chamber line. Just as in the theory of W. Birnbaum and H. Glauert, this means a good approximation only for moderate chamber of the blades, as in the case of compressor cascades. We shall also use this simplification; however, an extension to large blade cambers, like those in turbine cascades, is possible in principle.

For the rest, we choose for the solution of the second main problem a method which has already proved satisfactory for the single airfoil (refs. 19 and 20). From this application it is known that the exact solution leads to an integral equation which should be satisfied along the entire prescribed blade contour but may be solved approximately by satisfying it only at a few discrete points (the so-called control points). Thereby the solution of the integral equation is reduced to the solution of a linear system of equations. Since convenient methods with high accuracy are known for determining the velocity distribution on the single profile (refs. 10 and 11), we shall, in the calculation method for the cascade, omit representing simultaneously the single profile with great accuracy. Rather we shall emphasize a good expression of the influence of the "cascade geometry," that is, the pitch ratio and the stagger angle.

The method for determining the aerodynamic coefficients for a prescribed cascade described below leads to two systems of linear equations for the coefficients of the circulation distribution and the source distribution (usually two systems of six equations with six unknowns each). Certain fixed values which appear in these systems of equations and are rather hard to calculate, were listed universally in tables as functions of the pitch ratio t/l and of the stagger angle λ (so-called downwash tables). By this means, the greatest part of the calculation is taken care of, once and for all, for every individual case of a cascade; there remains only the solution of the two systems of equations and, then, the determination of the aerodynamic coefficients and the pressure distribution. According to experience up till now,[3] the complete calculation of a cascade according to potential theory (aerodynamic coefficients and pressure distribution) for six different inflow angles requires about 20 to 25 hours for a trained computer.

---

[3]The calculation method served as a basis for systematic theoretical investigations regarding the loss coefficients of cascades; a few results had already been given in references 1 and 3.

2. BASIS OF THE METHOD

2.1 The Kinematic Flow Conditions

The flow of a frictionless incompressible fluid about a prescribed body is obtained, according to the singularity method, by replacing the body by a suitable source-sink and vortex distribution in its interior and superimposing a translational flow on this field. The singularities are determined from the kinematic flow condition, according to which on the entire boundary of the body the resulting velocity, that is, the sum of the translational velocity and the velocity induced by the sources and vortices is tangential to the contour. In order to produce the flow about a cascade blade according to this method, we choose a suitable linear-type continuous source distribution $q(x)$ and a vortex distribution $\gamma(x)$, where x signifies the coordinate in the direction of the blade chord l.

The general case of a profile of finite thickness and a camber different from zero may be represented, for moderate thicknesses and cambers, by superposition of a thickness distribution and a mean camber line (figs. 2(a) to 2(e)). If $y_u(x)$ and $y_o(x)$ signify the profile coordinates perpendicular to the x-direction on the lower and upper sides of the profile, respectively, and if $y_d(x)$ and $y_s(x)$ are the corresponding coordinates of the thickness distribution or the mean camber line, there applies

$$y_s(x) = \frac{1}{2}\left[y_o(x) + y_u(x)\right] \tag{1}$$

and

$$y_d(x) = \frac{1}{2}\left[y_o(x) - y_u(x)\right] \tag{2}$$

According to the singularity method, we may represent the flow around a cambered, lift-producing profile as a superposition of the flow about the uncambered profile without incidence and the flow about the mean camber line with incidence. We have therefore to superimpose: (1) the flow about the uncambered profile (source distribution $q(x)$ and the velocity component U_∞ of the translational flow parallel to the chord) and (2) the flow about the mean camber line (circulation distribution $\gamma(x)$ and the translational flow which consists of the components V_∞ and U_∞.

Strictly speaking, the singularity distributions q and γ should be placed on the mean camber line. For moderate heights of camber f, however, they may be located with good approximation on the profile chord, as mentioned before; considerable simplification of the calculation is thus obtained. The range of application of the method remains thereby limited to cascades of moderate camber (about $f/l \leqq 0.1$ to 0.15). For compressor cascades this is sufficient in most cases, whereas the calculation method for strongly cambered turbine cascades requires an extension.

The integral over the circulation distribution $\gamma(x)$ per unit length gives the total circulation Γ of a blade according to

$$\Gamma = \int_{x=0}^{l} \gamma(x)dx \tag{3}$$

Hence follows, according to W. Kutta and N. Joukowsky, the lift A of a blade per unit width as

$$A = \rho W_\infty \Gamma = \rho W_\infty \int_{x=0}^{l} \gamma(x)dx \tag{4}$$

with ρ as density of the fluid and $W_\infty = \sqrt{U_\infty^2 + V_\infty^2}$ as amount of the translational velocity. For the single profile, the lift A acts perpendicular to W_∞. Equation (4) likewise applies to the cascade if we understand by W_∞ the vectorial mean of the inflow velocity W_1 and the outflow velocity W_2. (Compare fig. 1(a).) The source-sink distribution $q(x)$ must satisfy the condition

$$\int_{x=0}^{l} q(x)dx = 0 \tag{5}$$

so that a closed contour (uncambered profile) results for the thickness distribution.

The kinematic flow condition for the relationship between the prescribed contour and the pertaining singularity distribution likewise may be split up into two conditions, corresponding to the decomposition of the profiles into the mean camber line and the thickness distribution. If u and v denote the x- and the y-component of the velocities induced by the vortex and by the source-sink distribution, the kinematic flow condition for the mean camber line according to figure 3(a) (first kinematic flow condition) reads

$$dy_s/dx = \left(V_\infty + v\right)\Big/\left(U_\infty + u\right) \tag{6}$$

For the thickness distribution, the source distribution $q(x)$ lies, according to figure 3(b), on the profile chord. Here the condition must be satisfied that the contour is identical with the streamline which separates the external translational flow from the internal source-sink flow. By applying the continuity equation to the area thickly outlined in figure 3(b), we obtain

$$\left(U_\infty + u\right)y_d + \frac{1}{2}\, q\, dx = \left(U_\infty + u\right)\left(y_d + \frac{dy_d}{dx}\, dx\right)$$

or

$$dy_d/dx = q(x)\Big/2\left(U_\infty + u\right) \tag{7}$$

as the second kinematic flow condition. Here, too, we shall take the values of u and v, not on the contour, but on the blade chord (thus, for $y = 0$). Equations (6) and (7) apply in the same manner for the single profile and for the blade in the cascade configuration. The influence of the cascade is contained implicitly in the induced velocities u and v. The single profile results as the limiting case of a cascade with the pitch ratio $t/l = \infty$.

2.2 The Induced Velocities

For a prescribed cascade we calculate, first, from equations (6) and (7) the singularity distributions $\gamma(x)$ and $q(x)$ and, next, from these, the aerodynamic coefficients. The first step of this calculation (determination of $\gamma(x)$ and $q(x)$) is rather laborious since the induced velocities must first be determined from Biot-Savart's law. The second step (determination of the aerodynamic coefficients for known circulation distribution), in contrast, proves to be very simple.

For the single profile (characterized by subscript E) which extends from $x = 0$ to $x = l$ (compare figs. 2(a) to 2(e)) and has a circulation distribution $\gamma(x)$ and a source-sink distribution $q(x)$ along the chord, we obtain for the induced velocity $w_E(z)$ at an arbitrary point of the x,y-plane, in complex notation

$$w_E(z) = u_E - iv_E = \frac{1}{2\pi}\int_{x'=0}^{l} \frac{q(x') + i\gamma(x')}{z - x'}\,dx' \tag{8}$$

where x and x' denote, respectively, the real coordinates of the control point and the running point along the source distribution. According to assumption, the induced velocity is needed only on the chord, that is, for $z = x$ with $0 \leqq x \leqq l$. This velocity is, according to equation (8)

$$w_E(x,0) = \frac{1}{2\pi}\int_{x'=0}^{l} \frac{q(x') + i\gamma(x')}{x - x'}\,dx' \tag{9}$$

with a singularity at $x' = x$. The integral is to be interpreted as a Cauchy main value. If the induced velocity is split up into the contributions of the vortex and source distributions (denoted by subscripts γ and q), that is, if we write

$$u_E = u_{\gamma E} + u_{qE} \qquad v_E = v_{\gamma E} + v_{qE} \tag{10}$$

there follows from equation (9)

$$u_{\gamma E} = \pm \frac{1}{2}\gamma(x) \qquad v_{\gamma E} = \frac{1}{2\pi}\int_{x'=0}^{l} \frac{\gamma(x')}{x' - x}\,dx' \tag{11}$$

and

$$u_{qE} = \frac{1}{2\pi}\int_{x'=0}^{l} \frac{q(x')}{x - x'}\,dx' \qquad v_{qE} = \pm \frac{1}{2} q(x) \tag{12}$$

The plus sign applies for the upper side, the minus sign for the lower side of the profile.

For the cascade whose geometry is fixed, according to figure 1(b), by the angle of stagger λ and the pitch ratio t/l, we obtain, if $\gamma(x)$ and $q(x)$ are prescribed along each of the blade chords, the following expression for the induced velocity field (compare E. Pistolesi (ref. 15) or N. Scholz (ref. 4)):

$$w(z) = \frac{e^{i\lambda}}{2t} \int_{x'=0}^{l} \left[q(x') + i\gamma(x')\right] \coth\left(\pi \frac{z - x'}{t} e^{i\lambda}\right) dx' \qquad (13)$$

or for the value on the chord $(z = x)$

$$\left.\begin{aligned} w(x,0) &= u(x) - iv(x) \\ &= \frac{e^{i\lambda}}{2t} \int_{x'=0}^{l} \left[q(x') + i\gamma(x')\right] \coth\left(\pi \frac{x - x'}{t} e^{i\lambda}\right) dx' \end{aligned}\right\} \qquad (14)$$

This integral also is to be interpreted as a Cauchy main value. For the limiting case $t/l \rightarrow \infty$, equation (14) is transformed into equation (9) for the single airfoil.

If we now visualize the expressions resulting for the induced velocities u and v (for the single airfoil equations (11) and (12), for the cascade by splitting-up of equation (14)) as introduced into equations (6) and (7), we recognize that from them two coupled integral equations for $\gamma(x)$ and $q(x)$ result. An analytic or an exact numerical solution of these integral equations does not appear possible for the general case of an arbitrary cascade. We therefore choose an approximation method where we satisfy the two kinematic flow conditions which have to be fulfilled over the entire length of the blade chord $0 \leqq x \leqq l$, only at a few discrete control points. Thus we reduce the solution of the integral equations to the solution of two systems of linear equations for certain free coefficients of the circulation and source distribution. We shall discuss below this method of control points, first, for the case of the single blade and shall transfer it later to the cascade.

3. PERFORMANCE OF THE CALCULATION FOR THE SINGLE PROFILE

3.1 Expansion in Series According to H. Glauert

For the single profile, the angle of attack α_∞ of the chord with respect to the direction of the translational flow, according to figure 2(b) is, generally, small; thus $u \ll U_\infty$. We may therefore simplify equations (6) and (7) by neglecting u compared to U_∞. Furthermore, we may replace the y-component of the induced velocity $v_E = v_{\gamma E} + v_{qE}$ by $v_E = v_{\gamma E}$ because on both sides of the chord, according to equation (12), v_{qE} has opposite signs, thus is, on the average, equal to zero on the chord. Thus, the simplified kinematic flow conditions for the single profile read

$$dy_s/dx = \left(V_\infty + v_{\gamma E}\right)/U_\infty \tag{15}$$

and

$$dy_d/dx = q(x)/2U_\infty \tag{16}$$

By the simplification we perceive that, first, both conditions are now independent of one another (the first contains only the circulation distribution, the second only the source distribution) and, second, that now only the first condition represents an integral equation for $\gamma(x)$ whereas $q(x)$ may be determined from the second condition by a simple quadrature. Both circumstances contribute considerably to facilitating the calculation.[4]

Another circumstance which makes the calculation for the single profile much simpler than that for the cascade is the fact that, if $\gamma(x)$ and $q(x)$ are suitably selected, the integrals for the induced velocities on the single airfoil may be evaluated analytically according to equations (11) and (12), which is impossible for the corresponding integrals of the cascade according to equation (14). This is the more significant, as in both cases these integrals contain for the induced velocities a singularity which is rather inconvenient for a numerical quadrature.

In order to be able to calculate the induced velocities for the single profile conveniently, we expand $\gamma(x)$ and $q(x)$ according to H. Glauert (ref. 9) and H. J. Allen (ref. 11) into a trigonometric series and introduce instead of the coordinate x the trigonometric variable φ according to

$$x = \frac{l}{2}\left(1 - \cos\varphi\right) \tag{17}$$

---

[4]We shall note here that neglecting u compared to U_∞, which leads to this essential simplification for the single profile, is generally no longer permissible for the cascade, since, in the case of narrow spacing or large deflection, the induced velocities u and v become comparable to U_∞, due to the mutual interference of the blades.

so that $\varphi = 0$ denotes the leading edge and $\varphi = \pi$ the trailing edge. For the circulation distribution we write

$$\gamma(x) = 2U_\infty\left(A_0 \cot\frac{\varphi}{2} + A_1 \sin\varphi + A_2 \sin 2\varphi + \ldots\right) \tag{18}$$

and, correspondingly, for the source distribution

$$q(x) = 2U_\infty\left\{B_0\left(\cot\frac{\varphi}{2} - 2\sin\varphi\right) + B_2 \sin 2\varphi + \ldots\right\} \tag{19}$$

with A_0, A_1, A_2, . . . and B_0, B_1, B_2, . . . as free coefficients which have to be ascertained from the kinematic flow conditions. In the expression for the source distribution, the first two terms must be combined so that the closed-contour requirement, equation (5), is satisfied term by term.

By evaluating equations (11) and (12) with equations (18) and (19) we obtain for the induced velocities the explicit analytical expressions

$$u_{\gamma E} = \pm U_\infty\left[A_0 \cot\frac{\varphi}{2} + A_1 \sin\varphi + A_2 \sin 2\varphi + \ldots\right] \tag{20}$$

$$v_{\gamma E} = U_\infty\left[-A_0 + A_1 \cos\varphi + A_2 \cos 2\varphi + \ldots\right] \tag{21}$$

$$u_{qE} = U_\infty\left[B_0(1 + 2\cos\varphi) - B_2 \cos 2\varphi - B_3 \cos 3\varphi - \ldots\right] \tag{22}$$

$$v_{qE} = \pm U_\infty\left[B_0\left(\cot\frac{\varphi}{2} - 2\sin\varphi\right) + B_2 \sin 2\varphi + B_3 \sin 3\varphi + \ldots\right] \tag{23}$$

3.2 Systems of Equations for the Coefficients of the Singularity Distributions

For a prescribed camber distribution $y_s(x)$ and thickness distribution $y_d(x)$, the coefficients A_0, A_1, A_2, . . . and B_0, B_2, B_3, . . . are to be determined from the kinematic flow conditions, equations (15) and (16). From these there results, if we introduce $v_{\gamma E}$ according to equation (21), and $q(x)$ according to equation (19) and denote derivatives with respect to x by primes

$$-A_0 + A_1 \cos \varphi + A_2 \cos 2\varphi + \ldots = -K + y_s'(x) \tag{24}$$

and

$$B_0\left(\cot \frac{\varphi}{2} - 2 \sin \varphi\right) + B_2 \sin 2\varphi + \ldots = y_d'(x) \tag{25}$$

In equation (24)

$$K = \tan \alpha_\infty = V_\infty/U_\infty \tag{26}$$

denotes the parameter for the angle of attack of the profile. Since equations (24) and (25) are to be satisfied in the entire profile region $0 \leqq x \leqq l$, an infinite number of coefficients is required in the general case. In practical calculations, however, we try to manage with the smallest possible number of coefficients. Then the kinematic flow conditions can be satisfied at only as many discrete points (control points) along the length of the blade chord as terms are taken in equations (18) and (19). Thus the question arises as to the distribution of these control points over the length of the blade chord in order to attain an optimum approximation to the exact solution with the smallest possible number of terms.

For this purpose, the so-called three-quarter chord theorem has been successfully applied in a number of cases (refs. 19 and 20). This theorem states that, if only one control point is selected, it is to be placed at the point $x = \frac{3}{4} l$. For n control points, we divide the entire length of the profile chord into n equal strips each with a chord $l_n = \frac{l}{n}$ and assume the control points at the $\frac{3}{4} l_n$ points. Thus we have one control point at $x_1 = \frac{3}{4} l$, two control points at $x_1 = \frac{3}{8} l$ and $x_2 = \frac{7}{8} l$, three control points at $x_1 = \frac{3}{12} l$, $x_2 = \frac{7}{12} l$, and $x_3 = \frac{11}{12} l$, or generally n control points at

$$x_\nu^{(n)} = \frac{4\nu - 1}{4n} l \tag{27}$$

with $\nu = 1, 2, \ldots n$. With use of the three-quarter chord theorem, the kinematic flow conditions, equations (24) and (25), are replaced by the two systems of equations

$$-A_0 + A_1 \cos \varphi_\nu^{(n)} + A_2 \cos 2\varphi_\nu^{(n)} + \ldots A_{n-1} \cos\left[(n - 1)\varphi_\nu^{(n)}\right] =$$

$$-K + y_s'\left[x_\nu^{(n)}\right] \tag{28}$$

and

$$B_0\left[\cot \frac{\varphi_\nu^{(n)}}{2} - 2 \sin \varphi_\nu^{(n)}\right] + B_2 \sin 2\varphi_\nu^{(n)} + \ldots B_n \sin\left[n\varphi_\nu^{(n)}\right] =$$

$$y_d'\left[x_\nu^{(n)}\right] \tag{29}$$

with

$$\cos \varphi_\nu^{(n)} = 1 - (4\nu - 1)/2n \tag{30}$$

We thus obtain for n control points two systems of n equations each for $A_0, A_1, \ldots A_{n-1}$ and $B_0, B_2, \ldots B_n$. The values of the trigonometric functions at the control points $\varphi_\nu^{(n)}$ may be calculated universally.

It is expedient, for the evaluation of equation (28), to subdivide the coefficients $A_0, A_1, \ldots$ into a contribution of the angle of attack (second subscript β) and a portion independent of the angle of attack (second subscript 0).[5] We assume

$$\left.\begin{aligned} A_0 &= A_{00} + KA_{0\beta} \\ A_1 &= A_{10} + KA_{1\beta} \ldots \end{aligned}\right\} \tag{31}$$

[5]For the single airfoil the portion independent of the angle of attack is given by the profile camber; for the cascade it is produced by the induced velocities of the cascade; thus it appears also for symmetrical profiles.

Thereby we obtain, instead of equation (28), the two systems

$$-A_{00} + A_{10} \cos \varphi_\nu^{(n)} + A_{20} \cos 2\varphi_\nu^{(n)} + \ldots + A_{(n-1),0} \cos\left[(n - 1)\varphi_\nu^{(n)}\right] = y_s'\left[x_\nu^{(n)}\right] \tag{32}$$

$$-A_{0\beta} + A_{1\beta} \cos \varphi_\nu^{(n)} + A_{2\beta} \cos 2\varphi_\nu^{(n)} + \ldots + A_{(n-1),\beta} \cos\left[(n - 1)\varphi_\nu^{(n)}\right] = -1 \tag{33}$$

The system according to equation (33) has for an arbitrary $n \geqq 1$ the solution

$$A_{0\beta} = 1 \quad A_{1\beta} = A_{2\beta} = \ldots = 0$$

so that equation (31) is simplified to $A_0 = A_{00} + K$, $A_1 = A_{10}$, . . .
This means that, for arbitrary thickness and camber distribution, the circulation distribution stemming from the angle-of-attack parameter $\tan \alpha_\infty = K$ is, as for the flat plate, equal to $2V_\infty \cot (\varphi/2)$.

For a prescribed single profile we must therefore solve the two systems, equations (32) and (29). The solution of equation (32) yields the additional circulation distribution due to the camber; the solution of equation (29), the additional velocities due to the thickness. The explicit systems of equations for one control point as well as for two and three control points are given in table 1.

3.3 Aerodynamic Coefficients

After the coefficients of the singularity distributions have been determined, the aerodynamic coefficients can be obtained from them very simply. In the total circulation only the two first terms of equation (18) make any contribution. From equations (3) and (18) there follows

$$\Gamma = U_\infty l\pi\left(A_0 + \frac{1}{2} A_1\right) \tag{34}$$

and thus from equation (4) for the total lift of the wing per unit width

$$A = \rho U_\infty W_\infty l\pi\left(A_0 + \frac{1}{2} A_1\right) \tag{35}$$

For the lift coefficient c_A defined by

$$c_A = A\Big/\frac{\rho}{2} W_\infty^2 l \tag{35a}$$

there results, consequently

$$\begin{aligned} c_A &= 2\pi\left(A_0 + \frac{1}{2} A_1\right)\cos \alpha_\infty \\ &= 2\pi\left[\left(A_{00} + \frac{1}{2} A_{10}\right)\cos \alpha_\infty + \sin \alpha_\infty\right] \end{aligned} \tag{36}$$

and

$$\left(dc_A/d\alpha_\infty\right)_{\alpha_\infty=0} = 2\pi \tag{36a}$$

This value is exactly correct for the flat plate.

The velocity distribution $W_K(x)$ along the contour is obtained from the velocity distribution $U_s(x)$ along the chord line by means of the relationship indicated by F. Riegels (ref. 10)

$$W_K/U_\infty = \left(U_s/U_\infty\right)\left(1\Big/\sqrt{1 + {y_d'}^2}\right) \tag{37}$$

Here $1\Big/\sqrt{1 + {y_d'}^2}$ is the so-called Riegels factor known from the thickness distribution. The velocity distribution on the chord follows from

$$U_s = U_\infty + u_{qE} + u_{\gamma E}$$

or, after substitution of equations (20), (22), and (31) from

$$\frac{U_s}{U_\infty} = \left[1 + B_0(1 + 2\cos\varphi) - B_2\cos 2\varphi - B_3\cos 3\varphi - \ldots\right] \pm$$

$$\left(A_{00}\cot\frac{\varphi}{2} + A_{10}\sin\varphi + A_{20}\sin 2\varphi + \ldots\right) \pm K\cot\frac{\varphi}{2} \qquad (38)$$

with the upper and lower signs for the suction and pressure sides, respectively. $W_K(x)$ may be conveniently determined from equations (37) and (38), after the coefficients of the singularity distributions have been ascertained. In equation (38), the first term, in brackets, gives the velocity distribution of the symmetrical profile for symmetrical approach flow; the second term, in parentheses, gives the contribution of the camber for zero angle of attack, and the third term gives the contribution of the incidence of the profile with the angle $\alpha_\infty = \arctan K$. This third term is the same as in the case of the flat plate with incidence.

At the profile nose ($x = 0$, $\varphi = 0$) generally $U_s = \infty$ and thus for the infinitely thin profile also, $W_K = \infty$. The pressure then has in the neighborhood of the nose very large negative values (minimum-pressure peak). The profile nose is in a flow either from below or from above. The infinitely large velocity does not appear, however, if in equation (38) the terms with $\cot(\varphi/2)$ vanish, that is, for

$$A_0 = 0 \qquad (38a)$$

In this case there is no flow about the leading edge; that is, shock-free inflow occurs. At an angle of attack in the case of shock-free inflow, which plays a role in the older literature on turbo-machines, the front stagnation point, for an infinitely thin profile, lies exactly on the leading edge. From equation (38a) there results for the angle of attack pertaining to shock-free inflow (denoted by subscript st)

$$A_0 = A_{00} + K_{st} = A_{00} + \tan\alpha_{\infty st} = 0$$

$$\tan\alpha_{\infty st} = -A_{00} \qquad (38b)$$

For profiles of finite thickness, the velocity at the nose remains finite. Equation (37) yields for W_K/U_∞ at $x = 0$ the limiting value ∞/∞ which, with R_N as the nose radius, is calculated to be

$$\left(W_K/U_\infty\right)_{x=0} = A_0\sqrt{2l/R_N} \tag{38c}$$

(Compare ref. 3.) The concept of shock-free inflow according to equation (38a) is retained also for profiles of finite thickness since, with such profiles, for $\alpha_\infty \neq \alpha_{\infty st}$ a large local minimum pressure point appears also in the neighborhood of the nose.

A comparison of the aerodynamic coefficients calculated according to this approximation method with exact solutions follows later in section 3.5.

3.4 Checking of the Profile Shape

Since in the approximate method the prescribed profile is approximated at only a few control points by the tangents of the mean camber line and the thickness distribution, it is expedient to check whether it is represented with sufficient accuracy. This is possible by comparison of the prescribed mean camber line and thickness distribution with the corresponding values of the approximation polynomial. The formulas required for this will be given here.

For the mean camber line, the approximate calculation yields, by integration of equation (24) with $V_\infty = 0$:[6]

$$\frac{y_s}{l} = \frac{1}{8} A_1(1 - \cos 2\varphi) + \frac{1}{12} A_2(\cos \varphi - \cos 3\varphi) -$$

$$\frac{1}{16} A_3(1 - 2 \cos 2\varphi + \cos 4\varphi) + \ldots \tag{39}$$

The thickness distribution follows likewise by integration from equation (27)

[6]For $V_\infty \neq 0$ we obtain merely an additional inclination of the mean camber line (angle of incidence) which is unimportant here.

$$\frac{y_d}{l} = \frac{1}{2} B_0 \left(\sin \varphi + \frac{1}{2} \sin 2\varphi\right) +$$

$$\frac{1}{12} B_2(3 \sin \varphi - \sin 3\varphi) +$$

$$\frac{1}{16} B_3(2 \sin 2\varphi - \sin 4\varphi) + \ldots \qquad (40)$$

The numerical evaluation of equations (39) and (40) is discussed in section 3.5.

3.5 Examples

Before transferring the approximate method to the cascade, we shall examine its usefulness for the single profile with the aid of a few examples for which exact solutions are known.

3.5.1 The flat plate.- We assume the flat plate to have an angle of attack α_∞. Since the camber is zero and therefore $y_s \equiv 0$, there results from equation (32), independently of the number of control points selected

$$A_{00} = A_{10} = A_{20} = \ldots = 0$$

According to equation (29) we have also

$$B_0 = B_2 = B_3 = \ldots = 0$$

Thus there follows, in complete agreement with the exact solution, from equation (36) for the lift coefficient

$$c_A = 2\pi \sin \alpha_\infty$$

and from equation (18), because of $A_0 = K = V_\infty/U_\infty$ and $A_1 = A_2 = \ldots = 0$, for the circulation distribution

$$\gamma(x) = 2V_\infty \cot \frac{\varphi}{2}$$

3.5.2 Parabolic profile.- For a parabolic profile with the camber f, the chord of which coincides with the x-axis, there applies

$$y_s(x) = 4f\,\frac{x}{l}\left(1 - \frac{x}{l}\right)$$

We assume the direction of the approach flow to be parallel to the chord ($\alpha_\infty = 0$, that is, $K = 0$), and one control point to be chosen at $x_1 = \frac{3}{4}\,l$. From the fulfillment of the kinematic flow conditions (equation (34)) at this control point, we obtain the coefficient A_1 whereas we have to assume

$$A_{00} = A_{20} = A_{30} = \ldots = 0$$

For A_{10} we obtain, because of

$$\cos\varphi_1^{(1)} = -\frac{1}{2} \quad \text{and} \quad \left(y_s'\right)_{x=3l/4} = -2f/l$$

the values

$$-\frac{1}{2}\,A_{10} = -2f/l \quad \text{or} \quad A_{10} = 4f/l$$

respectively. According to equation (31), $B_0 = B_2 = B_3 = \ldots = 0$. Thus there results, according to equation (36), for the lift coefficient

$$c_A = 4\pi f/l$$

and, according to equation (20), for the circulation distribution

$$\gamma(x) = 8(f/l)U_\infty \sin\varphi$$

Both expressions agree completely with the solution of W. Birnbaum for the parabolic profile in the case of shock-free inflow (zero angle of attack). If we calculate with several control points, we arrive at the same result, as may be easily confirmed.

3.5.3 Symmetrical Joukowsky profile.- Within the scope of the approximate calculation, the symmetrical Joukowsky profile is the simplest case of a profile of finite thickness, since it is represented by the first term in equation (19). A Joukowsky profile of the thickness d has, for a moderate thickness ratio d/l, the thickness distribution

$$y_d(x) = \frac{8}{3\sqrt{3}}\, d\sqrt{\frac{x}{l}}\left(1 - \frac{x}{l}\right)^{3/2} \tag{41}$$

The greatest thickness lies at $x = \frac{l}{4}$. For the calculation with one control point we need y_d' for $x = \frac{3}{4}\, l$. From equation (41) there follows

$$\left(y_d'\right)_{x=3l/4} = -8d/9l$$

and thus from equation (29) as the qualifying equation for B_0

$$-\left(2/\sqrt{3}\right)B_0 = -8d/9l$$

or

$$B_0 = \left(4/3\sqrt{3}\right)(d/l) \qquad B_2 = B_3 = \ .\ .\ . = 0$$

The approximate calculation with one control point yields, therefore, according to equations (40) and (17), for the contour

$$y_d(x) = \frac{2}{3\sqrt{3}}\, d\left(\sin\varphi + \frac{1}{2}\sin 2\varphi\right)$$

$$= \frac{8}{3\sqrt{3}}\, d\sqrt{\frac{x}{l}}\left(1 - \frac{x}{l}\right)^{3/2}$$

in complete agreement with equation (41). The calculation with several control points leads to the same result.

In the further examples, for single profiles as well as, later on, for the cascade, we shall select three control points since this number yields for the cascade results with fully sufficient accuracy so that the considerably larger calculation expenditure for a higher number of control points is not worth while.

3.5.4 NACA 0010 profile.- As another single profile we shall treat a symmetrical profile of the old NACA system[7] which will later be used in the cascade also. The NACA 0010 profile has the thickness distribution

$$\frac{y_d}{l} = 0.1485\sqrt{\frac{x}{l}} - 0.0630\,\frac{x}{l} - 0.1758\left(\frac{x}{l}\right)^2 + 0.1422\left(\frac{x}{l}\right)^3 - 0.0508\left(\frac{x}{l}\right)^4 \qquad (42)$$

with

$$y_d' = 0.07423\sqrt{\frac{l}{x}} - 0.0630 - 0.3516\,\frac{x}{l} + 0.4265\left(\frac{x}{l}\right)^2 - 0.203\left(\frac{x}{l}\right)^3 \qquad (43)$$

Tables 2 and 3 contain, among others, the values of y_d/l according to equation (42), of y_d' at the three control points as well as the factor $\sqrt{1 + {y_d'}^2}$ which is required for the calculation of the velocity distribution according to equation (37). The solution of the system of equations for B_0, B_2, B_3 with these values of y_{d1}', y_{d2}', y_{d3}' yields the numerical values in table 4. Because of $y_s \equiv 0$, the coefficients A_{00}, A_{10}, A_{20} are all equal to zero. With these values we can, first, check the profile contour according to equation (40). The approximate calculation agrees satisfactorily with the prescribed contour (fig. 4). For the velocity distribution in symmetrical approach flow, calculated according to equations (37) and (38) with $K = 0$, figure 4 likewise shows good agreement with the exact solution. Only in the neighborhood of the trailing edge do somewhat larger deviations appear which are, however, to be expected because of the differences in the contours.

3.5.5 NACA 8410 profile.- Finally we shall calculate a cambered profile of finite thickness which will also be used in the cascade later on. The NACA 8410 profile, with the coordinates according to

---

[7]Systematics of the National Advisory Committee for Aeronautics. Regarding the old NACA systematics, compare Jacobs, E. N., Ward, K. E., and Pinkerton, R. M.: The Characteristics of 78 Related Airfoil Sections From Tests in the Variable-Density Wind Tunnel. NACA TR 460, 1933.

tables 2 and 3,[8] has a relative thickness $\frac{d}{l} = 0.1$ and a relative camber $\frac{f}{l} = 0.08$. Table 4 contains the coefficients for the singularity distributions. Figure 5 shows the result of the check of the profile contour. The agreement with the prescribed variation is satisfactory here, too. Figure 6 contains the velocity distribution for different angles of attack. The angle of attack $\alpha_{\infty 0}$ of zero lift is $\alpha_{\infty 0} = -7.3^{\circ}$; the shock-free inflow corresponds to $\alpha_{\infty st} = 2.0^{\circ}$. For larger angles of attack, a pronounced minimum-pressure peak appears in the neighborhood of the nose on the suction side.

4. PERFORMANCE OF THE CALCULATION FOR THE CASCADE

4.1 The Kinematic Flow Conditions

We shall now transfer to the cascade the three-quarter chord theorem whose applicability for the single profile was proved with the aid of the preceding examples. In contrast to the single blade, there exist, for the cascade, generally larger angles between the direction of the approach flow and the blade chord, and the deflection caused by the cascade, that is, the difference in direction between W_1 and W_2, can no longer be regarded as a small angle. Figures 7(a) and 7(b) show the velocity diagram of a staggered cascade. The translational velocity W_{∞} has, just as in the case of the single airfoil, the components U_{∞} parallel and V_{∞} perpendicular to the blade chord; however V_{∞} now is not always small compared to U_{∞}. The quantity W_{∞} denotes the translational velocity of the cascade, free from circulation (free from deflection). For the cascade with deflection (with circulation) the cascade induces an additional velocity parallel to the cascade front $\pm\Delta w$ which, far ahead of and far behind the cascade, has the same magnitude but opposite signs. The inflow velocity W_1 far ahead of the cascade is the resultant of W_{∞} and $+\Delta w$; the outflow velocity W_2 is the resultant of W_{∞} and $-\Delta w$. Between the circulation Γ of a blade and the induced velocity Δw there exists the relationship immediately following from figures 7(a) and 7(b)

$$\Delta w = \Gamma/2t \tag{44}$$

---

[8] We want to point out that the thickness distribution of the NACA 8410 profile given in table 2 slightly deviates from that according to footnote 7.

Since, for the cascade, the induced velocities u and v generally must not be neglected compared to U_∞, as they are for the single airfoil, we have now to use the complete kinematic flow conditions according to equations (6) and (7). For the further calculation, we shall write the latter in the form

$$\frac{V_\infty}{U_\infty} + \frac{v}{U_\infty} = y_s'\left(1 + \frac{u}{U_\infty}\right) \tag{45}$$

and

$$\frac{1}{2}\,\frac{q(x)}{U_\infty} = y_d'\left(1 + \frac{u}{U_\infty}\right) \tag{46}$$

These conditions, with the values of u and v, will be satisfied on the chord also for the cascade.

4.2 The Induced Velocities

In order to be able to evaluate the kinematic flow conditions according to equations (45) and (46) for the determination of the singularity distributions, we must first obtain the induced velocities u and v on the blade chord for the cascade just as before, for the single airfoil. The general formula for these induced velocities of the cascade was furnished by equation (14); however, the integral contained in it cannot be solved analytically for the general case of the staggered cascade ($\lambda \neq 0$). Thus we are dependent on numerical methods for the evaluation of this integral. In these methods the singularity of the integrand of equation (14) is again troublesome for $x' = x$ which, however, stems only from the contribution of the single airfoil. Since, for the single airfoil, all components of the induced velocity could be evaluated analytically for the singularity distributions on the basis of the series according to H. Glauert (compare section 3.1), it is possible to eliminate the singularity of the integrand by subtracting the induced velocity field of the single airfoil from that of the cascade. Therefore

$$w = w_E + w_G \tag{47}$$

The subscript G denotes the "remainder of the cascade," that is, the contribution of "all remaining" blades without the single blade considered. The explicit expression for w_G follows from equations (9) and (14) by taking the difference, after introducing, in addition, the dimensionless x-coordinates

$$\xi = x/l \qquad \xi' = x'/l \tag{48}$$

we obtain

$$w_G(\xi) = u_G - iv_G$$

$$= \frac{1}{2}\frac{l}{t}\int_{\xi'=0}^{1}\left[q(\xi') + i\gamma(\xi')\right]\left[e^{i\lambda}\coth\left(\pi\frac{\xi - \xi'}{t/l}e^{i\lambda}\right) - \frac{1}{\pi}\frac{t/l}{\xi - \xi'}\right]d\xi' \tag{49}$$

This induced velocity field of the remainder of the cascade can be conveniently evaluated numerically since the influence function

$$F(\xi - \xi') = e^{i\lambda}\coth\left(\pi\frac{\xi - \xi'}{t/l}e^{i\lambda}\right) - \frac{1}{\pi}\frac{t/l}{\xi - \xi'} \tag{50}$$

is regular for $\xi' = \xi$ (on the further calculation of equation (49) compare the following section 4.3 and later section 7.1).

4.3 Expansion in Series

Corresponding to equation (47), the two components u and v of the induced complex velocity $w = u - iv$ also are split up into the contribution of the single airfoil and that of the remainder of the cascade

$$u = u_E + u_G \qquad v = v_E + v_G \tag{51}$$

We divide these parts again, as before for the single airfoil according to equation (10), into the contributions of the circulation distribution (subscript γ) and of the source distribution (subscript q)

$$\left.\begin{aligned} u_E &= u_{\gamma E} + u_{qE} \qquad & u_G &= u_{\gamma G} + u_{qG} \\ v_E &= v_{\gamma E} + v_{qE} \qquad & v_G &= v_{\gamma G} + v_{qG} \end{aligned}\right\} \tag{52}$$

The four components of the single airfoil $u_{\gamma E}$, u_{qE}, $v_{\gamma E}$, and v_{qE} are given in integral form by equations (11) and (12) and as explicit formulas by equations (20) to (23), respectively.

Similarly we obtain for the four components $u_{\gamma G}$, u_{qG}, $v_{\gamma G}$, and v_{qG} of the remainder of the cascade from equation (49), by splitting, the integral representations

$$u_{\gamma G} = -\frac{1}{2}\frac{l}{t}\int_{\xi'=0}^{1} \gamma(\xi')J(F)d\xi' \tag{53}$$

$$v_{\gamma G} = -\frac{1}{2}\frac{l}{t}\int_{\xi'=0}^{1} \gamma(\xi')R(F)d\xi' \tag{54}$$

$$u_{qG} = \frac{1}{2}\frac{l}{t}\int_{\xi'=0}^{1} q(\xi')R(F)d\xi' \tag{55}$$

$$v_{qG} = -\frac{1}{2}\frac{l}{t}\int_{\xi'=0}^{1} q(\xi')J(F)d\xi' \tag{56}$$

with $R(F)$ and $J(F)$ as real and imaginary parts, respectively, of the function $F(\xi - \xi')$ according to equation (50). If we introduce, furthermore, into equations (53) to (56) for $\gamma(x)$ and $q(x)$ the Glauert series according to equations (18) and (19), we obtain, in analogy to equations (20) to (23)

$$u_{\gamma G} = U_\infty\left(A_0 g_{\gamma 0} + A_1 g_{\gamma 1} + A_2 g_{\gamma 2} + \cdot \cdot \cdot\right) \tag{57}$$

$$v_{\gamma G} = U_\infty\left(A_0 f_{\gamma 0} + A_1 f_{\gamma 1} + A_2 f_{\gamma 2} + \cdot \cdot \cdot\right) \tag{58}$$

$$u_{qG} = U_\infty\left(B_0 g_{q0} + B_2 g_{q2} + B_3 g_{q3} + \cdot \cdot \cdot\right) \tag{59}$$

$$v_{qG} = U_\infty\left(B_0 f_{q0} + B_2 f_{q2} + B_3 f_{q3} + \cdot \cdot \cdot\right) \tag{60}$$

In equations (57) to (60), the quantities $g_{\gamma 0}$, $g_{\gamma 1}$, . . . and g_{q0}, g_{q2}, . . . denote the dimensionless induced velocities in the x-direction caused by the vortex distribution (subscript γ) and the source distribution (subscript q), respectively. The same applies for the quantities $f_{\gamma 0}$, $f_{\gamma 1}$, . . . and f_{q0}, f_{q2}, . . . regarding the y-direction. All these quantities are functions of x/l, t/l, and λ. In the limiting process toward the single airfoil ($t/l \to \infty$) all these functions tend toward zero; they have been universally calculated in dependence on the three parameters x/l, t/l, and λ. (Compare later section 7.1 and the appendix "Cascade-Downwash Tables".) This signifies an important advantage for the application of the calculation method as will be shown later.

Since the kinematic flow conditions, equations (45) and (46), are satisfied on the blade chord for the calculation method with the values of u and v, the two components of which $u_{\gamma E}$ and v_{qE} have, according to equations (11) and (12), opposite and equal values on both sides of the chord, these two components are on the average, equal to zero on the chord. Thus the values of u and v to be substituted into equations (45) and (46) become, according to equations (51) and (52)

$$u = u_{qE} + u_{qG} + u_{\gamma G} \tag{61}$$

$$v = v_{\gamma E} + v_{\gamma G} + v_{qG} \qquad (62)^{9}$$

If we substitute into equations (61) and (62) the values according to equations (57) to (60) and according to equations (21) and (22), we obtain, if we limit ourselves to three series terms, the expressions

$$u = U_\infty\left[\left(A_0 g_{\gamma 0} + A_1 g_{\gamma 1} + A_2 g_{\gamma 2}\right) + \left(B_0 g^*_{q0} + B_2 g^*_{q2} + B_3 g^*_{q3}\right)\right] \tag{63}$$

$$v = U_\infty\left[\left(A_0 f^*_{\gamma 0} + A_1 f^*_{\gamma 1} + A_2 f^*_{\gamma 2} + A_3 f^*_{\gamma 3}\right) + \left(B_0 f_{q0} + B_2 f_{q2} + B_3 f_{q3}\right)\right] \tag{64}$$

which are also valid for the kinematic flow conditions only, with the abbreviations

$$\left.\begin{aligned} g^*_{q0} &= g_{q0} + 2\cos\varphi + 1 & f^*_{\gamma 0} &= f_{\gamma 0} - 1 \\ g^*_{q2} &= g_{q2} - \cos 2\varphi & f^*_{\gamma 1} &= f_{\gamma 1} + \cos\varphi \\ g^*_{q3} &= g_{q3} - \cos 3\varphi & f^*_{\gamma 2} &= f_{\gamma 2} + \cos 2\varphi \\ & & f^*_{\gamma 3} &= f_{\gamma 3} + \cos 3\varphi \end{aligned}\right\} \tag{65}$$

[9] This is not valid for determining the velocity distribution on the contour. For this, only u is needed. The different signs of $u_{\gamma E}$ indicate the velocity difference at the opposite points of the suction and pressure side.

which represent the total dimensionless induced velocities for the remainder of the cascade plus the single blade. Thereby the induced velocities are furnished to the extent that the coefficients of the circulation and the source distribution can be determined from the kinematic flow conditions.

4.4 Systems of Equations for the Coefficients of the Singularity Distributions

The coefficients A_0, A_1, . . . and B_0, B_2, . . . according to equations (18) and (19) are determined for the cascade from the kinematic flow conditions in the same manner as for the single profile. For the cascade, however, we shall take as a basis the complete kinematic flow conditions according to equations (45) and (46). For the location of the control points we shall also use the three-quarter chord theorem as we did in the case of the single airfoil. This implies a hypothesis, the justification of which we shall check later on a few examples for which exact solutions exist.

If we satisfy the two kinematic flow conditions at n control points, we obtain 2n linear equations for the 2n unknowns A_0, A_1, . . . A_{n-1} and B_0, B_2, . . . B_n. In the case of the single airfoil this system was transformed into two systems of n equations each: into one system for A_0, A_1, . . . A_{n-1}, and a second for B_0, B_2, . . . B_n. Both systems could be solved independently of one another. In the case of the cascade there results generally a system of 2n equations which only in a few special cases has to be transformed into two systems of n equations each.

By substituting equations (63) and (64) into equations (45) and (46) and satisfying the two equations thus formed at the n control points at the points corresponding to $\varphi_\nu^{(n)}$ (with ν = 1, 2, . . . n), we obtain with $y'_{d\nu} = y'_d\left[x_\nu^{(n)}\right]$ and $y'_{s\nu} = y'_s\left[x_\nu^{(n)}\right]$ the system of equations

$$\left.\begin{aligned}
&B_0\left\{\left[\cot\frac{\varphi_\nu^{(n)}}{2} - 2\sin\varphi_\nu^{(n)}\right] - y'_{d\nu}g^*_{q0}\right\} + \\
&B_2\left[\sin 2\varphi_\nu^{(n)} - y'_{d\nu}g^*_{q2}\right] + B_3\left[\sin 3\varphi_\nu^{(n)} - y'_{d\nu}g^*_{q3}\right] \\
&= y'_{d\nu}\left[1 + A_0g_{\gamma 0} + A_1g_{\gamma 1} + A_2g_{\gamma 2}\right] \\
&A_0\left[f^*_{\gamma 0} - y'_{s\nu}g_{\gamma 0}\right] + A_1\left[f^*_{\gamma 1} - y'_{s\nu}g_{\gamma 1}\right] + A_2\left[f^*_{\gamma 2} - y'_{s\nu}g_{\gamma 2}\right] \\
&= -K + y'_{s\nu}\left[1 + B_0g^*_{q0} + B_2g^*_{q2} + B_3g^*_{q3}\right] - \left[B_0f_{q0} + B_2f_{q2} + B_3f_{q3}\right]
\end{aligned}\right\} \quad (66)$$

The quantities $y'_{d\nu}$ and $y'_{s\nu}$ are given with the geometry of the profile. The functions $f_{\gamma 0}$, $f_{\gamma 1}$, . . . and $g_{\gamma 0}$, $g_{\gamma 1}$, . . . can be taken from the cascade-downwash tables (in the appendix); in addition to depending on t/l and λ, they depend on the position of the control point, thus on ν. The quantity $K = \frac{V_\infty}{U_\infty} = \tan\alpha_\infty$ determines the direction of the inflow and is to be interpreted as a free parameter.

The system (eq. (66)), is arranged in such a manner that the terms with A_0, A_1, . . . and B_0, B_2, . . . on the right side are, in general, small compared to the remaining terms and may be neglected for an approximate solution.

For the further treatment of the system according to equation (66) we shall take the case of three control points, thus $n = 3$, as a basis, since this case has proved to be particularly suitable for the cascade calculations and the downwash tables were therefore made accordingly. With $n = 3$, equation (66) is a system of six equations for A_0, A_1, A_2, B_0, B_2, B_3. With the abbreviations

$$\left.\begin{aligned} q_{0\nu} &= \cot\frac{\varphi_\nu^{(3)}}{2} - 2\sin\varphi_\nu^{(3)} \\ q_{2\nu} &= \sin 2\varphi_\nu^{(3)} \\ q_{3\nu} &= \sin 3\varphi_\nu^{(3)} \end{aligned}\right\} \qquad (67)^{10}$$

$$\left.\begin{aligned} q_{0\nu} - y'_{d\nu} g^*_{q0} &= Q_{0\nu} \qquad & f^*_{\gamma 0} - y'_{s\nu} g_{\gamma 0} &= P_{0\nu} \\ q_{2\nu} - y'_{d\nu} g^*_{q2} &= Q_{2\nu} \qquad & f^*_{\gamma 1} - y'_{s\nu} g_{\gamma 1} &= P_{1\nu} \\ q_{3\nu} - y'_{d\nu} g^*_{q3} &= Q_{3\nu} \qquad & f^*_{\gamma 2} - y'_{s\nu} g_{\gamma 2} &= P_{2\nu} \end{aligned}\right\} \qquad (68)$$

$$\left.\begin{aligned} y'_{d\nu} g_{\gamma 0} &= S_{0\nu} \qquad & f_{q0} - y'_{s\nu} g^*_{q0} &= R_{0\nu} \\ y'_{d\nu} g_{\gamma 1} &= S_{1\nu} \qquad & f_{q2} - y'_{s\nu} g^*_{q2} &= R_{2\nu} \\ y'_{d\nu} g_{\gamma 2} &= S_{2\nu} \qquad & f_{q3} - y'_{s\nu} g^*_{q3} &= R_{3\nu} \end{aligned}\right\} \qquad (69)$$

and with $\nu = 1$ to 3, equation (66) obtains the simpler form

$$\left.\begin{aligned} B_0 Q_{0\nu} + B_2 Q_{2\nu} + B_3 Q_{3\nu} &= y'_{d\nu} + A_0 S_{0\nu} + A_1 S_{1\nu} + A_2 S_{2\nu} \\ A_0 P_{0\nu} + A_1 P_{1\nu} + A_2 P_{2\nu} &= -K + y'_{s\nu} - \left(B_0 R_{0\nu} + B_2 R_{2\nu} + B_3 R_{3\nu}\right) \end{aligned}\right\} \qquad (70)$$

---

[10]For $n = 3$ we obtain the following numerical values (compare table 1):

$$\begin{aligned} q_{01} &= 0 \qquad & q_{21} &= 0.8660 \qquad & q_{31} &= 0 \\ q_{02} &= -1.1269 \qquad & q_{22} &= -0.3287 \qquad & q_{32} &= -0.8765 \\ q_{03} &= -0.8040 \qquad & q_{23} &= -0.9213 \qquad & q_{33} &= 0.9827 \end{aligned}$$

By profile geometry $(y_s', \ y_d')$ and cascade geometry $(t/l, \ \lambda)$ all coefficients of the system according to equation (70) are fixed. The coefficients A_0 to B_3 have then to be ascertained as functions of $K = \tan \alpha_\infty$ (inflow direction). We can see from equation (70) that all coefficients are linear functions of K. In order to eliminate the repeated solving of equation (70), corresponding to the number of different desired inflow directions, it is suitable to introduce this linear dependence (as for the single blade in equation (31)) according to

$$\left.\begin{aligned} A_0 &= A_{00} + KA_{0\beta} & B_0 &= B_{00} + KB_{0\beta} \\ A_1 &= A_{10} + KA_{1\beta} & B_2 &= B_{20} + KB_{2\beta} \\ A_2 &= A_{20} + KA_{2\beta} & B_3 &= B_{30} + KB_{3\beta} \end{aligned}\right\} \tag{71}$$

and to split the equations into components free from K and involving K. We thus obtain two systems of six equations each with $\nu = 1$ to 3. The first system for the six coefficients A_{00} to B_{30} describes the translational flow parallel to the chord ($K = 0$, $\alpha_\infty = 0$) and reads

$$\left.\begin{aligned} A_{00}P_{0\nu} + A_{10}P_{1\nu} + A_{20}P_{2\nu} &= y_{s\nu}' - \left(B_{00}R_{0\nu} + B_{20}R_{2\nu} + B_{30}R_{3\nu}\right) \\ B_{00}Q_{0\nu} + B_{20}Q_{2\nu} + B_{30}Q_{3\nu} &= y_{d\nu}' + \left(A_{00}S_{0\nu} + A_{10}S_{1\nu} + A_{20}S_{2\nu}\right) \end{aligned}\right\} \tag{72}$$

The second system yields $A_{0\beta}$ to $B_{3\beta}$ as variations of A_0 to B_3 for changed inflow direction and has the form

$$\left.\begin{aligned} A_{0\beta}P_{0\nu} + A_{1\beta}P_{1\nu} + A_{2\beta}P_{2\nu} &= -1 - \left(B_{0\beta}R_{0\nu} + B_{2\beta}R_{2\nu} + B_{3\beta}R_{3\nu}\right) \\ B_{0\beta}Q_{0\nu} + B_{2\beta}Q_{2\nu} + B_{3\beta}Q_{3\nu} &= A_{0\beta}S_{0\nu} + A_{1\beta}S_{1\nu} + A_{2\beta}S_{2\nu} \end{aligned}\right\} \tag{73}$$

In the general case for staggered cascades with cambered profiles of finite thickness, we have two systems of six linear equations each, with six unknowns. In a few special cases considerable simplifications are possible for the solution of the systems of equations which we shall briefly enumerate below.

4.4.1 Cascades with infinitely thin blades and arbitrary stagger.- Because of $y'_{d\nu} = 0$ for infinitely thin blades, we obtain

$S_{0\nu} = S_{1\nu} = S_{2\nu} = 0$ and thus also

$$B_{00} = B_{20} = B_{30} = 0 \qquad B_{0\beta} = B_{2\beta} = B_{3\beta} = 0$$

Equations (72) and (73) are reduced to

$$A_{00}P_{0\nu} + A_{10}P_{1\nu} + A_{20}P_{2\nu} = y'_{s\nu}$$

$$A_{0\beta}P_{0\nu} + A_{1\beta}P_{1\nu} + A_{2\beta}P_{2\nu} = -1$$

thus, to two systems of three equations each.

4.4.2 Unstaggered cascade with blades of arbitrary camber and thickness.- Because of $\lambda = 0$ for unstaggered cascades there applies (compare later section 7.1)

$$g_{\gamma 0} = g_{\gamma 1} = g_{\gamma 2} = f_{q0} = f_{q2} = f_{q3} = 0$$

Thereby we obtain $B_{0\beta} = B_{2\beta} = B_{3\beta} = 0$, and equations (70) and (71) are reduced to

$$\left.\begin{aligned} &B_{00}Q_{0\nu} + B_{20}Q_{2\nu} + B_{30}Q_{3\nu} = y'_{d\nu} \\ &A_{00}P_{0\nu} + A_{10}P_{1\nu} + A_{20}P_{2\nu} = y'_{s\nu} - \left(B_{00}R_{0\nu} + B_{20}R_{2\nu} + B_{30}R_{3\nu}\right) \\ &A_{0\beta}P_{0\nu} + A_{1\beta}P_{1\nu} + A_{2\beta}P_{2\nu} = -1 \end{aligned}\right\} \quad (74)$$

thus, to three systems of three equations each.

4.4.3 Single profile.- Because of $t/l = \infty$ for the single profile

$$g_{\gamma 0} = g_{\gamma 1} = g_{\gamma 2} = f_{q0} = f_{q2} = f_{q3} = 0$$

is valid.

Thus, according to equation (69), $S_{0\nu} = S_{1\nu} = S_{2\nu} = 0$ and consequently $B_{0\beta} = B_{2\beta} = B_{3\beta} = 0$. Furthermore, we obtain, according to equations (68) and (65)

$$P_{0\nu} = -1 \qquad P_{1\nu} = \cos \varphi_\nu^{(3)} \qquad P_{2\nu} = \cos 2\varphi_\nu^{(3)}$$

Accordingly, equations (70) and (71) are again reduced to equation (74); now, however, with P_{01} to P_{23} as fixed numbers.[11] With these, the solution of the last system of equation (74) reads

$$A_{0\beta} = 1 \qquad A_{1\beta} = 0 \qquad A_{2\beta} = 0$$

For the single profile, we have therefore to solve the first two systems of equation (74) with three equations each. The latter do not agree exactly with equations (29) and (32) for the single profile. The reason is that there the calculation was on the basis of the simplified kinematic flow conditions, equations (15) and (16); here, on the other hand we use the complete kinematic flow conditions, equations (7) and (8). In the numerical evaluation, however, the difference for the single profile is very small.

4.4.4 General case.- In the general case of the staggered cascade with cambered profile of finite thickness, where two systems of six equations each are to be solved, it proves to be expedient to choose a method of successive approximation. Equation (72) as well as equation (73) is split up into two systems of three equations each. (Compare for more details later, section 7.2.)[12]

4.5 Aerodynamic Coefficients

Below, the formulas are furnished according to which the aerodynamic coefficients of the cascade can be determined from the coefficients of the singularity distributions.

4.5.1 Lift.- Equation (4) for the resultant force on a single blade applies also for the blade in the cascade configuration if we understand W_∞ to be the vertical mean of W_1 and W_2 according to figure 7(a).

---

[11] The numerical values are (compare table 1):

$$P_{01} = -1 \qquad P_{11} = 0.5 \qquad P_{21} = -0.5$$
$$P_{02} = -1 \qquad P_{12} = -0.1667 \qquad P_{22} = -0.9444$$
$$P_{03} = -1 \qquad P_{13} = -0.8333 \qquad P_{23} = 0.3889$$

[12] This method corresponds approximately to the one for the single profile with the simplified kinematic flow conditions.

A is perpendicular to the direction of W_∞. If we insert Γ from equation (44) into equation (4), there follows

$$A = 2\rho W_\infty t \, \Delta w \tag{75}$$

or

$$c_A = A \Big/ \frac{\rho}{2} W_\infty^2 l = 4(\Delta w/W_\infty)(t/l) \tag{76}$$

From equation (4) we obtain with Γ according to equation (34) and with A_0 and A_1 according to equation (71)

$$c_A = 2\pi\left(A_0 + \frac{1}{2} A_1\right)\cos \alpha_\infty$$

$$= 2\pi\left[\left(A_{00} + \frac{1}{2} A_{10}\right)\cos \alpha_\infty + \left(A_{0\beta} + \frac{1}{2} A_{1\beta}\right)\sin \alpha_\infty\right] \tag{77}$$

Hence there results for the lift increase of the blade in the cascade for $\alpha_\infty = 0$ the expression

$$\left(\frac{dc_A}{d\alpha_\infty}\right)_{\alpha_\infty=0} = 2\pi\left(A_{0\beta} + \frac{1}{2} A_{1\beta}\right) \tag{78}$$

4.5.2 Inflow and outflow angles.- According to the velocity diagram in figure 7(a) there applies for the components $W_{\infty t}$ and $W_{\infty n}$ of W_∞ parallel (subscript t) or, respectively, perpendicular (subscript n) to the cascade front

$$\left.\begin{aligned} W_{\infty t} &= U_\infty \sin \lambda + V_\infty \cos \lambda \\ W_{\infty n} &= W_{1n} = W_{2n} = U_\infty \cos \lambda - V_\infty \sin \lambda \end{aligned}\right\} \tag{79}$$

Furthermore, we have according to figure 7(a) $\left(\text{with } W_n = W_{\infty n} = W_{1n} = W_{2n}\right.$ for abbreviation$\left.\right)$

$$\cot \beta_1 - \cot \beta_2 = \frac{2\,\Delta w}{W_n} \qquad \sin \beta_\infty = \frac{W_n}{W_\infty}$$

and thus

$$\left(\cot \beta_1 - \cot \beta_2\right)\sin \beta_\infty = 2\ \Delta w/W_\infty \tag{80}$$

or, respectively, according to equation (76)

$$c_A = 2\frac{t}{l}\sin \beta_\infty\left(\cot \beta_1 - \cot \beta_2\right) \tag{81}$$

This is the relationship between the lift coefficient and the flow angles, which is fundamental for the cascade theory.

In addition to the angles β_1, β_2, and β_∞ between W_1, W_2, and W_∞, respectively, and the cascade front, we shall introduce the angles α_1, α_2, and α_∞ between these velocities and the blade chord. According to figure 7(a) there applies, because of $\beta_s = (\pi/2) + \lambda$

$$\left.\begin{aligned}
\lambda + \alpha_1 &= \beta_1 - (\pi/2) \qquad & \alpha_1 &= \beta_1 - \beta_s \\
\lambda + \alpha_2 &= \beta_2 - (\pi/2) \qquad & \alpha_2 &= \beta_2 - \beta_s \\
\lambda + \alpha_\infty &= \beta_\infty - (\pi/2) \qquad & \alpha_\infty &= \beta_\infty - \beta_s
\end{aligned}\right\} \tag{82}$$

For the blade in the cascade configuration, the angle α_∞ between the blade chord and the velocity W_∞ plays the role of the angle of attack insofar as the resultant blade force A is perpendicular to the direction of W_∞. (Compare figs. 1(a) to 1(c).)

Between the velocities and angles there apply the relationships to be seen from figure 7(a).

$$-\cot \beta_1 = \frac{W_{\infty t} + \Delta w}{W_n} = \frac{U_\infty \sin \lambda + V_\infty \cos \lambda + \Delta w}{U_\infty \cos \lambda - V_\infty \sin \lambda}$$

$$-\cot \beta_2 = \frac{W_{\infty t} - \Delta w}{W_n} = \frac{U_\infty \sin \lambda + V_\infty \cos \lambda - \Delta w}{U_\infty \cos \lambda - V_\infty \sin \lambda}$$

$$\begin{aligned}
-\cot \beta_\infty &= -\frac{1}{2}\left(\cot \beta_1 + \cot \beta_2\right) \\
&= \frac{W_{\infty t}}{W_n} = \frac{U_\infty \sin \lambda + V_\infty \cos \lambda}{U_\infty \cos \lambda - V_\infty \sin \lambda}
\end{aligned}$$

Hence follows with equation (26)

$$-\cot \beta_1 = \frac{\tan \lambda + K + (1/\cos \lambda)(\Delta w/U_\infty)}{1 - K \tan \lambda} \tag{83}$$

$$-\cot \beta_2 = \frac{\tan \lambda + K - (1/\cos \lambda)(\Delta w/U_\infty)}{1 - K \tan \lambda} \tag{84}$$

$$-\cot \beta_\infty = (\tan \lambda + K)/(1 - K \tan \lambda) \tag{85}$$

where, according to equations (44), (34), and (71)

$$\frac{\Delta w}{U_\infty} = \frac{1}{2} \frac{\Gamma}{U_\infty t} = \frac{\pi}{2} \frac{l}{t}\left[\left(A_{00} + \frac{1}{2} A_{10}\right) + K\left(A_{0\beta} + A_{1\beta}\right)\right] \tag{86}$$

From equations (83) to (86) we can calculate the inflow and outflow angles as functions of $K = \tan \alpha_\infty$ after having first determined the coefficients A_{00}, A_{10}, $A_{0\beta}$, $A_{1\beta}$ from the systems according to equations (72) and (73). If we have obtained in this manner β_1 and β_2, there follows the velocity ratio W_2/W_1 from the continuity equation according to

$$W_2/W_1 = \sin \beta_1/\sin \beta_2 \tag{87}$$

The pressure rise in the cascade thus attains, according to the Bernoulli equation $p_1 + \frac{\rho}{2} W_1^2 = p_2 + \frac{\rho}{2} W_2^2$, the form

$$\frac{p_2 - p_1}{\frac{\rho}{2} W_1^2} = 1 - \frac{\sin^2\beta_1}{\sin^2\beta_2} \tag{88}$$

or, referred to the rate of flow W_n

$$\frac{p_2 - p_1}{\frac{\rho}{2} W_n^2} = \cot^2\beta_1 - \cot^2\beta_2 \tag{88a}$$

In the calculations so far, the component of the translational velocity U_∞ parallel to the chord was used for the formation of dimensionless velocities. For the final representation of the results and in the comparison of the theory with test results it is more expedient to refer all velocities to the inflow velocity W_1 or the outflow velocity W_2. From figure 7(a) we take for the conversion

$$W_1/U_\infty = (\cos\lambda - K\sin\lambda)/\sin\beta_1 \tag{89}$$

4.5.3 Velocity distribution.- The velocity distribution on the blade contour is obtained from the velocity U_s on the blade chord according to equation (37) with

$$U_s = U_\infty + u = U_\infty + u_{\gamma E} + u_{\gamma G} + u_{qE} + u_{qG} \tag{90}$$

The sum of the three terms $u_{\gamma G} + u_{qE} + u_{qG}$ was previously given in equation (63), the term $u_{\gamma E}$ in equation (20). If we divide up all coefficients of the singularity distributions according to equation (71), we obtain U_s/U_∞ in the form best suited for the numerical evaluation (with the upper sign for the upper side, the lower sign for the lower side of the profile)

$$\begin{aligned}\frac{U_s}{U_\infty} = 1 &+ B_{00}g^*_{q0} + B_{20}g^*_{q2} + B_{30}g^*_{q3} + \\ &K\left(B_{0\beta}g^*_{q0} + B_{2\beta}g^*_{q2} + B_{3\beta}g^*_{q3}\right) + \\ &A_{00}g_{\gamma 0} + A_{10}g_{\gamma 1} + A_{20}g_{\gamma 2} + \\ &K\left(A_{0\beta}g_{\gamma 0} + A_{1\beta}g_{\gamma 1} + A_{2\beta}g_{\gamma 2}\right) \pm \\ &\left[\left(A_{00}\cot\frac{\varphi}{2} + A_{10}\sin\varphi + A_{20}\sin 2\varphi\right) + \right. \\ &\left. K\left(A_{0\beta}\cot\frac{\varphi}{2} + A_{1\beta}\sin\varphi + A_{2\beta}\sin 2\varphi\right)\right]\end{aligned} \tag{91}$$

Once we have determined the coefficients B_{00}, B_{20}, . . . $A_{2\beta}$ from equations (72) and (73), we can calculate the velocity distribution from equations (37) and (91) with the aid of the downwash tables.

The velocity at the profile nose follows according to equation (38c) to be

$$\left(\frac{W_K}{U_\infty}\right)_{x=0} = A_0\sqrt{\frac{2l}{R_N}} = \left(A_{00} + KA_{0\beta}\right)\sqrt{\frac{2l}{R_N}} \tag{92}$$

Finally, we obtain from the velocity distribution, by means of the Bernoulli equation, the distribution of the pressure p on the contour, in the form

$$\frac{p - p_1}{\frac{1}{2}\rho W_1^2} = 1 - \left(\frac{W_K}{W_1}\right)^2 \tag{93}$$

4.5.4 Special inflow angles.- If the inflow direction (that is, $K = V_\infty/U_\infty$) for a prescribed staggered cascade is varied within sufficiently wide limits, flow conditions with pumping effect $(p_2 > p_1)$ and flow conditions with turbine effect $(p_2 < p_1)$ are obtained. Some special inflow directions also result which we shall now discuss briefly.

The shock-free inflow is characterized by that inflow angle for which the minimum-pressure peak at the nose is not present. Because of equation (38a) there applies here

$$K = \tan\alpha_{\infty st} = -A_{00}/A_{0\beta} \tag{94}$$

For a cascade free from deflection the inflow and outflow directions are parallel to one another, thus $\beta_1 = \beta_2 = \beta_\infty$. For this cascade the resultant blade force is zero $(c_A = 0)$. An unstaggered cascade of symmetrical profiles is, for reasons of symmetry, free from deflection when the inflow coincides with the direction of the chord $(\alpha_1 = \alpha_2 = \alpha_\infty = 0)$. For a staggered cascade of symmetrical profiles this is no longer true. On the contrary, as will be shown by the examples later, for such a cascade there must be, for a flow free from deflection, $\beta_1 \neq \beta_s$ (fig. 8(a)). The value of K for the cascade free from deflection results from $c_A = 0$ according to equation (77)

$$K_{cA=0} = \left(\tan\alpha_\infty\right)_{cA=0} = -\frac{A_{00} + \frac{1}{2}A_{10}}{A_{0\beta} + \frac{1}{2}A_{1\beta}} \tag{95}$$

For an inflow parallel to the chord $(\alpha_1 = 0)$ a deflection of the flow appears for the staggered cascade of symmetrical profiles (fig. 8(b)). In this case we obtain, because of $\alpha_1 = 0$ according to equation (82), $\tan \lambda = -\cot \beta_1$, and thus equation (83) yields

$$K = \tan \alpha_\infty = -\left(\Delta w / U_\infty\right) \cos \lambda$$

With $\Delta w / U_\infty$ according to equation (86) there follows

$$K = \frac{-\frac{\pi}{2}\frac{l}{t}\left(A_{00} + \frac{1}{2} A_{10}\right)}{\frac{\pi}{2}\frac{l}{t}\left(A_{0\beta} + \frac{1}{2} A_{1\beta}\right) + \frac{1}{\cos \lambda}} \tag{96}$$

The remaining aerodynamic coefficients for these particular flow states result by substitution of the given K-values into the formulas given above (equations (83) to (91)).

5. CALCULATION EXAMPLES

We shall test the accuracy of the calculation method first on examples for which exact solutions also exist.

5.1 The Unstaggered Plate Cascade

The simplest cascade is the unstaggered plate cascade with $\lambda = 0$ and $\beta_s = 90^\circ$ for which R. Grammel (ref. 21) indicated an exact solution which N. Scholz (ref. 22) represented in detail. The exact solution yields for the efficiency factor κ (ratio of the lift increase of the blade in the cascade configuration to the lift increase of the single blade)

$$\kappa = \frac{dc_A}{d\alpha_\infty} \Big/ \left(\frac{dc_A}{d\alpha_\infty}\right)_E = \frac{2}{\pi}\frac{t}{l} \tanh\left(\frac{\pi l}{2t}\right) \tag{97}$$

and for the ratio of the outflow angle to the inflow angle

$$\cot \beta_2 / \cot \beta_1 = e^{-\pi l/t} \tag{98}$$

The approximate solution yields according to equations (36a) and (78)

$$\kappa = A_{0\beta} + \frac{1}{2} A_{1\beta} \tag{99}$$

and according to equations (83), (84), and (86)

$$\frac{\cot \beta_2}{\cot \beta_1} = \frac{1 - \frac{l}{t}\frac{\pi}{2}\left(A_{0\beta} + \frac{1}{2} A_{1\beta}\right)}{1 + \frac{l}{t}\frac{\pi}{2}\left(A_{0\beta} + \frac{1}{2} A_{1\beta}\right)} \tag{100}$$

For the coefficients of the singularity distributions there applies according to equations (72) and (73)

$$A_{00} = A_{10} = \ldots = 0 \qquad B_{00} = B_{20} = \ldots = 0$$

$$B_{0\beta} = B_{2\beta} = \ldots = 0$$

and

$$A_{0\beta}P_{0\nu} + A_{1\beta}P_{1\nu} + A_{2\beta}P_{2\nu} = -1$$

with

$$P_{0\nu} = f^*_{\gamma 0} \qquad P_{1\nu} = f^*_{\gamma 1} \qquad P_{2\nu} = f^*_{\gamma 2}$$

according to equation (68) for the determination of $A_{0\beta}$, $A_{1\beta}$, and $A_{2\beta}$. The results of the calculation for three control points (n = 3) are given in table 5.

Figure 9 shows the efficiency factor κ (curve $\beta_s = 90^\circ$) as a function of the pitch ratio; agreement of the approximate calculation with the exact solution is very good. Figure 10 contains the result for the inflow and the outflow angles; here also the agreement of the approximate solution for three control points with the exact solution is excellent. In table 5 the position of the center of lift (aerodynamic center) was given also; its x-value we denote by x_{Neutr}. For the single plate the aerodynamic center lies at the point $\frac{x_{Neutr}}{l} = \frac{1}{4}$. With narrowing spacing it shifts considerably forward. Finally, figure 11 shows the circulation distribution over the plate chord for several pitch ratios. The approximate solution agrees again perfectly with the exact solution. Because of the narrow spacing $\frac{t}{l} = 0.5$ the rear half of the plate contributes almost nothing to the lift.

5.2 The Staggered Plate Cascade

For the staggered two-dimensional plate cascade, also, there exists an exact solution (on the basis of the conformal mapping, compare refs. 15 and 22), although not in closed form. The results of the approximate calculation for several blade angles β_s are contained in table 6. Figure 9 shows the efficiency factor. Here again, the agreement of the approximate solution for three control points and the exact solution is excellent.

On the whole, since these results of the approximation method are so satisfactory for the cascade also, good calculation accuracy may be expected as well in other cases for which no exact solutions exist.

5.3 Parabolic Cascade

Whereas no difference between positive and negative angles of stagger λ exists for the plate cascade, we find that generally, for cascades with cambered profiles, the arrangements with $\lambda < 0$ $(0 < \beta_s < 90^\circ)$ have turbine effect; those with $\lambda > 0$ $(90^\circ < \beta_s < 180^\circ)$, pump effect. The following results, calculated for the entire λ-range, give a first survey of the characteristic differences of the aerodynamic cascade coefficients for pumping and turbine cascades.

As the simplest case of a cascade with cambered profiles, we shall treat a cascade of infinitely thin parabolic profiles. With f as the height of camber, the equation of the mean camber line is given by the expression for $y_s(x)$ in section 3.5.2.

For the parabola as a single profile, the lift coefficient is

$$c_A = 2\pi\left[\alpha_\infty + 2\left(\frac{f}{l}\right)\right] \tag{101}$$

in perfect agreement for the exact and the approximate solutions. The angle of the shock-free inflow is $\alpha_{\infty st} = 0$ with $c_{Ast} = \frac{4\pi f}{l}$. For zero lift there applies $\left(\alpha_\omega\right)_{c_A=0} = \frac{-2f}{l}$.

For the parabolic profile in the cascade, the camber was based on the value $\frac{f}{l} = 0.1$. Thus, the values according to table 7 result for the inclination of the mean camber line at the three control points. Table 8 contains the coefficients of the singularity distributions. Of the extensive results, we shall give only those for the total lift. Figure 12 shows the coefficients for the lift increase. For the unstaggered parabolic cascade, agreement with the plate cascade exists, whereas the lift increase for higher λ-values is considerably smaller than for the plate cascade in the case of the parabolic cascade with pumping effect, and considerably larger in the case of the parabolic cascade with turbine effect. Figure 13 contains the results for the zero-lift direction. For the single blade $\left(\frac{t}{l} = \infty\right)$, $\left(\alpha_\infty\right)_{c_A=0} = \frac{-2f}{l} = -0.2 = -11.3^\circ$ is valid. For the other limiting case of the blades spaced very closely $\left(\frac{t}{l} = 0\right)$, we have the blade-congruent flow with a zero-lift angle which is equal to the angle δ_H of the end tangent with the chord: $-\left(\alpha_\infty\right)_{c_A=0} = \delta_H = \frac{4f}{l} = 0.4 = 21.8^\circ$. For finite values of the spacing, the values of $\left(\alpha_\infty\right)_{c_A=0}$ lie approximately between these limits for all angles of stagger. Figure 14 shows the outflow angle α_2 as a function of the inflow angle α_1. For the limiting case of the very closely spaced blades (blade-congruent flow, streamline theory), the outflow angle - independently of the inflow angle - is equal to δ_H (thus $-\alpha_2 = \delta_H = 21.8^\circ$). For spacings of finite magnitude, the outflow angle also depends only slightly on the inflow angle, particularly in the case of narrow spacing. However, the difference compared to the blade-end tangent, the so-called exaggeration angle (ref. 27) is considerable, for instance, approximately 9° for $\frac{t}{l} = 1.0$.

5.4 Cascade of Blades With Symmetrical Profiles

Furthermore, an extensive methodical system of cascades of blades with symmetrical profiles has been investigated (profile NACA 0010, cf. sec. 3.5.4). Such cascades are excellent for fundamental investigations due to the fact that the angle of stagger need be changed only in one direction, in the same manner as for the plate cascade and in contrast to cascades of cambered blades; there exists no difference between positive and negative stagger angles. This cascade shows, therefore, the thickness effect in a particularly clear form. Twelve arrangements were calculated, namely the blade angles $\beta_s = 90^\circ$, 120°, and 150° for the pitch ratios $\frac{t}{l} = 0.5$, 0.75, 1.0, and 1.5. We shall give only a very limited selection from the extremely voluminous results. Figure 15 shows the efficiency factor κ as a function of β_s and of t/l. (For comparison, the values of the plate cascade according to figure 9 have also been plotted.) As in the case of the single airfoil, the thickness has only a very slight influence on the lift increase. A particularly remarkable result is obtained for the zero-lift direction also contained in figure 15. It is identical with the inflow and outflow direction of the cascade free from deflection. Whereas an unstaggered cascade of symmetrical profiles has the effect of being free from deflection for an inflow parallel to the chord, a staggered cascade of such profiles gives, for an inflow parallel to the chord, a deviation in such a manner that the direction of outflow is turned from the direction of the chord toward the cascade front. The flow is free from deflection only when the cascade is approached by the flow at a certain angle with respect to the chord. For narrow spacing and considerable stagger, values $(\alpha_\infty)_{c_A=0}$ of 3° to 4° are attained. The values of $(\alpha_\infty)_{c_A=0}$ are probably about proportional to the profile thickness. Information regarding this effect may also be found in reference 23 by B. Eckert.

Figures 16 to 24 contain a small selection from the pressure distributions. It can be seen from the added velocity triangles whether we deal with pumping or with turbine cascades. For the unstaggered cascades $\beta_s = 90^\circ$ the pressure variation is of a similar nature as in the case of the single profile. However, the lift loading of the blade in the cascade lies closer to the profile nose, compared to the single blade. The entire rear half of the blade does not contribute anything to the lift, particularly in the case of narrow spacing.[13] For the staggered cascade $(\beta_s \neq 90^\circ)$, the pressure variation, for an inflow parallel to the chord $(\alpha_1 = 0)$, is different on both sides of the blade. The larger negative pressure lies close to the blade nose. Narrow spacings even cause overlapping of the pressure distribution on the upper and lower sides on the rear part of the blade. If the direction of inflow deviates from the direction parallel to the chord, a large negative-pressure peak is always produced at the profile nose. The positive α_1-values now

---

[13]Much more numerous results for unstaggered cascades, including the loss coefficients (also for other profile thicknesses and for cambered profiles) have been presented by L. Speidel (ref. 3).

correspond to pumping cascades, the negative α_1 -values, to turbine cascades. The differences in the pressure distribution are striking, particularly on the rear part of the blade. For the pumping cascades the loading on the rear part of the profile increases with increasing angle of attack; whereas for the turbine cascades, particularly in the case of narrow spacing, the overlapping of the pressure distributions already present at $\alpha_1 = 0$ is still increased. The rear parts of the blades of turbine cascades (particularly for narrow spacings and large stagger) make, therefore, a negative contribution to the lift. For equal total lift we obtain, therefore, larger negative-pressure peaks on the turbine than on the pumping cascades.

5.5 Cascades of Blades With Cambered Thick Profiles

Finally, we shall report a few results from a voluminous methodical system of cascades with blades of cambered thick profiles NACA 8410. (Cf. sec. 3.5.5.)[14] In this case, the influences of the thickness and the camber are superimposed in the cascade. The blade profile selected here, of 8-percent camber and 10-percent thickness, is usable both as a turbine and as a pumping cascade, as has been shown by investigations on loss coefficients. Twenty different arrangements of this profile in the cascade configuration were investigated: the blade angles $\beta_s = 30^\circ$ and 60° with turbine effect, the blade angle $\beta_s = 90^\circ$ and the angles $\beta_s = 120^\circ$ and 150° with pumping effect at pitch ratios 0.5, 0.75, 1.0, and 1.5. The complete calculation for a cascade from this series may be found in section 7.2; table 9 contains the coefficients of the singularity distributions. Figure 25 shows the results for the efficiency factor κ (relative lift increase) as a function of the reciprocal pitch ratio and of the blade angle; for comparison, the variation for the plate cascade has also been given. For extremely large stagger, corresponding to $\beta_s = 30^\circ$ and 150°, large differences between the pumping and the turbine cascades, and also compared to the plate cascade, appear. Figure 25 contains, in addition, the variation of the lift coefficient for $\alpha_\infty = 0$. For cambered profiles this value is more suitable for characterizing the lift curve $c_A(\alpha_\infty)$ than the value given for the former examples, α_∞ for $c_A = 0$, because the latter frequently lies in the region of separated flow, for cambered profiles. Figures 26 to 30 show for all cascades of this systematic family the inflow and outflow angles. The so-called

[14]The results of this section are taken from an unpublished report by L. Speidel (ref. 24) which also contains extensive results on loss coefficients.

exaggeration angle δ, that is, the angle between the outflow direction and the tangent to the mean camber line at the trailing edge, is given in the range of the inflow angles β_1 for which no significant flow separation occurs (according to the boundary-layer calculations not given here). For wide spacings this angle exaggeration always has higher values than for narrow spacings. We note, however, that the amount of δ is, in addition, considerably modified by the friction effect. Furthermore, we see from figures 26 to 30 that for turbine cascades $\beta_s = 30^\circ$ and 60° the range of permissible angles of attack α_1 of the cascade is considerably larger than for pumping cascades $\left(\beta_s = 120^\circ \text{ and } 150^\circ\right)$.

Figure 31 shows the velocity distribution along the profile contour for the calculation example according to section 7.2 for several K-values. A comparison with figure 6 shows that, particularly on the suction side, the pressure distribution in the cascade deviates considerably from that on the single profile. In figures 32 to 98, finally, a large number of pressure distributions has been compiled. For the pumping cascades, usable pressure distributions result in a range $\Delta\alpha_1$ of the inflow angle α_1, referred to the blade chord, which amounts at most to about $\Delta\alpha_1 = 20^\circ$; for turbine cascades, in contrast, up to $\Delta\alpha_1 = 70^\circ$. This is in good agreement with experience, according to which pumping cascades in general are much more sensitive to variations of the inflow angle than are turbine cascades.

We shall omit giving more details on the pressure distributions since the latter represent, primarily, the starting point for the calculation of the loss coefficients which we shall not treat in this report.

6. COMPARISON WITH TEST RESULTS

In conclusion, we shall give, to a limited extent, a comparison of the theoretical results with measurements, with the aid of the pressure distribution on the profile since this is rather sensitive to variations of the geometric parameters and of the inflow angle, and also is relatively little influenced by the viscosity effects (neglected in the theory) as long as no strong separation occurs. The pressure-distribution measurements on two-dimensional cascades with the blade profile NACA 8410 have been taken from extensive systematic measurements of N. Scholz. The two-dimensional cascade tunnel used for the measurements has been described in detail in references 1 and 25.[15] The following parameters

---

[15]Compare also reference 26, especially figure 1 on page 130 of that report.

could be varied: the pitch ratio t/l, the angle of stagger $\lambda = \beta_s - 90^o$, and the inflow angle β_1. The length of the blade chord was $l = 200$ mm, the height of the blade $h = 600$ mm. The average blade was provided, in its center section, with 28 pressure-tap orifices distributed over the circumference. Particular care was used in order to obtain a two-dimensional flow. For this purpose, the side walls of the cascade tunnel were provided with a suction device (porous walls). The outflow velocity was for all tests approximately $W_2 = 40$ m/s; the Reynolds number referred to the outflow velocity and the blade chord was therefore $W_2 l/\nu \approx 6 \times 10^5$ and the Mach number relative to the sonic velocity c was $M_2 = W_2/c = 0.12$; the flow showed, therefore, incompressible behavior.

In figures 99 to 112, a small selection from the pressure-distribution measurements has been compared with the theoretical results above; table 10 contains the pertaining lift coefficients c_A and outflow angles β_2. Figures 99 to 104 show, for constant spacing $\left(\frac{t}{l} = 1\right)$, the variation of the pressure distribution with the angle of attack α_1, for the turbine cascade with $\beta_s = 60^o$ and for the pumping cascade with $\beta_s = 120^o$. No separation occurs for the turbine cascade; whereas the pumping cascade shows, on the suction side, a slight separation at $\alpha_1 = 15^o$ and a somewhat more marked one at $\alpha_1 = 20^o$. The agreement between calculation and measurement is excellent for the turbine cascade; it is not quite as good for the pumping cascade, because of this separation, but on the whole still quite satisfactory. Figures 105 to 112 show the variation of the pressure distribution with the pitch ratio t/l for constant angle of attack α_1, for a series of turbine cascades with $\beta_s = 60^o$ and pumping cascades with $\beta_s = 120^o$. Here, the agreement of the calculation with the test is very good for both turbine and pumping cascades; particularly, if one takes into consideration that the theoretical pressure distributions do not contain the friction effect.

7. DETAILS OF THE CALCULATION

7.1 Calculation of the Tables of Functions for the Induced Velocities

The induced velocities $u_{\gamma G}$, $v_{\gamma G}$, u_{qG}, and v_{qG} of the remainder of the cascade must be calculated numerically as functions of the pitch ratio t/l, of the angle of stagger λ, and the relative coordinate x/l along the chord. These velocities are defined by equations (53) to (56) with the influence function F according to equation (50). Since we obtain for $\lambda = 0$ also $J(F) = 0$

$$\left(u_{\gamma G}\right)_{\lambda=0} = 0 \qquad \left(v_{qG}\right)_{\lambda=0} = 0 \tag{102}$$

is valid. In addition, there exist, as can be easily determined, the following symmetry relations

$$\left.\begin{aligned} u_{\gamma G}(-\lambda) &= -u_{\gamma G}(\lambda) & v_{\gamma G}(-\lambda) &= v_{\gamma G}(\lambda) \\ u_{qG}(-\lambda) &= u_{qG}(\lambda) & v_{qG}(-\lambda) &= -v_{qG}(\lambda) \end{aligned}\right\} \tag{103}$$

Thus it is necessary only to calculate the downwash functions for positive stagger angles λ.

If the series expressions according to equations (18) and (19) for $\gamma(x)$ and $q(x)$ are introduced into equations (53) to (56), one obtains, with φ' as the φ-value pertaining to x', by comparison with equations (57) to (60), the formulas for the downwash functions

$$\left.\begin{aligned} g_{\gamma 0} &= -\frac{l}{t}\int_{\xi'=0}^{1} \cot\frac{\varphi'}{2}\, J(F)d\xi' \\ g_{\gamma 1} &= -\frac{l}{t}\int_{\xi'=0}^{1} \sin\varphi' J(F)d\xi' \\ g_{\gamma 2} &= -\frac{l}{t}\int_{\xi'=0}^{1} \sin(2\varphi')J(F)d\xi' \\ &\cdots\cdots\cdots\cdots \end{aligned}\right\} \tag{104}$$

$$\left.\begin{aligned} f_{\gamma 0} &= -\frac{l}{t}\int_{\xi'=0}^{1} \cot\frac{\varphi'}{2}\, R(F)d\xi' \\ f_{\gamma 1} &= -\frac{l}{t}\int_{\xi'=0}^{1} \sin\varphi' R(F)d\xi' \\ f_{\gamma 2} &= -\frac{l}{t}\int_{\xi'=0}^{1} \sin(2\varphi')R(F)d\xi' \\ &\cdots\cdots\cdots\cdots \end{aligned}\right\} \tag{105}$$

$$\left.\begin{aligned}
g_{q0} &= \frac{l}{t}\int_{\xi'=0}^{1}\left(\cot\frac{\varphi'}{2} - 2\sin\varphi'\right)R(F)d\xi' \\
g_{q2} &= \frac{l}{t}\int_{\xi'=0}^{1}\sin(2\varphi')R(F)d\xi' \\
g_{q3} &= \frac{l}{t}\int_{\xi'=0}^{1}\sin(3\varphi')R(F)d\xi' \\
&\cdots\cdots\cdots\cdots\cdots\cdots
\end{aligned}\right\} \tag{106}$$

$$\left.\begin{aligned}
f_{q0} &= -\frac{l}{t}\int_{\xi'=0}^{1}\left(\cot\frac{\varphi'}{2} - 2\sin\varphi'\right)J(F)d\xi' \\
f_{q2} &= -\frac{l}{t}\int_{\xi'=0}^{1}\sin(2\varphi')J(F)d\xi' \\
f_{q3} &= -\frac{l}{t}\int_{\xi'=0}^{1}\sin(3\xi')J(F)d\xi' \\
&\cdots\cdots\cdots\cdots\cdots\cdots
\end{aligned}\right\} \tag{107}$$

The influence function F depends, according to equation (50), on $(\xi - \xi')l/t$ and λ. Its real and imaginary parts are[16]

$$R(F) = \frac{\cos\lambda\,\sinh\left(2\pi\,\frac{x - x'}{t}\,\cos\lambda\right) + \sin\lambda\,\sin\left(2\pi\,\frac{x - x'}{t}\,\sin\lambda\right)}{\cosh\left(2\pi\,\frac{x - x'}{t}\,\cos\lambda\right) - \cos\left(2\pi\,\frac{x - x'}{t}\,\sin\lambda\right)} - \frac{t}{\pi(x - x')} \tag{108}$$

[16] Compare reference 4, especially equations (16a) and (16b) on page 29. There one finds also in the table 1 on page 30 the numerical values of $R(F)$ and $J(F)$ for $\frac{(x - x')}{t} = 0$ to ∞ for angles of stagger $\lambda = 0^\circ, 15^\circ, 30^\circ, 45^\circ, 60^\circ, 75^\circ$, and 90°.

$$J(F) = \frac{\sin\lambda \sinh\left(2\pi \frac{x - x'}{t} \cos\lambda\right) - \cos\lambda \sin\left(2\pi \frac{x - x'}{t} \sin\lambda\right)}{\cosh\left(2\pi \frac{x - x'}{t} \cos\lambda\right) - \cos\left(2\pi \frac{x - x'}{t} \sin\lambda\right)} \tag{109}$$

We need calculate only the functions $g_{\gamma 0}$, $g_{\gamma 1}$, . . . , $f_{\gamma 0}$, $f_{\gamma 1}$, . . . of the circulation distribution. The functions g_{q0}, g_{q2}, . . ., f_{q0}, f_{q2}, . . . of the source distribution then result very simply according to the relationships following from equations (104) to (107)

$$\left.\begin{array}{lll} g_{q0} = -f_{\gamma 0} + 2f_{\gamma 1} & & f_{q0} = g_{\gamma 0} - 2g_{\gamma 1} \\ g_{q2} = -f_{\gamma 2} & g^{*}_{q2} = -f^{*}_{\gamma 2} & f_{q2} = g_{\gamma 2} \\ g_{q3} = -f_{\gamma 3} & g^{*}_{q3} = -f^{*}_{\gamma 3} & f_{q3} = g_{\gamma 3} \end{array}\right\} \tag{110}$$

Because of equations (102) and (103) there applies for $\lambda = 0$

$$\left.\begin{array}{l} g_{\gamma 0} = g_{\gamma 1} = g_{\gamma 2} = \ldots = 0 \\ f_{q0} = f_{q2} = f_{q3} = \ldots = 0 \end{array}\right\} \tag{111}$$

and for arbitrary λ-values

$$\left.\begin{array}{ll} g_{\gamma 0}(-\lambda) = -g_{\gamma 0}(\lambda) & g_{q0}(-\lambda) = g_{q0}(\lambda) \\ g_{\gamma 1}(-\lambda) = -g_{\gamma 1}(\lambda) & g_{q2}(-\lambda) = g_{q2}(\lambda) \\ \vdots & \vdots \\ f_{\gamma 0}(-\lambda) = f_{\gamma 0}(\lambda) & f_{q0}(-\lambda) = -f_{q0}(\lambda) \\ f_{\gamma 1}(-\lambda) = f_{\gamma 1}(\lambda) & f_{q2}(-\lambda) = -f_{q2}(\lambda) \\ \vdots & \vdots \end{array}\right\} \tag{112}$$

The downwash functions were calculated for pitch ratios $\frac{t}{l} = 0.5$, 0.75, 1.0, 1.25, 1.5, and 2.0 and for stagger angles $\lambda = 0^\circ$, 15°, 30°, 45°, 60°, and 75°. The Simpson rule, based on 20 points, served for calculating the integrals in equations (104) and (105). The results have been compiled in the cascade downwash tables in the appendix.

7.2 Example for the Determination of the Coefficients in the Singularity Distributions and of the Aerodynamic Coefficients

For clarification of the entire calculation process, we shall fully calculate here, as an example, a staggered cascade with cambered blade profiles of finite thickness. This is the most general case where no simplifications occur in the solution of the systems of equations for the coefficients of the singularity distributions.

The calculation procedure consists of four steps:

1. Determining the coefficients of the systems of equations (equations (72) and (73))

2. Solving these systems of equations for the coefficients of the singularity distribution

3. Calculating the aerodynamic coefficients

4. Calculating the velocity distribution along the blade contour.

The first step, tables 11 and 12, requires, aside from writing down the fixed values $q_{0\nu}$, $q_{2\nu}$, $q_{3\nu}$ (compare also table 1), determining the slope of the mean camber line and of the thickness distribution at the three control points. Then the values of the 10 downwash functions at the three control points have to be taken from the downwash tables of the appendix (columns 8 to 17 in table 11), and with them the coefficients $Q_{0\nu}, \ldots, P_{0\nu}, \ldots, R_{0\nu}, \ldots, S_{0\nu}, \ldots$ have to be calculated according to equations (68) and (69) (table 12).

The second step includes writing down the systems of equations, equations (72) and (73), according to table 13, and their solution, table 14. A method of successive approximation is used. Both systems are split up into two systems of three equations each. For the first system of equation (72) one may use the method of first solving the first three equations with the assumption $B_{00} = B_{20} = B_{30} = 0$. The values of A_{00}, A_{10}, A_{20} thus obtained are substituted into the right sides of the last three equations of this system, which now yield B_{00}, B_{20}, B_{30} (first approximation). With these values one enters into the right sides of the first three equations and obtains improved values of A_{00}, A_{10}, A_{20} (second approximation), etc. This method converges very rapidly in all cases. (In table 14 we had to calculate only up to the third approximation.)

In the third step, the aerodynamic coefficients are calculated (inflow and outflow angles, lift coefficient, pressure gradient in the cascade, inflow and outflow velocities). Equations (83) to (89) are available for this purpose. Table 15 contains the results. The contour velocity, resulting in the fourth step from equations (37) and (89) to (91), from which follows the pressure distribution on the blade according to equation (93), have already been shown in figure 31.

8. SUMMARY

A simple method for calculating the frictionless incompressible flow through a two-dimensional cascade is described for the so-called second main problem where the entire blade and cascade geometries are prescribed and the aerodynamic coefficients and the pressure distribution are desired. The calculation method is set up in such a manner that each geometric parameter (pitch ratio, stagger angle, and blade profile) can be varied independently of the other parameters. The method represents a transfer of the theory of the single airfoil, according to W. Birnbaum and H. Glauert, to the cascade; thus a singularity method where every cascade blade is replaced by continuous vortex and source-sink distributions which are expanded into a series, according to H. Glauert. For the circulation and the source-sink distributions, there result two coupled integral equations whose solution, with the aid of the three-quarter-chord theorem, may be reduced to the solution of two systems of linear equations. The coefficients of these systems of equations are formed from the dimensionless induced velocities of the cascade which depend on the pitch ratio and the blade angle of the cascade. This induced velocity field of the cascade has been calculated universally (cascade-downwash tables) so that, for a prescribed cascade, essentially only two systems of six linear equations each have to be solved. Solutions according to this approximation method for the single profile and for the plate cascade agree well with the two known exact solutions. Furthermore, numerous cases have been calculated for cascades with a parabolic profile, with a symmetrical NACA profile, and with a cambered NACA profile. Measured values of the pressure distributions on

the blade, which have been taken for the case of the cambered NACA profile, show good agreement with the calculated distributions for pumping as well as for turbine cascades.

Translated by Mary L. Mahler
National Aeronautics and Space Administration

REFERENCES

1. Schlichting, H.: Ergebnisse und Probleme von Gitteruntersuchungen. Z. Flugtechn. Bd. 1, 1953, pp. 109-122; (see, also, English translation: Problems and Results of Investigations on Cascade Flow. Jour. Aero. Sci., Bd. 21, 1954, pp. 163-178.)

2. Schlichling H., and Scholz, N.: Über die theoretische Berechnung der Strömungsverluste eines ebenen Schaufelgitters. Ing.-Arch., Bd. 19, 1951, pp. 42-65.

3. Speidel, L.: Berechnung der Strömungsverluste von ungestaffelten ebenen Schaufelgittern. Diss. Techn. Hochschule Braunschweig, 1953; (see also: Ing.-Arch., Bd. 22, 1954, pp. 295-322.)

4. Scholz, N.: Strömungsuntersuchungen an Schaufelgittern. Teil II: Ein Berechnungsverfahren zum Entwurf von Schaufelgitterprofilen. VDI-Forsch.-Heft 442 (Düsseldorf), 1954; (see, also, Scholz, N.: On the Calculation of the Potential Flow Around Airfoils in Cascade. Jour. Aero. Sci., Bd. 18, 1951, pp. 68-69.)

5. Weinig, F.: Die Strömung um die Schaufeln von Turbomaschinen. Johann Ambrosius Barth, (Leipzig), 1935.

6. Garrick, I. E.: On the Plane Potential Flow Past a Lattice of Arbitrary Airfoils. NACA Rep. 788, 1944.

7. Traupel, W.: Die Berechnung der Potentialströmung durch Schaufelgitter. Sulzer Techn. Rdsch., No. 1, 1945.

8. Birnbaum, W.: Die tragende Fläche als Hilfsmittel zur Berechnung des ebenen Problems der Tragflügeltheorie. Z. a. M. M. vol. 3, 1923, pp. 290-297.

9. Glauert, H.: Die Grundlagen der Tragflügel- und Luftschraubentheorie. (Berlin), 1929; (see, also, The Elements of Aerofoil and Airscrew Theory. Second Ed., Cambridge Univ. Press, 1947. (Reprinted 1948.))

10. Riegels, F.: Das Umströmungsproblem bei inkompressiblen Potentialströmungen. Ing.-Arch., Bd. 16, 1948, pp. 373-376 and Bd. 17, 1949, pp. 94-106.

11. Allen, H. Julian: General Theory of Airfoil Sections Having Arbitrary Shape or Pressure Distribution. NACA Rep. 833, 1945.

12. Schilhansl, M.: Näherungsweise Berechnung von Auftrieb- und Druckverteilung in Flügelgittern. Jb. 1927 Wiss. Ges. Luftf., pp. 151-167.

13. Betz, A.: Diagramme zur Berechnung von Flügelreihen. Ing.-Arch., Bd. 2, 1931, pp. 359-371.

14. Ackeret, J.: Zum Entwurf dichtstehender Schaufelgitter. Schweiz. Bauztg. Bd. 60, 1942, p. 120.

15. Pistolesi, E.: Sul calcolo dei schiere infinite di ali sottili. Aerotechnica vol. 17, 1937. (Available as NACA TM 968, 1941.)

16. Lieblein, V.: Zur Berechnung der Auftriebscharakteristik eines Profiles im Gitterverband. Ing.-Arch., Bd. 18, 1950, pp. 281-290.

17. Spurr, Robert A.,and Allen, H. Julian: A Theory of Unstaggered Airfoil Cascades in Compressible Flow. NACA Rep. 888, 1947.

18. Katzoff, S., Finn, Robert S., and Laurence, James C.: Interference Method for Obtaining Potential Flow Past an Arbitrary Cascade of Airfoils. NACA Rep. 879, 1947. (Formerly NACA TN 1252.)

19. Wieghardt, K.: Über die Auftriebsverteilung des einfachen Rechteckflügels über die Tiefe. Z. a. M. M., Bd. 19, 1939, pp. 257-270.

20. Scholz, N.: Beiträge zur Theorie der tragenden Fläche. Ing.-Arch., Bd. 18, 1950, pp. 84-105.

21. Grammel, R.: Die hydrodynamischen Grundlagen des Fluges. (Braunschweig), 1917.

22. Scholz, N.: Berechnung der Druckverteilung der ebenen Platte im Gitterverband. Abh. Braunsch. Wiss. Ges., Bd. 5, 1953, pp. 152-163.

23. Eckert, B.: Axialkompressoren und Radialkompressoren. (Berlin-Göttingen-Heidelberg), 1953.

24. Speidel, L.: Ergebnisse systematischer Untersuchungen an ebenen Schaufelgittern. Teil IV: Theoretische Ergebnisse für das Profil NACA 8410. Bericht 54/8 des Instituts für Strömungsmechanik der Techn. Hochschule Braunschweig, 1954.

25. Scholz, N.: Über die Durchführung systematischer Messungen an ebenen Schaufelgittern. Habilitation schrift der Technischen Hochschule Braunschweig 1955. Bericht 54/2 des Instituts für Strömungsmechanik der Techn. Hochschule Braunschweig, 1954.

26. Speidel, L.: Einfluß der Oberflächenrauhigkeit auf die Strömungsverluste in ebenen Schaufelgittern. Forsch. Ing.-Wes., Bd. 20, 1954, pp. 129-140.

27. Pfleiderer, C.: Strömungsmaschinen. (Berlin), 1952.

TABLE 1

SYSTEMS OF EQUATIONS FOR THE COEFFICIENTS OF THE CIRCULATION DISTRIBUTION AND OF THE SOURCE DISTRIBUTION OF THE SINGLE PROFILE

Number of control points n	Coordinate of the control point x	System according to equation (29)	System according to equation (32)
1	$x_1 = \frac{3}{4} l$	$-1.1547B_0 = y'_{d1}$	$-A_{00} = y'_{s1}$ (or $A_{10} = y'_{s1}$)
2	$x_1 = \frac{3}{8} l$	$-0.6435B_0 + 0.4841B_2 = y'_{d1}$	$-A_{00} + 0.25A_{10} = y'_{s1}$
	$x_2 = \frac{7}{8} l$	$-0.9449B_0 - 0.9922B_2 = y'_{d2}$	$-A_{00} - 0.75A_{10} = y'_{s2}$
3	$x_1 = \frac{3}{12} l$	$0.8660B_2 = y'_{d1}$	$-A_{00} + 0.5A_{10} - 0.5A_{20} = y'_{s1}$
	$x_2 = \frac{7}{12} l$	$-1.1269B_0 - 0.3287B_2 - 0.8765B_3 = y'_{d2}$	$-A_{00} - 0.1667A_{10} + 0.9444A_{20} = y'_{s2}$
	$x_3 = \frac{11}{12} l$	$-0.8040B_0 - 0.9213B_2 + 0.9827B_3 = y'_{d3}$	$-A_{00} - 0.8333A_{10} + 0.3889A_{20} = y'_{s3}$

TABLE 2

CONTOURS OF THE NACA 0010 AND 8410 PROFILES

NACA 0010 profile			NACA 8410 profile					
Relative distance from the leading edge x/l	Relative profile thickness $10^2 \frac{y_d}{l}$	Riegels factor $\sqrt{1 + y_d'^2}$	Relative distance from the leading edge x/l	Relative distance from the chord of the lower side of the contour $10^2 \frac{y_u}{l}$	Relative distance from the chord of the upper side of the contour $10^2 \frac{y_o}{l}$	Relative profile thickness $10^2 \frac{y_d}{l}$	Relative distance of the mean camber line from the chord $10^2 \frac{y_s}{l}$	Riegels factor $\sqrt{1 + y_d'^2}$
0	0	∞	0	0	0	0	0	∞
.025	2.20	1.076	.02	-1.11	3.40	2.26	1.15	1.122
.05	2.96	1.031	.05	-1.10	5.45	3.28	2.18	1.032
.10	3.90	1.011	.075	-.80	6.77	3.79	2.99	1.014
.15	4.45	1.003	.10	-.34	7.85	4.10	3.76	1.008
.20	4.78	1.001	.15	.47	9.71	4.62	5.09	1.003
.25	4.95	1.000	.20	1.30	11.02	4.86	6.16	1.001
.30	5.00	1.000	.30	2.42	12.5	5.04	7.46	1.000
.40	4.84	1.000	.40	3.18	12.9	4.86	8.04	1.001
.50	4.41	1.001	.50	3.41	12.1	4.40	7.76	1.002
.60	3.80	1.002	.60	3.15	10.7	3.78	6.93	1.003
.70	3.05	1.003	.70	2.50	8.63	3.07	5.57	1.003
.80	2.19	1.004	.80	1.66	6.10	2.22	3.88	1.004
.90	1.21	1.005	.90	.80	3.24	1.22	2.02	1.005
.95	.67	1.005	.95	.32	1.70	.69	1.01	1.006
1.0	.10	1.006	1.0	.09	.09	.09	0	1.006

TABLE 3

SLOPES OF THE TANGENTS AT THE THREE CONTROL POINTS FOR THE NACA 0010 AND 8410 PROFILES

Number of control point, ν	Relative distance from the leading edge, x_ν/l	NACA 0010 profile	NACA 8410 profile	
		Tangential slope of the thickness distribution, $y'_{d\nu}$	Tangential slope of the thickness distribution, $y'_{d\nu}$	Tangential slope of the mean camber line, $y'_{s\nu}$
1	$\frac{3}{12} = 0.250$	0.0210	0.0156	0.150
2	$\frac{7}{12} = 0.583$	-.0660	-.0635	-.105
3	$\frac{11}{12} = 0.917$	-0.1055	-.1024	-.201

TABLE 4

COEFFICIENTS OF THE SINGULARITY DISTRIBUTIONS FOR THE NACA 0010 AND 8410 PROFILES AS SINGLE PROFILES

a calculated from the simplified kinematic flow conditions, equations (15) and (16); b calculated from the complete kinematic flow conditions, equations (6) and (7).

Coefficient	NACA 0010 profile		NACA 8410 profile	
	a	b	a	b
A_{00}	0	0	-0.0332	-0.0538
A_{10}	0	0	.3229	.3472
A_{20}	0	0	.0894	.1153
B_0	0.0716	0.0700	0.0728	0.0713
B_2	.0242	.0275	.0180	.0204
B_3	-.0260	-.0187	-.0278	-.0213

TABLE 5

RESULTS FOR THE UNSTAGGERED PLATE CASCADE ($\lambda = 0$, $\beta_s = 90^{\circ}$)

APPROXIMATE CALCULATION FOR THREE CONTROL

POINTS ($n = 3$, $\nu = 1$ to 3)

Pitch ratio, t/l	Coefficients			Efficiency factor κ of the lift increase		Angle ratio, $\frac{\cot \beta_2}{\cot \beta_1}$		Relative distance from the leading edge of the aerodynamic center, x_{Neutr}/l	
	$A_{0\beta}$	$A_{1\beta}$	$A_{2\beta}$	Approximation according to equation (99)	Exact according to equation (97)	Approximation according to equation (100)	Exact according to equation (98)	Approximation	Exact
0.5	0.5568	-0.4758	-0.1250	0.319	0.317	0.000	0.002	0.113	0.109
.75	.6865	-.4434	-.0806	.465	.463	.014	.015	.153	.151
1.0	.7693	-.3731	-.0447	.583	.584	.044	.043	.180	.186
1.25	.8257	-.2987	-.0261	.676	.677	.081	.081	.200	.199
1.5	.8654	-.2384	-.0142	.746	.746	.124	.124	.213	.212
2.0	.9147	-.1590	-.0054	.835	.835	.207	.208	.227	.227
∞	1	0	0	1	1	1	1	.25	.25

TABLE 6

RESULTS OF THE APPROXIMATE CALCULATION

FOR THE STAGGERED PLATE CASCADE

Approximate Calculation for Three Control Points (n = 3)

Blade angle, β_s	Pitch ratio, t/l	Coefficients			Efficiency factor of the lift
		$A_{0\beta}$	$A_{1\beta}$	$A_{2\beta}$	κ
60°	0.5	0.6270	-0.5168	-0.1224	0.359
	.75	.7415	-.4102	-.0384	.536
	1.0	.8203	-.3015	-.0034	.670
	2.0	.9477	-.0968	+.0026	.896
	∞	1	0	0	1
45°	0.5	0.7302	-0.5568	-0.0990	0.452
	.75	.8131	-.3176	+.0573	.654
	1.0	.8926	-.1632	.0629	.811
	2.0	.9891	-.0139	.0083	.982
	∞	1	0	0	1
30°	0.5	0.9207	-0.5679	-0.0090	0.637
	.75	.9131	+.0300	+.3350	.928
	1.0	1.0243	.2015	.1788	1.125
	2.0	1.0455	.1023	.0071	1.097
	∞	1	0	0	1

TABLE 7

SLOPE OF THE MEAN CAMBER LINE OF THE PARABOLIC

PROFILE WITH THE CAMBER

$\frac{f}{l} = 0.1$ AT THE THREE

CONTROL POINTS

Number of control point, ν	1	2	3	----
Relative distance, x_ν/l	3/12	7/12	11/12	1
Slope, $y'_{s\nu}$	0.2	-0.0667	-0.3333	-0.4

TABLE 8

COEFFICIENTS OF THE SINGULARITY DISTRIBUTIONS,

EFFICIENCY FACTOR AND ZERO-LIFT DIRECTION

FOR PARABOLIC CASCADES WITH THE

CAMBER RATIO $\frac{f}{l} = 0.1$

Blade angle, β_s, deg	Stagger angle, λ, deg	Pitch ratio, t/l	Coefficients						Efficiency factor of lift, κ	Angle of attack for zero lift, $(\alpha_\infty)_{c_A} = 0$, deg
			$10\ A_{00}$	$10\ A_{01}$	$10\ A_{02}$	$A_{0\beta}$	$A_{1\beta}$	$A_{2\beta}$		
30	-60	0.5	1.439	2.961	-1.682	1.362	-0.437	-0.502	1.143	-14.3
		.75	.629	4.764	-.469	1.242	.407	.064	1.445	-11.8
		1.0	.382	4.775	-.317	1.270	.488	-.041	1.514	-10.4
		2.0	.081	4.214	-.079	1.092	.151	-.039	1.167	-10.6
60	-30	0.5	0.360	1.904	-0.481	0.682	-0.474	-0.189	0.445	-16.4
		.75	.258	2.731	-.306	.807	-.362	-.111	.626	-14.5
		1.0	.185	3.210	-.199	.883	-.252	-.069	.756	-13.3
		2.0	.063	3.795	-.063	.977	-.070	-.027	.942	-11.8
90	0	0.5	0.065	1.857	-0.106	0.557	-0.476	-0.125	0.319	-17.3
		.75	.036	2.509	-.057	.687	-.443	-.081	.465	-15.6
		1.0	.019	2.934	-.027	.769	-.373	-.045	.583	-14.3
		2.0	.003	3.642	-.004	.915	-.159	-.005	.836	-12.3
120	30	0.5	-0.220	2.399	0.265	0.601	-0.580	-0.093	0.312	-17.5
		.75	-.202	3.003	.231	.698	-.466	.008	.465	-15.6
		1.0	-.161	3.345	.179	.773	-.352	.046	.597	-14.2
		2.0	-.060	3.808	.062	.922	-.123	.029	.860	-12.1
150	60	0.5	-1.101	4.807	1.412	0.839	-0.859	-0.056	0.410	-17.5
		.75	-.640	4.761	.664	.782	-.274	.132	.645	-15.5
		1.0	-.374	4.613	.366	.883	-.024	.143	.871	-13.6
		2.0	-.079	4.196	.078	1,004	.057	.045	1.003	-11.7
Single profile		∞	0	4	0	1	0	0	1	-11.3

TABLE 9

COEFFICIENTS OF THE SINGULARITY DISTRIBUTIONS

FOR CASCADES OF NACA 8410 PROFILES

Blade angle, β_s, deg	Stagger angle, λ, deg	Pitch ratio, t/l	Coefficients											
			A_{00}	A_{10}	A_{20}	$A_{0\beta}$	$A_{1\beta}$	$A_{2\beta}$	B_{00}	B_{20}	B_{30}	$B_{0\beta}$	$B_{2\beta}$	$B_{3\beta}$
30	-60	0.5	0.0652	0.3543	0.2543	1.1847	-0.2583	0.2661	0.1213	0.0199	-0.0504	0.2201	0.0134	-0.0965
		.75	.0312	.4295	.1548	1.1342	.3859	.3977	.0956	.0165	-.0413	.1556	.0031	-.0954
		1.0	.0042	.4129	.1106	1.1788	.4383	.1384	.0822	.0194	-.0315	.0976	.0010	-.0695
		1.25	-.0177	.3874	.1064	1.1590	.3446	.0258	.0764	.0196	-.0262	.0595	.0004	-.0432
		1.5	-.0305	.3715	.1113	1.1212	.2490	-.0001	.0741	.0199	-.0241	.0379	.0004	-.0272
60	-30	0.5	-0.0175	0.2088	0.1308	0.6439	-0.4493	-0.0804	0.0851	0.0214	-0.0270	0.0508	0.0068	-0.0190
		.75	-.0251	.2689	.1234	.7692	-.3463	-.0231	.0800	.0206	-.0265	.0436	.0035	-.0207
		1.0	-.0313	.3003	.1179	.8491	-.2451	-.0026	.0770	.0204	-.0251	.0351	.0019	-.0191
		1.25	-.0367	.3165	.1145	.8984	-.1727	-.0014	.0751	.0203	-.0240	.0275	.0012	-.0162
		1.5	-.0422	.3255	.1166	.9295	-.1244	-.0026	.0740	.0203	-.0232	.0215	.0007	-.0133
90	0	0.5	-0.0542	0.2258	0.1118	0.5550	-0.4751	-0.1224	0.0758	0.0224	-0.0206	0	0	0
		.75	-.0557	.2656	.1164	.6866	-.4432	-.0806	.0740	.0214	-.0213	0	0	0
		1.0	-.0560	.2920	.1190	.7693	-.3731	-.0447	.0730	.0209	-.0215	0	0	0
		1.25	-.0551	.3061	.1169	.8257	-.2988	-.0261	.0726	.0208	-.0215	0	0	0
		1.5	-.0548	.3164	.1167	.8653	-.2384	-.0137	.0723	.0207	-.0215	0	0	0
120	30	0.5	-0.1000	0.3043	0.1235	0.6544	-0.6331	-0.1574	0.0708	0.0234	-0.0165	-0.0425	-0.0074	0.0135
		.75	-.0873	.3135	.1213	.7431	-.4925	-.0499	.0701	.0220	-.0184	-.0379	-.0038	.0166
		1.0	-.0781	.3232	.1201	.8103	-.3643	-.0040	.0701	.0213	-.0193	-.0315	-.0021	.0164
		1.25	-.0720	.3281	.1189	.8594	-.2683	.0072	.0703	.0210	-.0198	-.0252	-.0013	.0146
		1.5	-.0678	.3323	.1183	.8943	-.2012	.0098	.0706	.0207	-.0202	-.0201	-.0008	.0122
150	60	0.5	-0.2060	0.5427	0.1957	1.0782	-1.1159	-0.1266	0.0674	0.0252	-0.0106	-0.1239	-0.0175	0.0353
		.75	-.1276	.4315	.1358	.9174	-.2755	.3314	.0680	.0220	-.0168	-.1076	-.0062	.0610
		1.0	-.0971	.3858	.1212	.9801	.0153	.2088	.0684	.0212	-.0185	-.0749	-.0022	.0511
		1.25	-.0822	.3702	.1215	1.0246	.0889	.0928	.0688	.0207	-.0191	-.0503	-.0010	.0357
		1.5	-.0734	.3640	.1197	1.0344	.0888	.0447	.0693	.0207	-.0197	-.0340	-.0007	.0240
Single profile*		∞	-0.0538	0.3472	0.1153	1	0	0	0.0713	0.0204	-0.0213	0	0	0

*Calculated with the complete kinematic flow conditions, equations (6) and (7); compare table 4, case b.

TABLE 10

THEORETICALLY DETERMINED FLOW ANGLES AND LIFT COEFFICIENTS FOR THE CASCADES COMPARED WITH MEASUREMENTS IN FIGURES 99 to 112

Figure number	Blade angle, β_s, deg	Pitch ratio, t/l	Angle of attack, α_1, deg	Angle-of-attack coefficient, $K = \tan \alpha_\infty$	Inflow angle, β_1, deg	Outflow angle, β_2, deg	Lift coefficient, c_A
105	60	0.5	15	-0.002	75	48.2	0.541
106	60	.75	15	.016	75	49.9	.747
99	60	1.0	5	-.041	65	51.4	.559
100	60	1.0	15	.038	75	51.8	.917
101	60	1.0	25	.116	85	52.1	1.268
107	60	1.25	15	.056	75	53.5	1.048
108	60	1.5	15	.073	75	55.1	1.152
109	120	.5	10	.028	130	111.2	.388
110	120	.75	10	.034	130	112.2	.548
102	120	1.0	10	.042	130	113.3	.690
103	120	1.0	15	.099	135	113.6	.911
104	120	1.0	20	.164	140	114.0	1.156
111	120	1.25	10	.050	130	114.4	.806
112	120	1.5	10	.060	130	115.5	.916

TABLE 11

COMPILATION OF THE QUANTITIES REQUIRED FOR SETTING UP THE SYSTEMS OF EQUATIONS, EQUATIONS (72) AND (73), FOR THE COEFFICIENTS OF THE SINGULARITY DISTRIBUTIONS (CONTINUED IN TABLE 12)

Calculation example: NACA 8410 blade profile, pitch ratio $\frac{t}{l} = 0.75$, blade angle $\beta_s = 90^\circ + \lambda = 120^\circ$

1	2	3	4	5	6	7	8	9	10	11	12	13	14	15	16	17
Number of control point	Relative coordinate of the control point	Fixed values according to equation (67)			Profile geometry (compare table 3): Tangential slope of the mean camber line	Profile geometry (compare table 3): Tangential slope of the thickness distribution	Downwash functions from "cascade downwash tables" in the appendix									
ν	$\frac{x_\nu}{l}$	$q_{0\nu}$	$q_{2\nu}$	$q_{3\nu}$	$y'_{s\nu}$	$y'_{d\nu}$	$\dot f_{\gamma 0}$	$\dot f_{\gamma 1}$	$\dot f_{\gamma 2} = -\dot g_{q2}$	$\dot f_{\gamma 3} = -\dot g_{q3}$	$\dot g_{q0}$	$g_{\gamma 0}$	$g_{\gamma 1}$	$g_{\gamma 2} = f_{q2}$	$g_{\gamma 3} = f_{q3}$	f_{q0}
1	$0.250 = \frac{3}{12}$	0	0.8660	0	0.150	0.0156	-0.999	0.697	-0.695	-1.000	2.393	-0.036	0.239	-0.218	-0.0505	-0.514
2	$0.583 = \frac{7}{12}$	-1.1269	-0.3287	-0.8765	-0.105	-0.0635	-1.537	-0.234	-1.132	0.4786	1.070	-0.625	-0.083	-0.262	0.0198	-0.459
3	$0.917 = \frac{11}{12}$	-0.8040	-0.9213	0.9827	-0.201	-0.1024	-1.977	-1.155	0.203	0.2016	-0.334	-0.926	-0.361	-0.154	0.0616	-0.204

TABLE 12

CONTINUATION OF THE CALCULATION EXAMPLE OF TABLE 11: CALCULATION OF THE COEFFICIENTS P_{01} TO S_{23} FOR THE SYSTEMS OF EQUATIONS, EQUATIONS (72) AND (73), FROM THE VALUES OF TABLE 11

In the explanation of the direction for the calculation, the columns named in Arabic numbers refer to table 11, those named in Roman numbers to table 12

I	II	III	IV	V	VI	VII	VIII	IX	X	XI	XII	XIII	XIV
Number of the control point, ν	Relative coordinate of the control point, $\frac{x_\nu}{l}$	Product of column 6 and			Coefficients $P_{0\nu}$ to $P_{2\nu}$ according to equation (68)			Product of column 6 and			Coefficients $R_{0\nu}$ to $R_{3\nu}$ according to equation (69)		
		column 13, $y'_{s\nu}\ g_{\gamma 0}$	column 14, $y'_{s\nu}\ g_{\gamma 1}$	column 15, $y'_{s\nu}\ g_{\gamma 2}$	column 8 minus column III, $P_{0\nu}$	column 9 minus column IV, $P_{1\nu}$	column 10 minus column V, $P_{2\nu}$	column 12, $y_{s\nu}\ g^*_{q2}$	column 10, $-y'_{s\nu}\ g^*_{q2}$	column 11, $-y'_{s\nu}\ g^*_{q3}$	column 17 minus column IX, $R_{0\nu}$	column 15 plus column X, $R_{2\nu}$	column 16 plus column XI, $R_{3\nu}$
1	0.250	-0.0054	0.0359	-0.0327	-0.9936	0.6611	-0.6623	0.3590	-0.1043	-0.1500	-0.8730	-0.3223	-0.2005
2	.583	.0656	.0087	.0275	-1.6026	-.2427	-1.1655	-.1124	.1195	-.0503	-.3466	-.1425	-.0305
3	.917	.1861	.0726	.0310	-2.1631	-1.2276	.1720	.0671	-.0408	-.0405	-.2711	-.1948	.0211

XV	XVI	XVII	XVIII	XIX	XX	XXI	XXII	XXIII	XXIV	XXV	XXVI	XXVII	XXVIII
Number of the control point, ν	Relative coordinate of the control point, $\frac{x_\nu}{l}$	Product of column 7 and			Coefficients $Q_{0\nu}$ to $Q_{3\nu}$ according to equation (68)			Product of column 7 and			Coefficients $S_{0\nu}$ to $S_{2\nu}$ according to equation (69)		
		column 12, $y'_{d\nu}\ g^*_{q0}$	column 10, $-y'_{d\nu}\ g^*_{q2}$	column 11, $-y'_{d\nu}\ g^*_{q3}$	column 3 minus column XVII, $Q_{0\nu}$	column 4 plus column XVIII, $Q_{2\nu}$	column 5 plus column XIX, $Q_{3\nu}$	column 13, $y'_{d\nu}\ g_{\gamma 0}$	column 14, $y'_{d\nu}\ g_{\gamma 1}$	column 15, $y'_{d\nu}\ g_{\gamma 2}$	from column XXIII, $S_{0\nu}$	from column XXIV, $S_{1\nu}$	from column XXV, $S_{2\nu}$
1	0.250	0.0373	-0.0108	-0.0156	-0.0373	0.8552	-0.0156	-0.0006	0.0037	-0.0034	-0.0006	0.0037	-0.0034
2	.538	-.0679	.0723	-.0304	-1.0590	-.2564	-.9069	.0397	.0053	.0166	.0397	.0053	.0166
3	.917	.0342	-.0208	-.0206	-.8382	-.9421	.9621	.0948	.0370	.0158	.0948	.0370	.0158

TABLE 13

THE TWO SYSTEMS OF EQUATIONS FOR THE COEFFICIENTS OF THE CIRCULATION DISTRIBUTION AND OF THE SOURCE DISTRIBUTION, ACCORDING TO EQUATIONS (72) AND (73), RESPECTIVELY

Calculation example: NACA 8410 blade profile, pitch ratio $\frac{t}{l} = 0.75$, blade angle $\beta_s = 120^{\circ}$

First system	$-0.9936\,A_{00} + 0.6611\,A_{10} - 0.6623\,A_{20} = 0.150 + 0.8730\,B_{00} + 0.3223\,B_{20} + 0.2005\,B_{30}$
	$-1.6026\,A_{00} - 0.2427\,A_{10} - 1.1655\,A_{20} = -0.105 + 0.3466\,B_{00} + 0.1425\,B_{20} + 0.0305\,B_{30}$
	$-2.1631\,A_{00} - 1.2276\,A_{10} + 0.1720\,A_{20} = -0.201 + 0.2711\,B_{00} + 0.1948\,B_{20} - 0.0211\,B_{30}$
	$-0.0373\,B_{00} + 0.8552\,B_{20} - 0.0156\,B_{30} = 0.0156 - 0.0006\,A_{00} + 0.0037\,A_{10} - 0.0034\,A_{20}$
	$-1.0590\,B_{00} - 0.2564\,B_{20} - 0.9069\,B_{30} = -0.0635 + 0.0397\,A_{00} + 0.0053\,A_{10} + 0.0166\,A_{20}$
	$-0.8382\,B_{00} - 0.9421\,B_{20} + 0.9621\,B_{30} = -0.1024 + 0.0948\,A_{00} + 0.0370\,A_{10} + 0.0158\,A_{20}$
Second system	$-0.9936\,A_{0\beta} + 0.6611\,A_{1\beta} - 0.6623\,A_{2\beta} = -1.0 + 0.8730\,B_{0\beta} + 0.3223\,B_{2\beta} + 0.2005\,B_{3\beta}$
	$-1.6026\,A_{0\beta} - 0.2427\,A_{1\beta} - 1.1655\,A_{2\beta} = -1.0 + 0.3466\,B_{0\beta} + 0.1425\,B_{2\beta} + 0.0305\,B_{3\beta}$
	$-2.1631\,A_{0\beta} - 1.2276\,A_{1\beta} + 0.1720\,A_{2\beta} = -1.0 + 0.2711\,B_{0\beta} + 0.1948\,B_{2\beta} - 0.0211\,B_{3\beta}$
	$-0.0373\,B_{0\beta} + 0.8552\,B_{2\beta} - 0.0156\,B_{3\beta} = - 0.0006\,A_{0\beta} + 0.0037\,A_{1\beta} - 0.0034\,A_{2\beta}$
	$-1.0590\,B_{0\beta} - 0.2564\,B_{2\beta} - 0.9069\,B_{3\beta} = + 0.0397\,A_{0\beta} + 0.0053\,A_{1\beta} + 0.0166\,A_{2\beta}$
	$-0.8382\,B_{0\beta} - 0.9421\,B_{2\beta} + 0.9621\,B_{3\beta} = + 0.0948\,A_{0\beta} + 0.0370\,A_{1\beta} + 0.0158\,A_{2\beta}$

TABLE 14

SOLUTION OF THE SYSTEMS OF EQUATIONS OF TABLE 13

BY SUCCESSIVE APPROXIMATION: NACA 8410 BLADE

PROFILE, PITCH RATIO $\frac{t}{l}$ = 0.75,

BLADE ANGLE β_s = 120°

Coefficient	1st approximation	2nd approximation	3rd approximation
A_{00}	-0.0455	-0.0885	-0.0873
A_{10}	.2578	.3169	.3153
A_{20}	.0989	.1219	.1213
B_{00}	0.0735	0.0702	0.0701
B_{20}	.0211	.0220	.0220
B_{30}	-.0218	.0184	-.0184
$A_{0\beta}$	0.7232	0.7429	0.7431
$A_{1\beta}$	-.4652	-.4921	-.4925
$A_{2\beta}$	-.0395	-.0498	-.0499
$B_{0\beta}$	-0.0374	-0.0379	-0.0379
$B_{2\beta}$	-.0037	-.0038	-.0038
$B_{3\beta}$	0.0165	0.0166	0.0166

TABLE 15

AERODYNAMIC COEFFICIENTS OF THE PUMPING CASCADE OF BLADES WITH NACA 8410 PROFILES, THE PITCH RATIO $\frac{t}{l}$ = 0.75, AND THE BLADE ANGLE $\beta_s = 120^\circ$ ($\lambda = 30^\circ$)

Angle-of-attack coefficient, $K = \tan \alpha_\infty$	Angle of attack, α_∞, deg	Angle of attack, β_∞, according to equation (85), deg	Inflow angle, β_1, according to equations (83) and (86), deg	Outflow angle, β_2, according to equations (84) and (86), deg	Angle of attack, α_1, according to equation (82), deg	Outflow angle, α_2, according to equation (82), deg	Lift coefficient, c_A, according to equation (81)	Pressure gradient, $\frac{p_2 - p_1}{\frac{1}{2}\rho W_n^2}$ according to equation (88a)	Velocity ratio, $\frac{W_2}{U_\infty}$, according to equations (87) and (89)	Velocity ratio, $\frac{W_2}{W_1}$, according to equation (87)
0	0	120.0	126.8	112.2	6.8	-7.8	0.442	0.392	0.934	0.863
0.05	2.9	122.9	131.4	112.2	11.4	-7.8	.597	.613	.909	.822
.10	5.7	125.7	135.8	112.3	15.8	-7.7	.750	.885	.882	.753
.14	8.0	128.0	139.0	112.4	19.0	-7.6	.870	1.150	.861	.709
.18	10.2	130.2	141.9	112.5	21.9	-7.5	.987	1.454	.841	.668
.22	12.4	132.4	144.7	112.6	24.7	-7.4	1.103	1.819	.819	.626
.26	14.6	134.6	147.2	112.7	27.2	-7.3	1.214	2.239	.798	.587

TABLE 16

DOWNWASH TABLE FOR THE SINGLE AIRFOIL (ANGLE FUNCTIONS IN EQUATIONS (20) TO (23) FOR PITCH RATIO $\frac{t}{l} = \infty$ AND ARBITRARY BLADE ANGLES β_s)

(A) Angle Functions

$\frac{x}{l}$	$\cot\frac{\varphi}{2}$	$\sin\varphi$	$\sin 2\varphi$	$\sin 3\varphi$	$\cos\varphi$	$\cos 2\varphi$	$\cos 3\varphi$	$1 + 2\cos\varphi$	$\cot\frac{\varphi}{2} - 2\sin\varphi$
0	∞	0	0	0	1.0	1.00	1.000	3.0	∞
.05	4.3589	.4359	.7846	.9764	.9	.62	.216	2.8	3.4871
.1	3.0000	.6000	.9600	.9360	.8	.28	-.352	2.6	1.8000
.15	2.3805	.7141	.9998	.6856	.7	-.02	-.728	2.4	.9522
.2	2.0000	.8000	.9600	.3520	.6	-.28	-.936	2.2	.4000
.25	1.7320	.8660	.8660	0	.5	-.50	-1.000	2.0	0
.3	1.5275	.9165	.7332	-.3300	.4	-.68	-.944	1.8	-.3055
.35	1.3628	.9539	.5724	-.6105	.3	-.82	-.792	1.6	-.5451
.4	1.2247	.9798	.3919	-.8215	.2	-.92	-.568	1.4	-.7349
.45	1.1055	.9950	.1990	-.9552	.1	-.98	-.296	1.2	-.8844
.5	1.0000	1.0000	0	-1.0000	0	-1.00	0	1.0	-1.0000
.55	.9045	.9950	-.1990	-.9552	-.1	-.98	.296	.8	-1.0855
.6	.8165	.9798	-.3919	-.8215	-.2	-.92	.568	.6	-1.1431
.65	.7338	.9539	-.5724	-.6105	-.3	-.82	.792	.4	-1.1741
.7	.6547	.9165	-.7332	-.3300	-.4	-.68	.944	.2	-1.1784
.75	.5774	.8660	-.8660	0	-.5	-.50	1.000	0	-1.1547
.8	.5000	.8000	-.9600	.3520	-.6	-.28	.936	-.2	-1.1000
.85	.4201	.7141	-.9998	.6856	-.7	-.02	.728	-.4	-1.0082
.9	.3333	.6000	-.9600	.9360	-.8	.28	.352	-.6	-.8667
.95	.2294	.4359	-.7846	.9764	-.9	.62	-.216	-.8	-.6424
1.0	0	0	0	0	-1.0	1.00	-1.000	-1.0	0
$\frac{3}{12}$	1.7320	.8660	.8660	0	0.5000	-.5000	-1.000	2.0	0
$\frac{7}{12}$	.8451	.9860	-.3287	-.8765	-.1667	-.9444	.4815	.6667	-1.1269
$\frac{11}{12}$	.3015	.5528	-.9213	.9827	-.8333	.3889	.1852	-.6667	-.8040

TABLE 17

CASCADE DOWNWASH TABLES FOR BLADE ANGLES OF $\beta_B = 90^o$ TO 165^o

(CORRESPONDING TO STAGGER ANGLES OF $\lambda = 0^o$ TO 75^o)

AND PITCH RATIO OF $\frac{t}{l} = 2$ TO 0.5

$\beta_B = 90^o$ $\lambda = 0^o$ $t/l = 2.0$

$\frac{x}{l}$	$10^3 g_{\gamma 0}$	$10^3 g_{\gamma 1}$	$10^3 g_{\gamma 2}$	$10^3 g_{\gamma 3}$	$10^3 f_{\gamma 0}$	$10^3 f_{\gamma 1}$	$10^3 f_{\gamma 2}$	$10^3 f_{\gamma 3}$	$10^3 g_{q0}$	$10^3 f_{\gamma 0}$
0	0	0	0	0	97.8	96.1	-44.2	-3.6	94.4	0
.05	0	0	0	0	78.1	86.9	-45.1	-3.4	95.7	0
.1	0	0	0	0	58.9	77.9	-46.0	-3.1	96.9	0
.15	0	0	0	0	38.9	68.5	-46.7	-2.9	98.1	0
.2	0	0	0	0	18.9	59.0	-47.5	-2.6	99.1	0
.25	0	0	0	0	-1.0	49.4	-48.1	-2.3	99.8	0
.3	0	0	0	0	-20.9	39.6	-48.7	-2.1	100.1	0
.35	0	0	0	0	-40.9	29.7	-49.1	-1.7	100.3	0
.4	0	0	0	0	-60.6	19.8	-49.5	-1.2	100.2	0
.45	0	0	0	0	-80.0	9.9	-49.7	-.6	99.8	0
.5	0	0	0	0	-99.2	0	-49.7	0	99.2	0
.55	0	0	0	0	-118.3	-9.9	-49.7	.6	98.5	0
.6	0	0	0	0	-137.3	-19.8	-49.5	1.2	97.7	0
.65	0	0	0	0	-156.2	-29.7	-49.1	1.7	96.8	0
.7	0	0	0	0	-174.9	-39.6	-48.7	2.1	95.7	0
.75	0	0	0	0	-193.2	-49.4	-48.1	2.3	94.4	0
.8	0	0	0	0	-210.8	-59.0	-47.5	2.6	92.8	0
.85	0	0	0	0	-228.1	-68.5	-46.7	2.9	91.1	0
.9	0	0	0	0	-245.0	-77.9	-46.0	3.1	89.2	0
.95	0	0	0	0	-261.0	-86.9	-45.1	3.4	87.2	0
1.0	0	0	0	0	-277.2	-96.1	-44.2	3.6	85.0	0
$\frac{3}{12}$	0	0	0	0	-1.0	49.4	-48.1	-2.3	99.8	0
$\frac{7}{12}$	0	0	0	0	-131.0	-16.5	-49.5	1.0	98.0	0
$\frac{11}{12}$	0	0	0	0	-250.1	-80.8	-45.7	3.2	88.5	0

$\beta_B = 90^o$ $\lambda = 0^o$ $t/l = 1.5$

$\frac{x}{l}$	$10^3 g_{\gamma 0}$	$10^3 g_{\gamma 1}$	$10^3 g_{\gamma 2}$	$10^3 g_{\gamma 3}$	$10^3 f_{\gamma 0}$	$10^3 f_{\gamma 1}$	$10^3 f_{\gamma 2}$	$10^3 f_{\gamma 3}$	$10^3 g_{q0}$	$10^3 f_{q0}$
0	0	0	0	0	167.5	162.5	-71.9	-8.5	157.5	0
.05	0	0	0	0	133.9	147.8	-74.2	-7.9	161.7	0
.1	0	0	0	0	99.6	132.6	-76.6	-7.3	165.6	0
.15	0	0	0	0	65.5	117.0	-78.6	-6.7	168.5	0
.2	0	0	0	0	30.5	101.0	-80.5	-5.9	171.5	0
.25	0	0	0	0	-4.1	84.7	-82.2	-5.2	173.5	0
.3	0	0	0	0	-38.1	68.1	-83.5	-4.2	174.3	0
.35	0	0	0	0	-72.6	51.2	-84.7	-3.3	175.0	0
.4	0	0	0	0	-106.3	34.2	-85.4	-2.2	174.7	0
.45	0	0	0	0	-139.7	17.2	-85.9	-1.1	174.1	0
.5	0	0	0	0	-173.2	0	-86.0	0	173.2	0
.55	0	0	0	0	-205.8	-17.2	-85.9	1.1	171.4	0
.6	0	0	0	0	-237.4	-34.2	-85.4	2.2	169.0	0
.65	0	0	0	0	-268.6	-51.2	-84.7	3.3	166.2	0
.7	0	0	0	0	-299.1	-68.1	-83.5	4.2	162.9	0
.75	0	0	0	0	-328.4	-84.7	-82.2	5.2	159.0	0
.8	0	0	0	0	-356.7	-101.0	-80.5	5.9	154.7	0
.85	0	0	0	0	-384.1	-117.0	-78.6	6.7	150.1	0
.9	0	0	0	0	-410.2	-132.6	-76.6	7.3	145.0	0
.95	0	0	0	0	-435.7	-147.8	-74.2	7.9	140.1	0
1.0	0	0	0	0	-457.1	-162.5	-71.9	8.5	132.1	0
$\frac{3}{12}$	0	0	0	0	-4.1	84.7	-82.2	-5.2	173.5	0
$\frac{7}{12}$	0	0	0	0	-226.3	-28.5	-85.6	1.8	169.3	0
$\frac{11}{12}$	0	0	0	0	-418.0	-137.5	-75.8	7.6	143.0	0

TABLE 17.- Continued

CASCADE DOWNWASH TABLES FOR BLADE ANGLES OF $\beta_s = 90^\circ$ TO 165°

(CORRESPONDING TO STAGGER ANGLES OF $\lambda = 0^\circ$ TO 75°)

AND PITCH RATIO OF $\frac{t}{l} = 2$ TO 0.5

$\beta_s = 90^\circ$					$\lambda = 0^\circ$			$t/l = 1.25$		
$\frac{x}{l}$	$10^3 g_{\gamma 0}$	$10^3 g_{\gamma 1}$	$10^3 g_{\gamma 2}$	$10^3 g_{\gamma 3}$	$10^3 f_{\gamma 0}$	$10^3 f_{\gamma 1}$	$10^3 f_{\gamma 2}$	$10^3 f_{\gamma 3}$	$10^3 g_{q0}$	$10^3 f_{q0}$
0	0	0	0	0	233.9	225.0	-96.2	-14.1	216.1	0
.05	0	0	0	0	187.4	205.3	-100.4	-13.4	223.2	0
.1	0	0	0	0	139.5	184.7	-104.3	-12.6	229.9	0
.15	0	0	0	0	90.6	163.4	-108.2	-11.5	236.2	0
.2	0	0	0	0	41.8	141.3	-111.6	-10.3	240.8	0
.25	0	0	0	0	-6.7	118.8	-114.7	-8.9	244.3	0
.3	0	0	0	0	-54.5	95.6	-117.3	-7.3	245.7	0
.35	0	0	0	0	-102.8	72.1	-119.3	-5.5	247.0	0
.4	0	0	0	0	-150.6	48.2	-120.6	-3.7	247.0	0
.45	0	0	0	0	-197.8	24.2	-121.5	-1.9	246.2	0
.5	0	0	0	0	-243.7	0	-121.8	0	243.7	0
.55	0	0	0	0	-288.9	-24.2	-121.5	1.9	240.5	0
.6	0	0	0	0	-333.0	-48.2	-120.6	3.7	236.6	0
.65	0	0	0	0	-375.2	-72.1	-119.3	5.5	231.0	0
.7	0	0	0	0	-415.6	-95.6	-117.3	7.3	224.4	0
.75	0	0	0	0	-454.5	-118.8	-114.7	8.9	216.9	0
.8	0	0	0	0	-491.9	-141.3	-111.6	10.3	209.3	0
.85	0	0	0	0	-527.8	-163.4	-108.2	11.5	201.0	0
.9	0	0	0	0	-562.5	-184.7	-104.3	12.6	193.1	0
.95	0	0	0	0	-595.2	-205.3	-100.4	13.4	184.6	0
1.0	0	0	0	0	-625.6	-225.0	-96.2	14.1	175.6	0
$\frac{3}{12}$	0	0	0	0	-6.7	118.8	-114.7	-8.9	244.3	0
$\frac{7}{12}$	0	0	0	0	-320.0	-41.0	-121.0	3.1	238.0	0
$\frac{11}{12}$	0	0	0	0	-573.0	-191.8	-103.0	12.9	189.4	0

$\beta_s = 90^\circ$					$\lambda = 0^\circ$			$t/l = 1.0$		
$\frac{x}{l}$	$10^3 g_{\gamma 0}$	$10^3 g_{\gamma 1}$	$10^3 g_{\gamma 2}$	$10^3 g_{\gamma 3}$	$10^3 f_{\gamma 0}$	$10^3 f_{\gamma 1}$	$10^3 f_{\gamma 2}$	$10^3 f_{\gamma 3}$	$10^3 g_{q0}$	$10^3 f_{q0}$
0	0	0	0	0	350	332	-133	-26.3	314	0
.05	0	0	0	0	285	307	-142	-25.8	329	0
.1	0	0	0	0	217	280	-150	-24.9	343	0
.15	0	0	0	0	145	250	-157	-23.5	355	0
.2	0	0	0	0	70	217	-164	-21.7	364	0
.25	0	0	0	0	-8	182	-170	-19.2	372	0
.3	0	0	0	0	-84	146	-176	-16.0	376	0
.35	0	0	0	0	-158	110	-181	-12.3	378	0
.4	0	0	0	0	-229	74	-184	-8.5	377	0
.45	0	0	0	0	-300	37	-186	-4.4	374	0
.5	0	0	0	0	-368	0	-187	0	368	0
.55	0	0	0	0	-434	-37	-186	4.4	360	0
.6	0	0	0	0	-498	-74	-184	8.5	350	0
.65	0	0	0	0	-558	-110	-181	12.3	338	0
.7	0	0	0	0	-616	-146	-176	16.0	324	0
.75	0	0	0	0	-672	-182	-170	19.2	308	0
.8	0	0	0	0	-727	-217	-164	21.7	293	0
.85	0	0	0	0	-775	-250	-157	23.5	275	0
.9	0	0	0	0	-818	-280	-150	24.9	258	0
.95	0	0	0	0	-855	-307	-142	25.8	241	0
1.0	0	0	0	0	-889	-332	-133	26.3	225	0
$\frac{3}{12}$	0	0	0	0	-8	182	-170	-19.2	372	0
$\frac{7}{12}$	0	0	0	0	-476	-61	-185	7.2	354	0
$\frac{11}{12}$	0	0	0	0	-830	-289	-147	25.2	252	0

TABLE 17.- Continued

CASCADE DOWNWASH TABLES FOR BLADE ANGLES OF $\beta_s = 90^\circ$ TO 165°

(CORRESPONDING TO STAGGER ANGLES OF $\lambda = 0^\circ$ TO 75°)

AND PITCH RATIO OF $\frac{t}{l} = 2$ TO 0.5

$\beta_s = 90^\circ$				$\lambda = 0^\circ$			$t/l = 0.75$			
$\frac{x}{l}$	$10^3 g_{\gamma 0}$	$10^3 g_{\gamma 1}$	$10^3 g_{\gamma 2}$	$10^3 g_{\gamma 3}$	$10^3 f_{\gamma 0}$	$10^3 f_{\gamma 1}$	$10^3 f_{\gamma 2}$	$10^3 f_{\gamma 3}$	$10^3 g_{q0}$	$10^3 f_{q0}$
0	0	0	0	0	574	530	-189	-52.5	486	0
.05	0	0	0	0	456	488	-206	-54.1	520	0
.1	0	0	0	0	336	444	-225	-54.1	552	0
.15	0	0	0	0	215	398	-243	-52.7	581	0
.2	0	0	0	0	89	347	-261	-49.7	605	0
.25	0	0	0	0	-35	294	-276	-45.0	623	0
.3	0	0	0	0	-158	238	-291	-38.4	634	0
.35	0	0	0	0	-276	181	-302	-30.4	638	0
.4	0	0	0	0	-394	121	-311	-21.2	636	0
.45	0	0	0	0	-502	62	-316	-11.1	626	0
.5	0	0	0	0	-611	0	-318	0	611	0
.55	0	0	0	0	-715	-62	-316	11.1	591	0
.6	0	0	0	0	-807	-121	-311	21.2	565	0
.65	0	0	0	0	-897	-181	-302	30.4	535	0
.7	0	0	0	0	-978	-238	-291	38.4	502	0
.75	0	0	0	0	-1,056	-294	-276	45.0	468	0
.8	0	0	0	0	-1,127	-347	-261	49.7	433	0
.85	0	0	0	0	-1,195	-398	-243	52.7	399	0
.9	0	0	0	0	-1,253	-444	-225	54.1	365	0
.95	0	0	0	0	-1,307	-488	-206	54.1	331	0
1.0	0	0	0	0	-1,360	-530	-189	52.5	300	0
$\frac{3}{12}$	0	0	0	0	-35	294	-276	-45.0	623	0
$\frac{7}{12}$	0	0	0	0	-778	-102	-313	18.5	574	0
$\frac{11}{12}$	0	0	0	0	-1,271	-459	-218	54.3	353	0

$\beta_s = 90^\circ$				$\lambda = 0^\circ$			$t/l = 0.5$			
$\frac{x}{l}$	$10^3 g_{\gamma 0}$	$10^3 g_{\gamma 1}$	$10^3 g_{\gamma 2}$	$10^3 g_{\gamma 3}$	$10^3 f_{\gamma 0}$	$10^3 f_{\gamma 1}$	$10^3 f_{\gamma 2}$	$10^3 f_{\gamma 3}$	$10^3 g_{q0}$	$10^3 f_{q0}$
0	0	0	0	0	1,106	968	-280	-115.0	830	0
.05	0	0	0	0	866	902	-322	-126.8	938	0
.1	0	0	0	0	633	833	-368	-136.0	1,033	0
.15	0	0	0	0	387	752	-416	-141.2	1,117	0
.2	0	0	0	0	132	659	-465	-140.6	1,186	0
.25	0	0	0	0	-118	559	-511	-133.4	1,236	0
.3	0	0	0	0	-354	455	-554	-118.4	1,264	0
.35	0	0	0	0	-583	347	-590	-96.6	1,270	0
.4	0	0	0	0	-792	233	-616	-68.3	1,258	0
.45	0	0	0	0	-992	117	-632	-35.6	1,226	0
.5	0	0	0	0	-1,176	0	-638	0	1,176	0
.55	0	0	0	0	-1,347	-117	-632	35.6	1,113	0
.6	0	0	0	0	-1,506	-233	-616	68.3	1,040	0
.65	0	0	0	0	-1,653	-347	-590	96.6	959	0
.7	0	0	0	0	-1,784	-455	-554	118.4	874	0
.75	0	0	0	0	-1.905	-559	-511	133.4	787	0
.8	0	0	0	0	-2,019	-659	-465	140.6	701	0
.85	0	0	0	0	-2,122	-752	-416	141.2	618	0
.9	0	0	0	0	-2,207	-833	-368	136.0	541	0
.95	0	0	0	0	-2,277	-902	-322	126.8	473	0
1.0	0	0	0	0	-2,345	-968	-280	115.0	409	0
$\frac{3}{12}$	0	0	0	0	-118	559	-511	-133.4	1,236	0
$\frac{7}{12}$	0	0	0	0	-1,457	-195	-623	57.6	1,067	0
$\frac{11}{12}$	0	0	0	0	-2,232	-857	-353	133.4	518	0

TABLE 17.- Continued

CASCADE DOWNWASH TABLES FOR BLADE ANGLES OF $\beta_s = 90^\circ$ TO 165°

(CORRESPONDING TO STAGGER ANGLES OF $\lambda = 0^\circ$ TO 75°)

AND PITCH RATIO OF $\frac{t}{l} = 2$ TO 0.5

$\beta_s = 105^\circ$ $\lambda = 15^\circ$ $t/l = 2.0$										
$\frac{x}{l}$	$10^3 g_{\gamma 0}$	$10^3 g_{\gamma 1}$	$10^3 g_{\gamma 2}$	$10^3 g_{\gamma 3}$	$10^3 f_{\gamma 0}$	$10^3 f_{\gamma 1}$	$10^3 f_{\gamma 2}$	$10^3 f_{\gamma 3}$	$10^3 g_{q 0}$	$10^3 f_{q 0}$
0	47.0	45.6	-20.1	-2.5	85.7	84.9	-40.2	-2.7	84.1	-44.2
.05	37.5	41.5	-20.8	-2.3	68.9	76.8	-40.7	-2.4	84.7	-45.5
.1	28.0	37.3	-21.5	-2.1	51.5	68.5	-41.2	-2.1	85.5	-46.6
.15	18.3	32.8	-22.1	-1.9	34.0	60.2	-41.6	-1.9	86.4	-47.3
.2	8.7	28.4	-22.7	-1.7	16.6	51.7	-42.0	-1.6	86.8	-48.1
.25	-1.0	23.8	-23.1	-1.4	-0.8	43.2	-42.3	-1.4	87.2	-48.6
.3	-10.6	19.1	-23.5	-1.1	-18.3	34.6	-42.6	-1.1	87.5	-48.8
.35	-20.2	14.4	-23.7	-.8	-35.9	26.0	-42.8	-.8	87.9	-49.0
.4	-29.8	9.6	-24.0	-.6	-53.1	17.4	-43.0	-.5	87.9	-49.0
.45	-39.3	4.8	-24.1	-.2	-70.5	8.7	-43.1	-.2	87.9	-48.9
.5	-48.8	0	-24.2	0	-87.9	0	-43.1	0	87.9	-48.8
.55	-57.9	-4.8	-24.1	.2	-104.9	-8.7	-43.1	.2	87.5	-48.3
.6	-66.8	-9.6	-24.0	.6	-121.7	-17.4	-43.0	.5	86.9	-47.6
.65	-75.6	-14.4	-23.7	.8	-138.4	-26.0	-42.8	.8	86.4	-46.8
.7	-84.2	-19.1	-23.5	1.1	-154.9	-34.6	-42.6	1.1	85.7	-46.0
.75	-92.2	-23.8	-23.1	1.4	-171.4	-43.2	-42.3	1.4	85.0	-44.6
.8	-100.1	-28.4	-22.7	1.7	-187.7	-51.7	-42.0	1.6	84.3	-43.3
.85	-107.7	-32.8	-22.1	1.9	-203.6	-60.2	-41.6	1.9	83.2	-42.1
.9	-114.9	-37.3	-21.5	2.1	-219.2	-68.5	-41.2	2.1	82.2	-40.3
.95	-121.7	-41.5	-20.8	2.3	-234.5	-76.8	-40.7	2.4	80.9	-38.7
1.0	-128.2	-45.6	-20.1	2.5	-250.7	-84.9	-40.2	2.7	80.9	-37.0
$\frac{3}{12}$	-1.0	23.8	-23.1	-1.4	-.8	43.2	-42.3	-1.4	87.2	-48.6
$\frac{7}{12}$	-63.8	-8.0	-24.1	.5	-115.5	-14.2	-43.0	.5	87.1	-47.8
$\frac{11}{12}$	-117.0	-38.7	-21.3	2.2	-224.0	-71.3	-41.0	2.2	81.4	-39.6

$\beta_s = 105^\circ$ $\lambda = 15^\circ$ $t/l = 1.5$										
$\frac{x}{l}$	$10^3 g_{\gamma 0}$	$10^3 g_{\gamma 1}$	$10^3 g_{\gamma 2}$	$10^3 g_{\gamma 3}$	$10^3 f_{\gamma 0}$	$10^3 f_{\gamma 1}$	$10^3 f_{\gamma 2}$	$10^3 f_{\gamma 3}$	$10^3 g_{q 0}$	$10^3 f_{q 0}$
0	79.1	75.2	-30.5	-6.1	149.5	146.5	-66.9	-6.6	143.5	-71.3
.05	63.3	68.9	-32.4	-5.8	119.6	132.9	-68.6	-6.0	146.2	-74.5
.1	47.0	62.3	-34.2	-5.4	89.5	119.0	-70.1	-5.3	148.5	-77.6
.15	30.6	55.2	-35.9	-4.9	59.0	104.7	-71.5	-4.6	150.4	-79.8
.2	14.2	48.0	-37.5	-4.3	28.6	90.3	-72.7	-4.0	152.0	-81.8
.25	-2.6	40.4	-38.8	-3.6	-2.2	75.6	-73.7	-3.2	153.4	-83.4
.3	-19.2	32.6	-39.9	-2.9	-32.8	60.7	-74.5	-2.6	154.2	-84.4
.35	-35.6	24.6	-40.7	-2.2	-63.5	45.6	-75.1	-1.9	154.7	-84.8
.4	-52.0	16.5	-41.4	-1.5	-94.2	30.5	-75.6	-1.4	155.2	-85.0
.45	-68.0	8.3	-41.8	-.8	-124.0	15.2	-75.8	-.7	154.4	-84.6
.5	-83.4	0	-41.9	0	-153.8	0	-76.0	0	153.8	-83.4
.55	-98.6	-8.3	-41.8	.8	-183.3	-15.2	-75.8	.7	152.9	-82.0
.6	-113.1	-16.5	-41.4	1.5	-212.6	-30.5	-75.6	1.4	151.6	-80.1
.65	-126.8	-24.6	-40.7	2.2	-241.3	-45.6	-75.1	1.9	150.1	-77.6
.7	-140.0	-32.6	-39.9	2.9	-269.3	-60.7	-74.5	2.6	147.9	-74.8
.75	-152.2	-40.4	-38.8	3.6	-296.1	-75.6	-73.7	3.2	144.9	-71.4
.8	-163.8	-48.0	-37.5	4.3	-322.7	-90.3	-72.7	4.0	142.1	-67.8
.85	-174.6	-55.2	-35.9	4.9	-348.6	-104.7	-71.5	4.6	139.2	-64.2
.9	-184.7	-62.3	-34.2	5.4	-373.4	-119.0	-70.1	5.3	135.4	-60.1
.95	-194.1	-68.9	-32.4	5.8	-397.5	-132.9	-68.6	6.0	131.7	-56.3
1.0	-202.5	-75.2	-30.5	6.1	-420.9	-146.5	-66.9	6.6	127.9	-52.1
$\frac{3}{12}$	-2.6	40.4	-38.8	-3.6	-2.2	75.6	-73.7	-3.2	153.4	-83.4
$\frac{7}{12}$	-108.0	-13.9	-41.5	1.3	-203.0	-25.5	-75.7	1.2	152.0	-80.2
$\frac{11}{12}$	-187.9	-64.6	-35.5	5.6	-382.0	-123.8	-69.8	5.5	134.4	-58.7

TABLE 17.- Continued

CASCADE DOWNWASH TABLES FOR BLADE ANGLES OF $\beta_s = 90^\circ$ TO 165°

(CORRESPONDING TO STAGGER ANGLES OF $\lambda = 0^\circ$ TO 75°)

AND PITCH RATIO OF $\frac{t}{l} = 2$ TO 0.5

$\beta_s = 105^\circ$				$\lambda = 15^\circ$				$t/l = 1.25$		
$\frac{x}{l}$	$10^3 g_{\gamma 0}$	$10^3 g_{\gamma 1}$	$10^3 g_{\gamma 2}$	$10^3 g_{\gamma 3}$	$10^3 f_{\gamma 0}$	$10^3 f_{\gamma 1}$	$10^3 f_{\gamma 2}$	$10^3 f_{\gamma 3}$	$10^3 g_{q0}$	$10^3 f_{q0}$
0	108.8	101.4	-38.0	-10.1	210.7	204.7	-90.4	-11.4	198.7	-94.0
.05	86.9	93.4	-41.3	-9.8	168.7	186.2	-93.6	-10.5	203.7	-99.9
.1	64.4	84.8	-44.6	-9.3	125.9	167.1	-96.6	-9.5	208.3	-105.2
.15	41.6	75.6	-47.6	-8.7	82.9	147.6	-99.3	-8.5	212.3	-109.6
.2	18.3	65.9	-50.4	-7.8	39.3	127.4	-101.7	-7.3	215.5	-113.5
.25	-4.9	55.8	-52.9	-6.8	-4.1	106.9	-103.8	-6.2	217.9	-116.5
.3	-28.2	45.1	-55.0	-5.6	-47.7	86.0	-105.4	-4.9	219.7	-118.4
.35	-51.1	34.2	-56.8	-4.4	-91.3	64.8	-106.8	-3.7	220.9	-119.5
.4	-73.3	22.9	-58.0	-2.9	-134.2	43.3	-107.7	-2.5	220.8	-119.1
.45	-95.1	11.5	-58.8	-1.5	-176.6	21.7	-108.3	-1.3	220.0	-118.1
.5	-116.1	0	-59.0	0	-218.7	0	-108.4	0	218.7	-116.1
.55	-136.1	-11.5	-58.8	1.5	-260.0	-21.7	-108.3	1.3	216.6	-113.1
.6	-155.1	-22.9	-58.0	2.9	-300.2	-43.3	-107.7	2.5	213.6	-109.3
.65	-172.8	-34.2	-56.8	4.4	-339.5	-64.8	-106.8	3.7	209.9	-104.4
.7	-189.4	-45.1	-55.0	5.6	-377.5	-86.0	-105.4	4.9	205.5	-99.2
.75	-204.8	-55.8	-52.9	6.8	-414.0	-106.9	-103.8	6.2	200.2	-93.2
.8	-219.0	-65.9	-50.4	7.8	-449.3	-127.4	-101.7	7.3	194.5	-87.2
.85	-231.9	-75.6	-47.6	8.7	-483.6	-147.6	-99.3	8.5	188.4	-80.7
.9	-243.6	-84.8	-44.6	9.3	-516.3	-167.1	-96.6	9.5	182.1	-74.0
.95	-254.3	-93.4	-41.3	9.8	-547.5	-186.2	-93.6	10.5	175.1	-67.5
1.0	-263.9	-101.4	-38.0	10.1	-576.9	-204.7	-90.4	11.4	167.5	-61.1
$\frac{3}{12}$	-4.9	55.8	-52.9	-6.8	-4.1	106.9	-103.8	-6.2	217.9	-116.5
$\frac{7}{12}$	-148.5	-19.2	-58.2	2.6	-286.0	-36.1	-108.0	2.1	213.8	-110.1
$\frac{11}{12}$	-247.5	-87.8	-43.5	9.6	-526.0	-173.6	-95.7	9.8	178.8	-71.9

$\beta_s = 105^\circ$				$\lambda = 15^\circ$				$t/l = 1.0$		
$\frac{x}{l}$	$10^3 g_{\gamma 0}$	$10^3 g_{\gamma 1}$	$10^3 g_{\gamma 2}$	$10^3 g_{\gamma 3}$	$10^3 f_{\gamma 0}$	$10^3 f_{\gamma 1}$	$10^3 f_{\gamma 2}$	$10^3 f_{\gamma 3}$	$10^3 g_{q0}$	$10^3 f_{q0}$
0	157.5	142.7	-47.1	-17.3	317.1	303.5	-126.7	-21.6	289.9	-127.9
.05	125.4	132.4	-53.1	-17.5	253.6	277.3	-133.4	-20.5	301.0	-139.4
.1	92.4	121.0	-59.1	-17.3	189.0	250.0	-139.6	-19.2	311.0	-149.6
.15	58.6	108.6	-64.9	-16.6	123.2	221.4	-145.5	-17.4	319.6	-158.6
.2	24.3	95.2	-70.4	-15.4	57.2	192.0	-150.8	-15.4	326.8	-166.1
.25	-10.5	80.9	-75.5	-13.7	-9.4	161.5	-155.4	-13.1	332.4	-172.3
.3	-44.7	65.8	-79.9	-11.7	-75.6	130.2	-159.4	-10.8	336.0	-176.3
.35	-78.2	50.0	-83.5	-9.1	-141.1	98.2	-162.4	-8.2	337.5	-178.2
.4	-110.5	33.6	-86.3	-6.3	-206.6	65.8	-164.7	-5.5	338.2	-177.7
.45	-141.2	16.9	-87.9	-3.2	-270.6	33.0	-166.1	-2.8	336.6	-175.0
.5	-170.1	0	-88.5	0	-332.6	0	-166.6	0	332.6	-170.1
.55	-197.4	-16.9	-87.9	3.2	-393.0	-33.0	-166.1	2.8	327.0	-163.6
.6	-222.8	-33.6	-86.3	6.3	-451.8	-65.8	-164.7	5.5	320.2	-155.6
.65	-246.0	-50.0	-83.5	9.1	-508.2	-98.2	-162.4	8.2	311.8	-146.0
.7	-267.2	-65.8	-79.9	11.7	-562.4	-130.2	-159.4	10.8	302.0	-135.6
.75	-286.4	-80.9	-75.5	13.7	-613.6	-161.5	-155.4	13.1	290.6	-124.6
.8	-303.7	-95.2	-70.4	15.4	-660.2	-192.0	-150.8	15.4	276.2	-113.3
.85	-319.0	-108.6	-64.9	16.6	-708.4	-221.4	-145.5	17.4	265.6	-101.8
.9	-332.4	-121.0	-59.1	17.3	-752.5	-250.0	-139.6	19.2	252.5	-90.4
.95	-344.2	-132.4	-53.1	17.5	-793.9	-277.3	-133.4	20.5	239.3	-79.4
1.0	-354.6	-142.7	-47.1	17.3	-832.8	-303.5	-126.7	21.6	225.8	-69.2
$\frac{3}{12}$	-10.5	80.9	-75.5	-13.7	-9.4	161.5	-155.4	-13.1	332.4	-172.3
$\frac{7}{12}$	-213.0	-28.3	-86.9	5.4	-432.0	-55.1	-165.2	4.6	321.8	-156.4
$\frac{11}{12}$	-337.0	-124.9	-57.0	17.4	-766.0	-259.2	-137.4	19.7	247.6	-87.2

TABLE 17.- Continued

CASCADE DOWNWASH TABLES FOR BLADE ANGLES OF $\beta_s = 90^\circ$ TO 165°

(CORRESPONDING TO STAGGER ANGLES OF $\lambda = 0^\circ$ TO 75°)

AND PITCH RATIO OF $\frac{t}{l} = 2$ TO 0.5

$\beta_s = 105^\circ$			$\lambda = 15^\circ$				$t/l = 0.75$			
$\frac{x}{l}$	$10^3 g_{\gamma 0}$	$10^3 g_{\gamma 1}$	$10^3 g_{\gamma 2}$	$10^3 g_{\gamma 3}$	$10^3 f_{\gamma 0}$	$10^3 f_{\gamma 1}$	$10^3 f_{\gamma 2}$	$10^3 f_{\gamma 3}$	$10^3 g_{q0}$	$10^3 f_{q0}$
0	247.1	213.8	-56.7	-30.1	527.8	492.8	-185.8	-47.4	457.8	-180.5
.05	195.2	200.3	-67.8	-32.7	421.3	453.0	-201.0	-46.1	484.7	-205.4
.1	141.5	184.6	-79.6	-34.3	312.9	411.5	-216.5	-44.8	510.1	-227.7
.15	86.1	167.1	-91.6	-34.8	201.3	366.4	-230.4	-41.7	531.5	-248.1
.2	29.4	147.4	-103.5	-33.9	88.5	319.8	-244.4	-38.0	551.1	-265.4
.25	-26.2	126.0	-114.7	-31.5	-24.5	269.9	-256.0	-33.4	564.3	-278.2
.3	-80.4	102.9	-124.7	-27.6	-136.6	218.9	-267.1	-27.1	574.4	-286.2
.35	-132.5	78.5	-133.1	-22.3	-247.9	165.5	-275.1	-21.4	578.9	-289.5
.4	-181.3	52.9	-139.5	-15.6	-355.5	111.3	-281.8	-13.6	578.1	-287.1
.45	-226.7	26.6	-143.5	-8.1	-460.0	55.6	-284.8	-7.6	571.2	-279.9
.5	-268.2	0	-144.8	0	-560.6	0	-285.9	0	560.6	-268.2
.55	-306.0	-26.6	-143.5	8.1	-662.4	-55.6	-284.8	7.6	551.2	-252.8
.6	-340.4	-52.9	-139.5	15.6	-753.0	-111.3	-281.8	13.6	530.4	-234.6
.65	-371.3	-78.5	-133.1	22.3	-835.2	-165.5	-275.1	21.4	504.2	-214.3
.7	-398.6	-102.9	-124.7	27.6	-917.4	-218.9	-267.1	27.1	479.6	-192.8
.75	-422.7	-126.0	-114.7	31.5	-991.3	-269.9	-256.0	33.4	451.5	-170.7
.8	-443.4	-147.4	-103.5	33.9	-1,062.8	-319.8	-244.4	38.0	423.2	-148.6
.85	-461.4	-167.1	-91.6	34.8	-1,126.6	-366.4	-230.4	41.7	393.8	-127.2
.9	-476.9	-184.6	-79.6	34.3	-1,187.1	-411.5	-216.5	44.8	364.1	-107.7
.95	-490.3	-200.3	-67.8	32.7	-1,240.6	-453.0	-201.0	46.1	334.6	-89.7
1.0	-501.2	-213.8	-56.7	30.1	-1,291.0	-492.8	-185.8	47.4	305.4	-73.6
$\frac{3}{12}$	-26.2	126.0	-114.7	-31.5	-24.5	269.9	-256.0	-33.4	564.3	-278.2
$\frac{7}{12}$	-328.0	-44.1	-141.1	13.5	-718.0	-93.0	-282.9	12.2	532.0	-239.8
$\frac{11}{12}$	-481.0	-190.1	-75.3	33.9	-1,025.0	-425.0	-211.3	45.8	355.0	-100.8

$\beta_s = 105^\circ$			$\lambda = 15^\circ$				$t/l = 0.5$			
$\frac{x}{l}$	$10^3 g_{\gamma 0}$	$10^3 g_{\gamma 1}$	$10^3 g_{\gamma 2}$	$10^3 g_{\gamma 3}$	$10^3 f_{\gamma 0}$	$10^3 f_{\gamma 1}$	$10^3 f_{\gamma 2}$	$10^3 f_{\gamma 3}$	$10^3 g_{q0}$	$10^3 f_{q0}$
0	442.5	356.2	-63.2	-50.1	1,028.3	913.7	-281.1	-109.1	799.1	-269.9
.05	343.6	337.4	-84.6	-61.2	815.9	850.0	-320.5	-116.4	884.1	-331.2
.1	237.9	314.1	-109.4	-71.4	594.0	778.7	-361.7	-121.1	963.4	-390.3
.15	129.4	286.3	-136.4	-79.4	366.7	700.5	-403.6	-121.8	1,034.3	-443.2
.2	22.3	254.1	-164.6	-83.5	136.2	615.1	-444.6	-118.3	1,094.0	-485.9
.25	-78.9	218.1	-192.1	-82.8	-91.3	523.4	-483.4	-109.7	1,138.1	-515.1
.3	-173.0	178.6	-217.4	-75.9	-313.2	426.1	-517.8	-95.7	1,165.4	-530.2
.35	-258.7	136.4	-238.9	-63.5	-528.0	323.9	-546.8	-76.9	1,175.8	-531.5
.4	-335.8	92.0	-255.2	-45.6	-731.2	218.0	-568.4	-53.8	1,167.2	-519.8
.45	-404.5	46.4	-265.6	-23.9	-923.8	109.7	-581.7	-27.7	1,143.2	-497.3
.5	-465.9	0	-268.9	0	-1,104.6	0	-586.3	0	1,104.6	-465.9
.55	-520.8	-46.4	-265.6	23.9	-1,272.0	-109.7	-581.7	27.7	1,052.6	-428.0
.6	-569.0	-92.0	-255.2	45.6	-1,426.7	-218.0	-568.4	53.8	990.7	-385.0
.65	-612.1	-136.4	-238.9	63.5	-1,567.9	-323.9	-546.8	76.9	920.1	-339.3
.7	-649.6	-178.6	-217.4	75.9	-1,697.2	-426.1	-517.8	95.7	845.0	-292.4
.75	-682.7	-218.1	-192.1	82.8	-1,815.0	-523.4	-483.4	109.7	768.2	-246.5
.8	-711.2	-254.1	-164.6	83.5	-1,921.8	-615.1	-444.6	118.3	691.6	-203.0
.85	-735.0	-286.3	-136.4	79.4	-2,017.7	-700.5	-403.6	121.8	616.7	-162.4
.9	-754.8	-314.1	-109.4	71.4	-2,106.2	-778.7	-361.7	121.1	548.8	-126.6
.95	-770.7	-337.4	-84.6	61.2	-2,180.3	-850.0	-320.5	116.4	480.3	-95.9
1.0	-783.2	-356.2	-63.2	50.1	-2,247.6	-913.7	-281.1	109.1	420.2	-70.8
$\frac{3}{12}$	-78.9	218.1	-192.1	-82.8	-91.3	523.4	-483.4	-109.7	1,138.1	-515.1
$\frac{7}{12}$	-552.5	-77.8	-259.3	38.7	-1,372.0	-183.0	-574.0	46.2	1,006.0	-396.9
$\frac{11}{12}$	-761.0	-322.5	-100.6	68.3	-2,132.0	-805.0	-347.0	119.9	522.0	-116.0

TABLE 17.- Continued

CASCADE DOWNWASH TABLES FOR BLADE ANGLES OF $\beta_s = 90^\circ$ TO 165°

(CORRESPONDING TO STAGGER ANGLES OF $\lambda = 0^\circ$ TO 75°)

AND PITCH RATIO OF $\frac{t}{l} = 2$ TO 0.5

$\beta_s = 120^\circ$				$\lambda = 30^\circ$			$t/l = 2.0$			
$\frac{x}{l}$	$10^3 g_{\gamma 0}$	$10^3 g_{\gamma 1}$	$10^3 g_{\gamma 2}$	$10^3 g_{\gamma 3}$	$10^3 f_{\gamma 0}$	$10^3 f_{\gamma 1}$	$10^3 f_{\gamma 2}$	$10^3 f_{\gamma 3}$	$10^3 g_{q0}$	$10^3 f_{q0}$
0	83.9	82.2	-37.6	-3.4	52.1	53.4	-27.6	0.2	54.7	-80.5
.05	66.9	74.5	-38.6	-3.1	41.8	48.0	-27.3	.2	54.2	-82.1
.1	50.0	66.7	-39.4	-2.8	31.6	42.6	-26.9	.2	53.6	-83.4
.15	33.0	58.7	-40.2	-2.5	21.0	37.1	-26.6	.1	53.2	-84.4
.2	16.1	50.6	-40.9	-2.2	10.7	31.7	-26.3	.1	52.7	-85.1
.25	-1.1	42.3	-41.4	-1.9	0	26.2	-26.1	.1	52.4	-85.7
.3	-18.0	34.0	-41.8	-1.6	-10.2	21.0	-25.9	.1	52.2	-86.0
.35	-35.1	25.5	-42.2	-1.2	-20.7	15.7	-25.8	.1	52.1	-86.0
.4	-51.8	17.1	-42.4	-.8	-31.2	10.5	-25.7	0	52.2	-86.0
.45	-68.7	8.5	-42.5	-.4	-41.9	5.2	-25.6	0	52.3	-85.7
.5	-85.4	0	-42.5	0	-52.5	0	-25.6	0	52.5	-85.4
.55	-101.9	-8.5	-42.5	.4	-63.2	-5.2	-25.6	0	52.8	-84.9
.6	-118.2	-17.1	-42.4	.8	-75.1	-10.5	-25.7	0	53.2	-84.2
.65	-134.3	-25.5	-42.2	1.2	-85.0	-15.7	-25.8	-.1	53.6	-83.3
.7	-150.1	-34.0	-41.8	1.6	-96.4	-21.0	-25.9	-.1	54.2	-82.1
.75	-165.2	-42.3	-41.4	1.9	-107.2	-26.2	-26.1	-.1	54.8	-80.6
.8	-180.2	-50.6	-40.9	2.2	-118.9	-31.7	-26.3	-.1	55.5	-79.0
.85	-194.5	-58.7	-40.2	2.5	-130.4	-37.1	-26.6	-.1	56.2	-77.1
.9	-208.4	-66.7	-39.4	2.8	-142.1	-42.6	-26.9	-.2	56.9	-75.0
.95	-221.9	-74.5	-38.6	3.1	-153.7	-48.0	-27.3	-.2	57.7	-72.9
1.0	-235.2	-82.2	-37.6	3.4	-165.2	-53.4	-27.6	-.2	58.4	-70.8
$\frac{3}{12}$	-1.1	42.3	-41.4	-1.9	0	26.2	-26.1	.1	52.4	-85.7
$\frac{7}{12}$	-112.9	-14.2	-42.4	.7	-70.4	-8.7	-25.7	0	53.0	-84.5
$\frac{11}{12}$	-213.1	-69.4	-39.2	2.9	-145.8	-44.3	-27.0	-.2	57.2	-74.3

$\beta_s = 120^\circ$				$\lambda = 30^\circ$			$t/l = 1.5$			
$\frac{x}{l}$	$10^3 g_{\gamma 0}$	$10^3 g_{\gamma 1}$	$10^3 g_{\gamma 2}$	$10^3 g_{\gamma 3}$	$10^3 f_{\gamma 0}$	$10^3 f_{\gamma 1}$	$10^3 f_{\gamma 2}$	$10^3 f_{\gamma 3}$	$10^3 g_{q0}$	$10^3 f_{q0}$
0	143.4	138.1	-59.4	-9.4	97.4	98.0	-50.0	0.1	98.6	-132.8
.05	114.0	126.0	-62.2	-8.5	77.5	88.1	-49.6	.3	98.7	-138.0
.1	84.9	113.3	-64.8	-7.6	57.6	77.9	-49.1	.4	98.2	-141.7
.15	56.2	100.2	-67.1	-6.6	38.4	68.0	-48.7	.3	97.6	-144.2
.2	26.9	86.7	-69.1	-5.5	18.9	58.0	-48.2	.2	97.1	-146.5
.25	-2.7	72.8	-70.6	-4.4	-.3	48.2	-47.9	0	96.7	-148.3
.3	-32.3	58.7	-71.9	-3.3	-19.4	38.4	-47.4	-.1	96.2	-149.7
.35	-62.1	44.2	-72.8	-2.4	-38.4	28.8	-47.3	-.2	96.0	-150.5
.4	-91.3	29.6	-73.5	-1.5	-57.6	19.1	-47.0	-.2	95.8	-150.5
.45	-120.7	14.8	-73.8	-.7	-77.0	9.6	-47.0	0	96.2	-150.3
.5	-149.7	0	-74.0	0	-96.6	0	-46.9	0	96.6	-149.7
.55	-177.7	-14.8	-73.8	.7	-115.9	-9.6	-47.0	0	96.4	-148.1
.6	-204.9	-29.6	-73.5	1.5	-135.8	-19.1	-47.0	.2	97.6	-145.7
.65	-231.3	-44.2	-72.8	2.4	-156.3	-28.8	-47.3	.2	98.7	-142.9
.7	-256.5	-58.7	-71.9	3.3	-176.8	-38.4	-47.4	.1	100.0	-139.1
.75	-280.4	-72.8	-70.6	4.4	-197.9	-48.2	-47.9	0	101.5	-134.8
.8	-303.1	-86.7	-69.1	5.5	-218.7	-58.0	-48.2	-.2	102.7	-129.7
.85	-324.5	-100.2	-67.1	6.6	-239.4	-68.0	-48.7	-.3	103.4	-124.1
.9	-345.0	-113.3	-64.8	7.6	-259.7	-77.9	-49.1	-.4	103.9	-118.4
.95	-364.0	-126.0	-62.2	8.4	-280.7	-88.1	-49.6	-.3	104.5	-112.0
1.0	-381.6	-138.1	-59.4	9.4	-301.0	-98.0	-50.0	-.1	105.0	-105.4
$\frac{3}{12}$	-2.7	72.8	-70.6	-4.4	-.3	48.2	-47.9	0	96.7	-148.3
$\frac{7}{12}$	-196.0	-24.7	-73.6	1.2	-129.2	-16.2	-47.0	.2	96.8	-146.6
$\frac{11}{12}$	-351.7	-117.4	-63.9	7.9	-267.0	-81.5	-49.3	-.3	104.0	-116.9

TABLE 17.- Continued

CASCADE DOWNWASH TABLES FOR BLADE ANGLES OF $\beta_s = 90^\circ$ TO 165°

(CORRESPONDING TO STAGGER ANGLES OF $\lambda = 0^\circ$ TO 75°)

AND PITCH RATIO OF $\frac{t}{l} = 2$ TO 0.5

$\beta_s = 120^\circ$				$\lambda = 30^\circ$			$t/l = 1.25$			
$\frac{x}{l}$	$10^3 g_{\gamma 0}$	$10^3 g_{\gamma 1}$	$10^3 g_{\gamma 2}$	$10^3 g_{\gamma 3}$	$10^3 f_{\gamma 0}$	$10^3 f_{\gamma 1}$	$10^3 f_{\gamma 2}$	$10^3 f_{\gamma 3}$	$10^3 g_{q0}$	$10^3 f_{q0}$
0	199.0	188.7	-75.8	-16.5	141.5	141.1	-72.3	-1.1	140.7	-178.4
.05	158.7	173.1	-81.0	-15.4	112.0	128.0	-72.1	-.3	144.0	-187.5
.1	118.1	156.5	-85.9	-14.2	84.1	113.5	-71.7	.1	142.9	-194.9
.15	77.5	139.0	-90.4	-12.7	56.1	99.0	-71.2	.4	141.9	-200.5
.2	36.0	120.8	-94.3	-10.9	28.1	84.6	-70.6	.6	141.1	-205.6
.25	-5.8	101.8	-97.7	-9.1	.3	70.3	-70.0	.7	140.3	-209.4
.3	-47.7	82.3	-100.5	-7.1	-27.3	56.1	-69.4	.6	139.5	-212.3
.35	-89.6	62.2	-102.8	-5.2	-55.4	41.9	-68.7	.4	139.2	-214.0
.4	-130.7	41.7	-104.3	-3.4	-83.3	27.9	-68.3	.3	139.1	-214.1
.45	-171.4	20.9	-105.2	-1.7	-111.7	13.9	-68.0	.2	139.5	-213.2
.5	-210.9	0	-105.5	0	-140.6	0	-67.9	0	140.6	-210.9
.55	-249.0	-20.9	-105.2	1.7	-169.6	-13.9	-68.0	-.2	141.8	-207.2
.6	-285.6	-41.7	-104.3	3.4	-199.2	-27.9	-68.3	-.3	143.4	-202.2
.65	-319.7	-62.2	-102.8	5.2	-229.1	-41.9	-68.7	-.4	145.3	-195.3
.7	-352.1	-82.3	-100.5	7.1	-259.2	-56.1	-69.4	-.6	147.0	-187.5
.75	-382.8	-101.8	-97.7	9.1	-288.4	-70.3	-70.0	-.7	147.8	-179.2
.8	-411.1	-120.8	-94.3	10.9	-317.9	-84.6	-70.6	-.6	148.7	-169.5
.85	-437.3	-139.0	-90.4	12.7	-347.6	-99.0	-71.2	-.4	149.6	-159.3
.9	-461.9	-156.5	-85.9	14.2	-376.5	-113.5	-71.7	-.1	149.5	-148.9
.95	-484.1	-173.1	-81.0	15.4	-404.8	-128.0	-72.1	.3	148.8	-137.9
1.0	-503.8	-188.7	-75.8	16.5	-433.0	-141.1	-72.3	1.1	150.8	-126.4
$\frac{3}{12}$	-5.8	101.8	-97.7	-9.1	.3	70.3	-70.0	.7	140.3	-209.4
$\frac{7}{12}$	-272.5	-35.0	-104.7	2.8	-189.5	-23.5	-68.2	-.2	142.5	-202.5
$\frac{11}{12}$	-470.0	-162.2	-84.4	14.6	-386.0	-118.4	-71.8	0	149.2	-145.6

$\beta_s = 120^\circ$				$\lambda = 30^\circ$			$t/l = 1.0$			
$\frac{x}{l}$	$10^3 g_{\gamma 0}$	$10^3 g_{\gamma 1}$	$10^3 g_{\gamma 2}$	$10^3 g_{\gamma 3}$	$10^3 f_{\gamma 0}$	$10^3 f_{\gamma 1}$	$10^3 f_{\gamma 2}$	$10^3 f_{\gamma 3}$	$10^3 g_{q0}$	$10^3 f_{q0}$
0	289	269	-96	-30.6	218	222	-112	-6.0	226	-249
.05	231	249	-107	-29.6	175	200	-113	-3.7	225	-267
.1	172	227	-117	-28.3	134	179	-113	-1.6	224	-282
.15	111	203	-126	-26.2	90	156	-113	.1	222	-295
.2	49	177	-134	-23.4	45	133	-112	1.4	220	-305
.25	-14	150	-142	-20.1	3	111	-110	2.2	219	-314
.3	-76	122	-148	-16.4	-43	88	-109	2.5	219	-320
.35	-139	92	-153	-12.4	-87	66	-108	2.3	219	-323
.4	-199	62	-157	-8.4	-132	44	-107	1.9	220	-323
.45	-258	31	-159	-4.3	-177	22	-106	1.1	221	-319
.5	-313	0	-160	0	-223	0	-106	0	223	-313
.55	-366	-31	-159	4.3	-268	-22	-106	-1.1	224	-304
.6	-416	-62	-157	8.4	-314	-44	-107	-1.9	226	-292
.65	-461	-92	-153	12.4	-360	-66	-108	-2.3	228	-277
.7	-504	-122	-148	16.4	-405	-88	-109	-2.5	229	-260
.75	-542	-150	-142	20.1	-452	-111	-110	-2.2	230	-242
.8	-576	-177	-134	23.4	-495	-133	-112	-1.4	229	-222
.85	-608	-203	-126	26.2	-539	-156	-113	-.1	227	-202
.9	-636	-227	-117	28.3	-582	-179	-113	1.6	224	-182
.95	-660	-249	-107	29.6	-619	-200	-113	3.7	219	-162
1.0	-680	-269	-96	30.6	-656	-222	-112	6.0	212	-142
$\frac{3}{12}$	-14	150	-142	-20.1	3	111	-110	2.2	219	-314
$\frac{7}{12}$	-400	-52	-158	7.0	-298	-36	-107	-1.7	226	-296
$\frac{11}{12}$	-645	-235	-114	28.7	-592	-185	-113	2.3	222	-175

TABLE 17.- Continued

CASCADE DOWNWASH TABLES FOR BLADE ANGLES OF $\beta_s = 90^\circ$ TO 165°

(CORRESPONDING TO STAGGER ANGLES OF $\lambda = 0^\circ$ TO 75°)

AND PITCH RATIO OF $\frac{t}{l} = 2$ TO 0.5

$\beta_s = 120^\circ$ $\lambda = 30^\circ$ $t/l = 0.75$										
$\frac{x}{l}$	$10^3 g_{\gamma 0}$	$10^3 g_{\gamma 1}$	$10^3 g_{\gamma 2}$	$10^3 g_{\gamma 3}$	$10^3 f_{\gamma 0}$	$10^3 f_{\gamma 1}$	$10^3 f_{\gamma 2}$	$10^3 f_{\gamma 3}$	$10^3 g_{q0}$	$10^3 f_{q0}$
0	460	409	-118	-58.7	379	380	-175	-25.8	381	-358
.05	366	381	-140	-61.1	304	345	-182	-20.2	386	-396
.1	270	351	-161	-61.6	231	310	-188	-14.5	389	-432
.15	170	317	-181	-60.1	155	273	-192	-9.2	391	-464
.2	68	280	-200	-56.4	78	235	-194	-4.3	392	-492
.25	-36	239	-218	-50.5	1	197	-195	0	393	-514
.3	-142	193	-234	-43.2	-78	158	-195	2.8	394	-528
.35	-241	147	-249	-34.3	-159	119	-195	3.9	397	-535
.4	-333	100	-259	-23.5	-239	80	-194	3.4	399	-533
.45	-423	50	-265	-12.1	-321	40	-194	1.8	401	-523
.5	-505	0	-267	0	-403	0	-194	0	403	-505
.55	-579	-50	-265	12.1	-484	-40	-194	-1.8	404	-479
.6	-648	-100	-259	23.5	-563	-80	-194	-3.4	403	-448
.65	-706	-147	-249	34.3	-637	-119	-195	-3.9	399	-412
.7	-760	-193	-234	43.2	-710	-158	-195	-2.8	394	-374
.75	-812	-239	-218	50.5	-779	-197	-195	0	385	-334
.8	-854	-280	-200	56.4	-843	-235	-194	4.3	373	-294
.85	-888	-317	-181	60.1	-903	-273	-192	9.2	357	-254
.9	-919	-351	-161	61.6	-959	-310	-188	14.5	339	-217
.95	-943	-381	-140	61.1	-1,010	-345	-182	20.2	320	-181
1.0	-966	-409	-118	58.7	-1,059	-380	-175	25.8	299	-148
$\frac{3}{12}$	-36	239	-218	-50.5	1	197	-195	0	393	-514
$\frac{7}{12}$	-625	-83	-262	19.8	-537	-67	-194	-2.9	403	-459
$\frac{11}{12}$	-926	-361	-154	61.6	-977	-322	-186	16.4	333	-204

$\beta_s = 120^\circ$ $\lambda = 30^\circ$ $t/l = 0.5$										
$\frac{x}{l}$	$10^3 g_{\gamma 0}$	$10^3 g_{\gamma 1}$	$10^3 g_{\gamma 2}$	$10^3 g_{\gamma 3}$	$10^3 f_{\gamma 0}$	$10^3 f_{\gamma 1}$	$10^3 f_{\gamma 2}$	$10^3 f_{\gamma 3}$	$10^3 g_{q0}$	$10^3 f_{q0}$
0	829	683	-129	-103.4	802	750	-279	-91.3	708	-537
.05	652	648	-171	-122.4	640	693	-307	-86.1	746	-644
.1	460	602	-217	-138.3	486	631	-332	-78.8	776	-744
.15	263	550	-268	-149.2	325	564	-356	-68.7	803	-837
.2	64	490	-319	-153.1	155	492	-377	-55.1	829	-916
.25	-133	420	-370	-148.8	-13	418	-395	-42.0	853	-973
.3	-318	344	-416	-134.7	-192	340	-410	-30.7	872	-1,006
.35	-487	263	-456	-111.5	-371	258	-423	-20.4	887	-1,013
.4	-642	177	-486	-79.5	-546	174	-432	-12.4	894	-996
.45	-776	90	-505	-41.5	-714	88	-438	-5.7	890	-956
.5	-898	0	-512	0	-876	0	-440	0	876	-898
.55	-1,005	-90	-505	41.5	-1,027	-88	-438	5.7	851	-825
.6	-1,096	-177	-486	79.5	-1,166	-174	-432	12.4	818	-742
.65	-1,179	-263	-456	111.5	-1,293	-258	-423	20.4	777	-653
.7	-1,250	-344	-416	134.7	-1,409	-340	-410	30.7	729	-562
.75	-1,314	-420	-370	148.8	-1,520	-418	-395	42.0	680	-474
.8	-1,370	-490	-319	153.1	-1,612	-492	-377	55.1	628	-390
.85	-1,412	-550	-268	149.2	-1,702	-564	-356	68.7	574	-312
.9	-1,448	-602	-217	138.3	-1,782	-631	-332	78.8	520	-244
.95	-1,480	-648	-171	122.4	-1,852	-693	-307	86.1	466	-184
1.0	-1,500	-683	-129	103.4	-1,916	-750	-279	91.3	416	-134
$\frac{3}{12}$	-133	420	-370	-148.8	-13	418	-395	-42.0	853	-973
$\frac{7}{12}$	-1,068	-149	-497	67.2	-1,122	-146	-435	10.0	830	-770
$\frac{11}{12}$	-1,460	-617	-201	133.6	-1,806	-652	-324	81.6	502	-226

TABLE 17.- Continued

CASCADE DOWNWASH TABLES FOR BLADE ANGLES OF $\beta_s = 90^\circ$ TO 165°

(CORRESPONDING TO STAGGER ANGLES OF $\lambda = 0^\circ$ TO 75°)

AND PITCH RATIO OF $\frac{t}{l} = 2$ TO 0.5

$\beta_s = 135^\circ$ $\lambda = 45^\circ$ $t/l = 2.0$

$\frac{x}{l}$	$10^3 g_{\gamma 0}$	$10^3 g_{\gamma 1}$	$10^3 g_{\gamma 2}$	$10^3 g_{\gamma 3}$	$10^3 f_{\gamma 0}$	$10^3 f_{\gamma 1}$	$10^3 f_{\gamma 2}$	$10^3 f_{\gamma 3}$	$10^3 g_{q0}$	$10^3 f_{q0}$
0	96.8	99.1	-49.3	-2.5	5.7	7.2	-6.7	2.9	8.7	-101.4
.05	79.5	90.6	-49.6	-2.2	4.2	5.8	-5.6	2.5	7.4	-101.7
.1	61.0	81.5	-49.9	-1.8	3.0	4.6	-4.6	2.2	6.2	-102.0
.15	41.0	71.6	-50.1	-1.4	1.9	3.6	-3.8	1.8	5.3	-102.2
.2	20.3	61.3	-50.2	-1.1	1.1	2.8	-3.1	1.4	4.5	-102.3
.25	0	51.2	-50.3	-.8	.3	2.1	-2.5	1.0	3.9	-102.4
.3	-20.7	40.9	-50.4	-.5	-.4	1.5	-2.1	.7	3.4	-102.5
.35	-41.1	30.7	-50.4	-.3	-1.0	1.1	-1.7	.5	3.2	-102.5
.4	-61.5	20.5	-50.4	-.1	-1.6	.7	-1.5	.3	3.0	-102.5
.45	-81.9	10.3	-50.4	0	-2.3	.3	-1.4	.1	2.9	-102.5
.5	-102.6	0	-50.4	0	-3.2	0	-1.4	0	3.2	-102.6
.55	-123.1	-10.3	-50.4	0	-4.4	-.3	-1.4	-.1	3.8	-102.5
.6	-143.4	-20.5	-50.4	.1	-6.0	-.7	-1.5	-.3	4.6	-102.4
.65	-163.6	-30.7	-50.4	.3	-7.9	-1.1	-1.7	-.5	5.7	-102.2
.7	-183.8	-40.9	-50.4	.5	-10.3	-1.5	-2.1	-.7	7.3	-102.0
.75	-204.0	-51.2	-50.3	.8	-13.1	-2.1	-2.5	-1.0	8.9	-101.6
.8	-223.7	-61.3	-50.2	1.1	-16.5	-2.8	-3.1	-1.4	10.9	-101.1
.85	-243.5	-71.6	-50.1	1.4	-20.2	-3.6	-3.8	-1.8	13.0	-100.3
.9	-262.9	-81.5	-49.9	1.8	-24.5	-4.6	-4.6	-2.2	15.3	-99.9
.95	-280.5	-90.6	-49.6	2.2	-29.6	-5.8	-5.6	-2.5	18.0	-99.3
1.0	-296.8	-99.1	-49.3	2.5	-35.3	-7.2	-6.7	-2.9	20.9	-98.6
$\frac{3}{12}$	0	51.2	-50.3	-.8	.3	2.1	-2.5	1.0	3.9	-102.4
$\frac{7}{12}$	-137.4	-17.5	-50.4	.1	-5.4	-.6	-1.5	-.2	4.2	-102.4
$\frac{11}{12}$	-268.9	-84.6	-49.8	1.9	-26.1	-5.0	-4.9	-2.3	16.1	-99.7

$\beta_s = 135^\circ$ $\lambda = 45^\circ$ $t/l = 1.5$

$\frac{x}{l}$	$10^3 g_{\gamma 0}$	$10^3 g_{\gamma 1}$	$10^3 g_{\gamma 2}$	$10^3 g_{\gamma 3}$	$10^3 f_{\gamma 0}$	$10^3 f_{\gamma 1}$	$10^3 f_{\gamma 2}$	$10^3 f_{\gamma 3}$	$10^3 g_{q0}$	$10^3 f_{q0}$
0	179.0	177.2	-83.4	-6.9	14.9	21.6	-20.6	8.2	28.3	-175.4
.05	143.4	160.4	-85.0	-5.8	12.5	17.5	-17.4	7.5	22.5	-177.4
.1	107.4	143.2	-86.3	-4.8	9.4	14.0	-14.5	6.7	18.5	-179.0
.15	71.7	125.9	-87.4	-3.8	6.6	11.0	-11.9	5.8	15.4	-180.1
.2	35.4	108.3	-88.2	-2.9	4.3	8.5	-9.7	4.9	13.7	-181.2
.25	-1.2	90.5	-88.7	-2.3	2.2	6.4	-7.8	4.0	10.6	-182.2
.3	-37.6	72.5	-89.1	-1.6	.4	4.6	-6.3	3.1	8.8	-182.6
.35	-74.4	54.5	-89.4	-1.2	-1.4	3.2	-5.0	2.2	7.8	-183.4
.4	-111.0	36.4	-89.6	-.7	-3.4	2.0	-4.1	1.4	7.4	-183.8
.45	-147.1	18.2	-89.8	-.3	-5.9	1.0	-3.5	.7	7.9	-183.5
.5	-183.6	0	-89.7	0	-9.6	0	-3.4	0	9.6	-183.6
.55	-219.9	-18.2	-89.8	.3	-14.1	-1.0	-3.5	-.7	12.1	-183.5
.6	-255.1	-36.4	-89.6	.7	-19.2	-2.0	-4.1	-1.4	15.2	-182.3
.65	-290.6	-54.5	-89.4	1.2	-25.6	-3.2	-5.0	-2.2	19.2	-181.6
.7	-325.7	-72.5	-89.1	1.6	-32.7	-4.6	-6.3	-3.1	23.5	-180.7
.75	-359.4	-90.5	-88.7	2.3	-41.1	-6.4	-7.8	-4.0	28.3	-178.4
.8	-392.8	-108.3	-88.2	2.9	-51.2	-8.5	-9.7	-4.9	34.2	-176.2
.85	-424.6	-125.9	-87.4	3.8	-62.6	-11.0	-11.9	-5.8	40.6	-172.8
.9	-455.5	-143.2	-86.3	4.8	-75.3	-14.0	-14.5	-6.8	47.3	-169.1
.95	-485.8	-160.4	-85.0	5.8	-89.5	-17.5	-17.1	-7.5	54.5	-165.0
1.0	-514.6	-177.2	-83.4	6.9	-104.9	-21.6	-20.6	-8.2	61.7	-160.2
$\frac{3}{12}$	-1.2	90.5	-88.7	-2.3	2.2	6.4	-7.8	4.0	10.6	-182.2
$\frac{7}{12}$	-243.5	-30.4	-89.6	.6	-17.3	-1.7	-3.9	-1.1	13.9	-182.7
$\frac{11}{12}$	-466.0	-149.0	-84.9	5.1	-80.2	-15.1	-15.4	-7.0	50.0	-168.0

TABLE 17.- Continued

CASCADE DOWNWASH TABLES FOR BLADE ANGLES OF $\beta_s = 90^o$ TO 165^o

(CORRESPONDING TO STAGGER ANGLES OF $\lambda = 0^o$ TO 75^o)

AND PITCH RATIO OF $\frac{t}{l} = 2$ TO 0.5

$\beta_s = 135^o$					$\lambda = 45^o$			$t/l = 1.25$		
$\frac{x}{l}$	$10^3 g_{\gamma 0}$	$10^3 g_{\gamma 1}$	$10^3 g_{\gamma 2}$	$10^3 g_{\gamma 3}$	$10^3 f_{\gamma 0}$	$10^3 f_{\gamma 1}$	$10^3 f_{\gamma 2}$	$10^3 f_{\gamma 3}$	$10^3 g_{q0}$	$10^3 f_{q0}$
0	253.1	248.3	-112.4	-14.2	31.2	42.2	-39.7	14.0	53.2	-243.5
.05	202.8	225.7	-116.3	-12.0	24.5	34.5	-34.4	13.7	44.5	-248.6
.1	152.3	202.3	-119.6	-9.9	18.7	27.8	-29.0	12.9	36.9	-252.3
.15	101.4	178.3	-122.2	-8.0	13.8	22.0	-24.2	11.7	30.2	-255.2
.2	50.1	153.8	-124.2	-6.2	9.5	17.0	-19.7	10.2	24.5	-257.5
.25	-2.1	128.9	-125.8	-4.5	5.7	12.8	-15.9	8.7	19.9	-259.9
.3	-54.6	103.5	-127.0	-3.2	2.1	9.3	-12.5	6.9	16.5	-261.6
.35	-106.8	77.9	-127.9	-2.1	-1.7	6.5	-9.9	5.3	14.7	-262.6
.4	-159.2	52.0	-128.4	-1.3	-6.7	4.1	-7.9	3.5	14.9	-263.2
.45	-211.1	26.0	-128.6	-.7	-12.8	2.0	-6.8	1.8	16.8	-263.1
.5	-262.6	0	-128.7	0	-20.1	0	-6.4	0	20.1	-262.6
.55	-314.1	-26.0	-128.6	.7	-28.6	-2.0	-6.8	-1.8	24.6	-262.1
.6	-364.2	-52.0	-128.4	1.3	-39.2	-4.1	-7.9	-3.5	31.0	-260.2
.65	-412.7	-77.9	-127.9	2.1	-51.7	-6.5	-9.9	-5.3	38.7	-256.9
.7	-459.6	-103.5	-127.0	3.2	-66.5	-9.3	-12.5	-6.9	47.9	-252.6
.75	-505.1	-128.9	-125.5	4.5	-83.2	-12.8	-15.9	-8.7	57.6	-247.3
.8	-549.2	-153.8	-124.2	6.2	-102.0	-16.1	-19.7	-10.2	69.8	-241.6
.85	-591.0	-178.3	-122.2	8.0	-123.2	-22.0	-24.2	-11.7	79.2	-234.4
.9	-630.0	-202.3	-119.6	9.9	-145.9	-27.8	-29.0	-12.9	90.3	-225.4
.95	-666.1	-225.7	-116.3	12.0	-170.0	-34.5	-34.4	-13.7	101.0	-214.7
1.0	-699.0	-248.3	-112.4	14.2	-194.6	-42.2	-39.7	-14.0	110.2	-202.4
$\frac{3}{12}$	-2.1	128.9	-125.8	-4.5	5.7	12.8	-15.9	8.7	19.9	-259.9
$\frac{7}{12}$	-348.0	-43.6	-128.4	1.1	-35.1	-3.4	-7.5	-3.0	28.3	-260.8
$\frac{11}{12}$	-642.0	-210.0	-118.5	10.6	-153.5	-30.0	-30.9	-13.2	93.5	-222.0

$\beta_s = 135^o$					$\lambda = 45^o$			$t/l = 1.0$		
$\frac{x}{l}$	$10^3 g_{\gamma 0}$	$10^3 g_{\gamma 1}$	$10^3 g_{\gamma 2}$	$10^3 g_{\gamma 3}$	$10^3 f_{\gamma 0}$	$10^3 f_{\gamma 1}$	$10^3 f_{\gamma 2}$	$10^3 f_{\gamma 3}$	$10^3 g_{q0}$	$10^3 f_{q0}$
0	379	365	-150	-33.6	67.8	89.6	-79.3	24.0	111.4	-351
.05	305	335	-160	-29.3	54.0	75.0	-71.1	23.9	96.0	-365
.1	228	302	-170	-24.9	42.0	61.7	-62.3	23.8	81.4	-376
.15	151	268	-178	-20.5	31.9	49.7	-52.8	23.1	67.5	-385
.2	72	233	-184	-16.3	22.8	39.0	-44.2	21.9	55.2	-394
.25	-7	196	-189	-12.7	14.4	30.1	-33.6	19.6	45.8	-399
.3	-87	158	-193	-9.6	5.6	22.4	-29.9	16.4	39.2	-403
.35	-165	119	-196	-6.8	-4.8	15.8	-23.8	12.7	36.4	-403
.4	-245	80	-198	-4.3	-16.9	10.0	-19.3	8.8	36.9	-405
.45	-323	40	-199	-2.1	-31.6	4.8	-16.4	4.5	41.2	-403
.5	-401	0	-200	0	-48.7	0	-15.7	0	48.7	-401
.55	-477	-40	-199	2.1	-69.2	-4.8	-16.4	-4.5	59.6	-397
.6	-550	-80	-198	4.3	-92.9	-10.0	-19.3	-8.8	72.9	-390
.65	-618	-119	-196	6.8	-120.4	-15.8	-23.8	-12.7	88.8	-380
.7	-684	-158	-193	9.6	-151.4	-22.4	-29.9	-16.4	106.6	-368
.75	-745	-196	-189	12.7	-184.6	-30.1	-36.6	-19.6	124.4	-353
.8	-799	-233	-184	16.3	-219.6	-39.0	-44.2	-21.9	141.6	-333
.85	-848	-268	-178	20.5	-256.8	-49.7	-52.8	-23.1	157.4	-312
.9	-892	-302	-170	24.9	-295.0	-61.7	-62.3	-23.8	171.6	-288
.95	-931	-335	-160	29.3	-333.3	-75.0	-71.1	-23.9	183.3	-261
1.0	-963	-365	-150	33.6	-371.6	-89.6	-79.3	-24.0	192.4	-233
$\frac{3}{12}$	-7	196	-189	-12.7	14.4	30.1	-36.6	19.6	45.8	-399
$\frac{7}{12}$	-525	-67	-198	3.6	-84.4	-8.2	-18.2	-7.4	68.0	-391
$\frac{11}{12}$	-907	-313	-167	26.1	-307.5	-66.0	-64.7	-23.8	175.5	-281

TABLE 17.- Continued

CASCADE DOWNWASH TABLES FOR BLADE ANGLES OF $\beta_B = 90^\circ$ TO 165°

(CORRESPONDING TO STAGGER ANGLES OF $\lambda = 0^\circ$ TO 75°)

AND PITCH RATIO OF $\frac{t}{l} = 2$ TO 0.5

$\beta_B = 135^\circ$				$\lambda = 45^\circ$			$t/l = 0.75$			
$\frac{x}{l}$	$10^3 g_{\gamma 0}$	$10^3 g_{\gamma 1}$	$10^3 g_{\gamma 2}$	$10^3 g_{\gamma 3}$	$10^3 f_{\gamma 0}$	$10^3 f_{\gamma 1}$	$10^3 f_{\gamma 2}$	$10^3 f_{\gamma 3}$	$10^3 g_{q0}$	$10^3 f_{q0}$
0	614	566	-188	-83	158	202	-156	26	246	-518
.05	493	526	-214	-79	132	174	-147	33	216	-559
.1	368	482	-241	-73	107	149	-137	38	191	-596
.15	241	434	-264	-65	85	124	-124	42	163	-627
.2	114	380	-285	-55	63	102	-110	44	141	-646
.25	-24	324	-304	-44	39	81	-94	43	123	-672
.3	-160	263	-319	-34	11	61	-80	40	111	-686
.35	-299	200	-331	-25	-18	44	-67	33	106	-699
.4	-431	135	-340	-16	-53	29	-56	24	111	-701
.45	-559	69	-345	-7	-95	14	-50	12	123	-697
.5	-683	0	-347	0	-142	0	-48	0	142	-683
.55	-800	-69	-345	7	-196	-14	-50	-12	168	-662
.6	-902	-135	-340	16	-254	-29	-56	-24	196	-632
.65	-992	-200	-331	25	-314	-44	-67	-33	226	-592
.7	-1,072	-263	-319	34	-375	-61	-80	-40	253	-546
.75	-1,145	-324	-304	44	-438	-81	-94	-43	276	-497
.8	-1,205	-380	-285	55	-500	-102	-110	-44	296	-445
.85	-1,259	-434	-264	65	-558	-124	-124	-42	310	-391
.9	-1,300	-482	-241	73	-613	-149	-137	-38	315	-336
.95	-1,336	-526	-214	79	-665	-174	-147	-33	317	-284
1.0	-1,367	-566	-188	83	-714	-202	-156	-26	310	-235
$\frac{3}{12}$	-24	324	-304	-44	39	81	-94	43	123	-672
$\frac{7}{12}$	-871	-114	-342	13	-234	-24	-54	-20	186	-643
$\frac{11}{12}$	-1,313	-498	-234	75	-634	-157	-140	-37	320	-317

$\beta_B = 135^\circ$				$\lambda = 45^\circ$			$t/l = 0.5$			
$\frac{x}{l}$	$10^3 g_{\gamma 0}$	$10^3 g_{\gamma 1}$	$10^3 g_{\gamma 2}$	$10^3 g_{\gamma 3}$	$10^3 f_{\gamma 0}$	$10^3 f_{\gamma 1}$	$10^3 f_{\gamma 2}$	$10^3 f_{\gamma 3}$	$10^3 g_{q0}$	$10^3 f_{q0}$
0	1,135	962	-202	-163	424	488	-279	-56	552	-789
.05	904	908	-263	-182	359	439	-285	-30	519	-912
.1	659	844	-326	-195	298	389	-288	-4	480	-1,029
.15	400	770	-392	-198	241	341	-284	23	441	-1,140
.2	131	684	-458	-193	175	293	-273	48	411	-1,237
.25	-135	590	-521	-179	96	245	-256	66	394	-1,315
.3	-401	485	-578	-156	0	197	-238	73	394	-1,371
.35	-655	372	-628	-124	-114	149	-221	70	412	-1,399
.4	-888	252	-671	-87	-241	100	-209	55	441	-1,392
.45	-1,097	127	-695	-46	-374	50	-199	33	474	-1,351
.5	-1,275	0	-704	0	-507	0	-195	0	507	-1,275
.55	-1,431	-127	-695	46	-635	-50	-199	-33	535	-1,177
.6	-1,562	-252	-671	87	-755	-100	-209	-55	555	-1,058
.65	-1,677	-372	-628	124	-864	-149	-221	-70	566	-933
.7	-1,776	-485	-578	156	-963	-197	-238	-73	569	-806
.75	-1,861	-590	-521	179	-1,054	-245	-256	-66	564	-681
.8	-1,935	-684	-458	193	-1,135	-293	-273	-48	549	-567
.85	-1,999	-770	-392	198	-1,210	-341	-284	-23	528	-459
.9	-2,050	-844	-326	195	-1,280	-389	-288	4	502	-362
.95	-2,093	-908	-263	182	-1,346	-439	-285	30	468	-277
1.0	-2,128	-962	-202	162	-1,407	-488	-279	56	431	-204
$\frac{3}{12}$	-135	590	-521	-179	96	245	-256	66	394	-1,315
$\frac{7}{12}$	-1,523	-210	-681	74	-715	-83	-205	-48	550	-1,103
$\frac{11}{12}$	-2,068	-866	-308	192	-1,300	-405	-288	11	490	-336

TABLE 17.- Continued

CASCADE DOWNWASH TABLES FOR BLADE ANGLES OF $\beta_s = 90^o$ TO 165^o

(CORRESPONDING TO STAGGER ANGLES OF $\lambda = 0^o$ TO 75^o)

AND PITCH RATIO OF $\frac{t}{l} = 2$ TO 0.5

$\beta_s = 150^o$				$\lambda = 60^o$				$t/l = 2.0$		
$\frac{x}{l}$	$10^3 g_{\gamma 0}$	$10^3 g_{\gamma 1}$	$10^3 g_{\gamma 2}$	$10^3 g_{\gamma 3}$	$10^3 f_{\gamma 0}$	$10^3 f_{\gamma 1}$	$10^3 f_{\gamma 2}$	$10^3 f_{\gamma 3}$	$10^3 g_{q0}$	$10^3 f_{q0}$
0	92.5	94.9	-50.0	1.1	-47.1	-46.4	20.6	3.3	-45.7	-97.3
.05	73.6	84.8	-49.1	1.2	-38.2	-42.3	21.5	2.7	-46.4	-96.0
.1	55.0	74.9	-48.2	1.2	-28.9	-38.0	22.3	2.2	-47.1	-94.8
.15	36.7	65.1	-47.4	1.2	-19.5	-33.6	22.9	1.7	-47.7	-93.5
.2	18.4	55.5	-46.6	1.1	-9.7	-29.0	23.3	1.3	-48.3	-92.6
.25	.2	46.1	-46.0	1.0	-.2	-24.3	23.7	.9	-48.8	-92.0
.3	-18.4	36.6	-45.3	.8	10.0	-19.6	24.0	.6	-49.2	-91.6
.35	-36.7	27.3	-44.8	.6	19.9	-14.8	24.2	.4	-49.5	-91.3
.4	-54.8	18.2	-44.5	.4	29.8	-9.9	24.3	.2	-49.6	-91.2
.45	-72.9	9.2	-44.3	.2	39.8	-4.9	24.4	.1	-49.6	-91.3
.5	-91.8	0	-44.1	0	49.5	0	24.4	0	-49.5	-91.8
.55	-111.1	-9.2	-44.3	-.2	59.0	4.9	24.4	-.1	-49.2	-92.7
.6	-130.2	-18.2	-44.5	-.4	68.6	9.9	24.3	-.2	-48.8	-93.8
.65	-149.5	-27.3	-44.8	-.6	77.7	14.8	24.2	-.4	-48.1	-94.9
.7	-169.2	-36.6	-45.3	-.8	86.2	19.6	24.0	-.6	-47.0	-96.0
.75	-189.7	-46.1	-46.0	-1.0	94.2	24.3	23.7	-.9	-45.6	-97.5
.8	-210.4	-55.5	-46.6	-1.1	102.1	29.0	23.3	-1.3	-44.1	-99.4
.85	-232.3	-65.1	-47.4	-1.2	109.5	33.6	22.9	-1.7	-42.3	-102.1
.9	-253.2	-74.9	-48.2	-1.2	116.2	38.0	22.3	-2.2	-40.2	-103.4
.95	-274.8	-84.8	-49.1	-1.2	122.1	42.3	21.5	-2.7	-37.5	-105.2
1.0	-296.8	-94.9	-50.0	-1.1	127.3	46.4	20.6	-3.3	-34.5	-107.0
$\frac{3}{12}$	.2	46.1	-46.0	1.0	.2	-24.3	23.7	.9	-48.8	-92.0
$\frac{7}{12}$	-123.6	-15.1	-44.4	-.3	65.3	8.2	24.3	-.1	-48.9	-93.4
$\frac{11}{12}$	-260.4	-78.2	-48.5	-1.2	118.4	39.4	22.0	-2.4	-39.3	-104.0

$\beta_s = 150^o$				$\lambda = 60^o$				$t/l = 1.5$		
$\frac{x}{l}$	$10^3 g_{\gamma 0}$	$10^3 g_{\gamma 1}$	$10^3 g_{\gamma 2}$	$10^3 g_{\gamma 3}$	$10^3 f_{\gamma 0}$	$10^3 f_{\gamma 1}$	$10^3 f_{\gamma 2}$	$10^3 f_{\gamma 3}$	$10^3 g_{q0}$	$10^3 f_{q0}$
0	173.0	176.6	-94.1	3.3	-77.1	-72.2	26.4	9.9	-67.3	-180.2
.05	137.4	157.7	-92.0	3.2	-62.2	-67.1	30.0	8.1	-72.0	-178.0
.1	102.6	138.9	-90.0	2.9	-46.2	-61.2	32.9	6.6	-76.2	-175.2
.15	68.9	120.8	-88.2	2.6	-30.4	-54.7	35.3	5.3	-79.0	-172.7
.2	35.0	102.8	-86.5	2.2	-13.9	-47.6	37.2	4.3	-81.3	-170.6
.25	1.3	85.2	-85.1	1.8	2.7	-40.2	38.7	3.5	-83.1	-169.1
.3	-31.8	67.8	-83.8	1.5	19.0	-32.4	39.7	2.7	-83.8	-167.4
.35	-66.3	50.7	-82.9	1.2	35.4	-24.4	40.5	2.2	-84.2	-167.7
.4	-100.5	33.7	-82.3	.7	51.2	-16.3	41.0	1.5	-83.8	-167.9
.45	-134.6	16.9	-81.9	.5	67.0	-8.2	41.4	.7	-83.4	-168.4
.5	-170.4	0	-81.7	0	82.7	0	41.4	0	-82.7	-170.4
.55	-205.4	-16.9	-81.9	-.5	97.9	8.2	41.4	-.7	-81.5	-171.6
.6	-241.1	-33.7	-82.3	-.7	112.6	16.3	41.0	-1.5	-80.0	-173.7
.65	-278.1	-50.7	-82.9	-1.2	126.7	24.4	40.5	-2.2	-77.9	-176.7
.7	-315.8	-67.8	-83.8	-1.5	139.6	32.4	39.7	-2.7	-74.8	-180.2
.75	-354.7	-85.2	-85.1	-1.8	150.6	40.2	38.7	-3.5	-70.2	-184.3
.8	-394.3	-102.8	-86.5	-2.2	159.9	47.6	37.2	-4.3	-64.7	-198.5
.85	-434.6	-120.8	-88.2	-2.6	167.1	54.7	35.3	-5.3	-57.7	-193.0
.9	-475.5	-138.9	-90.0	-2.9	171.4	61.2	32.9	-6.6	-49.0	-198.3
.95	-517.7	-157.7	-92.0	-3.2	173.1	67.1	30.0	-8.1	-38.9	-202.3
1.0	-559.8	-176.6	-94.1	-3.3	171.9	72.2	29.8	-9.9	-27.5	-206.6
$\frac{3}{12}$	1.3	85.2	-85.1	1.8	2.7	-40.2	38.7	3.5	-83.1	-169.1
$\frac{7}{12}$	-228.0	-28.0	-82.1	-.7	107.5	13.7	41.2	-1.3	-80.1	-172.0
$\frac{11}{12}$	-489.0	-145.2	-90.7	-3.0	172.3	63.2	32.0	-7.1	-45.9	-198.6

TABLE 17.- Continued

CASCADE DOWNWASH TABLES FOR BLADE ANGLES OF $\beta_s = 90^\circ$ TO 165°

(CORRESPONDING TO STAGGER ANGLES OF $\lambda = 0^\circ$ TO 75°)

AND PITCH RATIO OF $\frac{t}{l} = 2$ TO 0.5

$\beta_s = 150^\circ$				$\lambda = 60^\circ$				$t/l = 1.25$		
$\frac{x}{l}$	$10^3 g_{\gamma 0}$	$10^3 g_{\gamma 1}$	$10^3 g_{\gamma 2}$	$10^3 g_{\gamma 3}$	$10^3 f_{\gamma 0}$	$10^3 f_{\gamma 1}$	$10^3 f_{\gamma 2}$	$10^3 f_{\gamma 3}$	$10^3 g_{q0}$	$10^3 f_{q0}$
0	254.7	261.4	-140.5	4.2	-100.5	-88.4	20.5	23.8	-76.3	-268.1
.05	202.8	233.4	-137.9	5.4	-81.6	-84.6	29.2	19.9	-87.6	-264.0
.1	152.2	205.7	-134.8	5.7	-61.0	-79.1	36.5	16.4	-97.2	-259.2
.15	102.1	178.5	-131.7	5.6	-39.4	-72.1	42.7	13.1	-104.8	-254.9
.2	52.7	151.8	-128.7	5.0	-17.3	-63.9	47.6	10.4	-110.5	-250.9
.25	3.6	125.6	-126.0	4.5	5.2	-54.6	51.4	8.0	-114.4	-247.6
.3	-46.1	99.9	-123.6	3.6	27.6	-44.6	54.3	5.9	-116.8	-245.9
.35	-96.3	74.5	-121.7	2.8	50.1	-33.9	56.2	4.2	-117.9	-245.3
.4	-146.8	49.5	-120.4	1.7	72.3	-22.8	57.5	2.7	-117.0	-245.8
.45	-197.7	24.7	-119.6	.9	94.4	-11.5	58.2	1.3	-117.4	-247.1
.5	-249.2	0	-119.5	0	115.6	0	58.5	0	-115.6	-249.2
.55	-301.9	-24.7	-119.6	-.9	135.4	11.5	58.2	-1.3	-112.4	-252.5
.6	-356.6	-49.5	-120.4	-1.7	153.6	22.8	57.5	-2.7	-108.0	-257.6
.65	-412.4	-74.5	-121.7	-2.8	169.1	33.9	56.2	-4.2	-101.3	-263.4
.7	-469.4	-99.9	-123.6	-3.6	181.3	44.6	54.3	-5.9	-92.1	-269.6
.75	-527.8	-125.6	-126.0	-4.5	189.4	54.6	51.4	-8.0	-80.2	-276.6
.8	-587.0	-151.8	-128.7	-5.0	193.7	63.9	47.6	-10.4	-65.9	-283.4
.85	-646.8	-178.5	-131.7	-5.6	192.7	72.1	42.7	-13.1	-48.5	-289.8
.9	-706.6	-205.7	-134.8	-5.7	186.2	79.1	36.2	-16.4	-28.0	-295.2
.95	-765.0	-233.4	-137.9	-5.4	174.3	84.6	29.2	-19.9	-5.1	-298.2
1.0	-820.5	-261.4	-140.5	-4.2	157.1	88.4	20.5	-23.8	19.7	-297.7
$\frac{3}{12}$	3.6	125.6	-126.0	4.5	5.2	-54.6	51.4	8.0	-114.4	-247.6
$\frac{7}{12}$	-336.0	-41.5	-120.2	-1.6	146.1	19.0	58.0	-2.2	-108.1	-253.0
$\frac{11}{12}$	-726.0	-215.0	-135.7	-5.6	183.0	81.0	34.2	-17.5	-21.0	-296.0

$\beta_s = 150^\circ$				$\lambda = 60^\circ$				$t/l = 1.0$		
$\frac{x}{l}$	$10^3 g_{\gamma 0}$	$10^3 g_{\gamma 1}$	$10^3 g_{\gamma 2}$	$10^3 g_{\gamma 3}$	$10^3 f_{\gamma 0}$	$10^3 f_{\gamma 1}$	$10^3 f_{\gamma 2}$	$10^3 f_{\gamma 3}$	$10^3 g_{q0}$	$10^3 f_{q0}$
0	399	411	-214	-10	-126.4	-92.1	-18.3	57.6	-57.8	-423
.05	320	370	-216	-2	-103.6	-94.7	2.6	53.0	-85.8	-420
.1	242	328	-216	5	-76.8	-95.1	21.3	46.6	-113.3	-414
.15	165	286	-213	9	-49.0	-91.7	38.6	39.3	-134.4	-407
.2	88	244	-209	11	-17.5	-84.6	53.0	32.0	-151.8	-400
.25	10	202	-203	12	16.0	-74.7	65.0	25.3	-165.4	-394
.3	-68	161	-199	11	48.5	-62.8	74.5	19.1	-174.1	-390
.35	-150	119	-195	9	82.5	-48.2	81.7	13.7	-178.9	-388
.4	-231	79	-191	6	113.4	-33.3	86.5	8.8	-179.9	-389
.45	-314	39	-190	3	142.7	-16.8	89.3	4.3	-176.3	-392
.5	-398	0	-189	0	169.0	0	90.4	0	-169.0	-398
.55	-483	-39	-190	-3	190.8	16.8	89.3	-4.3	-157.2	-405
.6	-573	-79	-191	-6	206.0	33.3	86.5	-8.8	-139.5	-415
.65	-665	-119	-195	-9	212.7	48.2	81.7	-13.7	-116.3	-427
.7	-759	-161	-199	-11	213.7	62.8	74.5	-19.1	-88.1	-437
.75	-848	-202	-203	-12	202.2	74.7	65.0	-25.3	-52.8	-444
.8	-935	-244	-209	-11	182.5	84.6	53.0	-32.0	-13.2	-447
.85	-1,014	-286	-213	-9	153.9	91.7	38.6	-39.3	30.5	-442
.9	-1,086	-328	-216	-5	115.7	95.1	21.3	-46.6	74.8	-430
.95	-1,149	-370	-216	2	64.5	94.7	2.6	-53.0	124.9	-409
1.0	-1,202	-411	-214	10	19.6	92.1	-18.3	-57.5	164.6	-380
$\frac{3}{12}$	10	202	-203	12	16.0	-74.7	65.0	25.3	-165.4	-394
$\frac{7}{12}$	-542	-65	-191	-5	200.6	27.7	87.7	-7.3	-145.2	-412
$\frac{11}{12}$	-1,107	-342	-216	-2	98.4	95.3	15.3	-48.8	92.2	-423

TABLE 17.- Continued

CASCADE DOWNWASH TABLES FOR BLADE ANGLES OF $\beta_s = 90^\circ$ TO 165°

(CORRESPONDING TO STAGGER ANGLES OF $\lambda = 0^\circ$ TO 75°)

AND PITCH RATIO OF $\frac{t}{l}$ = 2 TO 0.5

$\beta_s = 150^\circ$			$\lambda = 60^\circ$				$t/l = 0.75$			
$\frac{x}{l}$	$10^3 g_{\gamma 0}$	$10^3 g_{\gamma 1}$	$10^3 g_{\gamma 2}$	$10^3 g_{\gamma 3}$	$10^3 f_{\gamma 0}$	$10^3 f_{\gamma 1}$	$10^3 f_{\gamma 2}$	$10^3 f_{\gamma 3}$	$10^3 g_{q0}$	$10^3 f_{q0}$
0	682	674	-281	-96	-128	-37.6	-127.9	91.7	53	-666
.05	553	620	-310	-73	-101	-55.7	-95.4	104.9	-10	-687
.1	428	564	-334	-50	-69	-70.2	-60.6	110.2	-71	-700
.15	296	502	-351	-27	-31	-79.2	-23.6	108.0	-128	-708
.2	160	436	-360	-7	11	-83.3	14.7	99.1	-177	-712
.25	21	368	-364	6	56	-81.1	50.5	85.7	-218	-715
.3	-124	296	-363	15	101	-73.6	80.7	69.3	-248	-716
.35	-274	222	-360	16	143	-60.6	105.6	51.3	-264	-718
.4	-425	149	-356	14	180	-43.2	124.8	33.4	-267	-723
.45	-585	74	-353	8	209	-22.5	135.8	16.1	-254	-733
.5	-747	0	-351	0	224	0	139.7	0	-224	-747
.55	-907	-74	-353	-8	221	22.5	135.8	-16.1	-176	-760
.6	-1,063	-149	-356	-14	199	43.2	124.8	-33.4	-113	-765
.65	-1,201	-222	-360	-16	158	60.6	105.6	-51.3	-37	-757
.7	-1,321	-296	-363	-15	102	73.6	80.7	-69.3	45	-729
.75	-1,429	-368	-364	-6	37	81.1	50.5	-85.7	125	-693
.8	-1,511	-436	-360	7	-33	83.3	14.7	-99.1	199	-639
.85	-1,576	-502	-351	27	-102	79.2	-23.6	-108.0	260	-572
.9	-1,624	-564	-334	50	-166	70.2	-60.6	-110.2	306	-496
.95	-1,658	-620	-310	73	-224	55.7	-95.4	-104.9	335	-418
1.0	-1,689	-674	-281	96	-274	37.6	-127.9	-91.7	349	-341
$\frac{3}{12}$	21	368	-364	6	56	-81.1	50.5	85.7	-218	-715
$\frac{7}{12}$	-1,010	-123	-355	-12	208	36.4	129.7	-27.4	-135	-764
$\frac{11}{12}$	-1,639	-583	-327	57	-186	65.8	-72.5	-109.4	318	-473

$\beta_s = 150^\circ$			$\lambda = 60^\circ$				$t/l = 0.5$			
$\frac{x}{l}$	$10^3 g_{\gamma 0}$	$10^3 g_{\gamma 1}$	$10^3 g_{\gamma 2}$	$10^3 g_{\gamma 3}$	$10^3 f_{\gamma 0}$	$10^3 f_{\gamma 1}$	$10^3 f_{\gamma 2}$	$10^3 f_{\gamma 3}$	$10^3 g_{q0}$	$10^3 f_{q0}$
0	1,300	1,160	-284	-243	-47	145	-284	-4	337	-1,020
.05	1,053	1,090	-358	-252	-11	107	-266	51	226	-1,127
.1	802	1,012	-432	-248	42	75	-236	106	108	-1,222
.15	533	922	-505	-228	104	48	-194	156	-8	-1,311
.2	252	824	-575	-196	168	27	-141	194	-114	-1,396
.25	-49	714	-639	-157	224	12	-81	217	-200	-1,477
.3	-371	593	-697	-113	262	3	-16	218	-256	-1,557
.35	-714	458	-745	-74	265	-1	46	196	-267	-1,630
.4	-1,044	314	-784	-41	219	-2	100	148	-223	-1,672
.45	-1,348	160	-809	-17	129	-1	136	80	-131	-1,668
.5	-1,605	0	-818	0	9	0	149	0	-9	-1,605
.55	-1,807	-160	-809	17	-117	1	136	-80	119	-1,487
.6	-1,963	-314	-784	41	-231	2	100	-148	235	-1,335
.65	-2,083	-458	-745	74	-325	1	46	-196	327	-1,167
.7	-2,184	-593	-697	113	-401	-3	-16	-218	395	-998
.75	-2,276	-714	-639	157	-465	-12	-81	-217	441	-848
.8	-2,353	-824	-575	196	-525	-27	-141	-194	471	-705
.85	-2,426	-922	-505	228	-570	-48	-194	-156	484	-582
.9	-2,487	-1,012	-432	248	-633	-75	-236	-106	483	-463
.95	-2,544	-1,090	-358	252	-688	-107	-266	-51	473	-364
1.0	-2,589	-1,160	-284	243	-745	-145	-284	4	454	-269
$\frac{3}{12}$	-49	714	-639	-157	224	12	-81	217	-200	-1,477
$\frac{7}{12}$	-1,911	-262	-794	32	-196	2	114	-126	200	-1,387
$\frac{11}{12}$	-2,506	-1,039	-408	251	-651	-85	-248	-87	481	-428

TABLE 17.- Continued

CASCADE DOWNWASH TABLES FOR BLADE ANGLES OF $\beta_B = 90^\circ$ TO 165°

(CORRESPONDING TO STAGGER ANGLES OF $\lambda = 0^\circ$ TO 75°)

AND PITCH RATIO OF $\frac{t}{l}$ = 2 TO 0.5

$\beta_B = 165^\circ$	$\lambda = 75^\circ$	$t/l = 2.0$								
$\frac{x}{l}$	$10^3 g_{\gamma 0}$	$10^3 g_{\gamma 1}$	$10^3 g_{\gamma 2}$	$10^3 g_{\gamma 3}$	$10^3 f_{\gamma 0}$	$10^3 f_{\gamma 1}$	$10^3 f_{\gamma 2}$	$10^3 f_{\gamma 3}$	$10^3 g_{q0}$	$10^3 f_{q0}$
0	56.3	58.5	-32.8	2.9	-91.2	-92.2	47.0	0.1	-93.2	-60.7
.05	44.8	51.8	-31.3	2.4	-72.8	-82.6	46.5	.1	-92.4	-58.8
.1	33.6	45.4	-30.1	2.0	-54.6	-73.2	46.0	.1	-91.8	-57.2
.15	22.5	39.2	-29.1	1.6	-36.5	-63.9	45.6	.1	-91.3	-55.9
.2	11.5	33.2	-28.2	1.2	-18.3	-54.6	45.3	0	-90.9	-54.9
.25	.6	27.4	-27.5	1.0	-.2	-45.4	44.9	0	-90.6	-54.2
.3	-10.3	21.8	-27.0	.7	18.1	-36.3	44.7	-.1	-90.7	-53.9
.35	-21.2	16.3	-26.6	.5	36.3	-27.2	44.5	-.1	-90.7	-53.8
.4	-32.2	10.8	-26.3	.3	54.6	-18.1	44.4	-.1	-90.8	-53.8
.45	-43.2	5.4	-26.2	.1	73.0	-9.0	44.3	0	-91.0	-54.0
.5	-54.4	0	-26.1	0	91.3	0	44.3	0	-91.3	54.4
.55	-66.0	-5.4	-26.2	-.1	109.8	9.0	44.3	0	-91.8	-55.2
.6	-77.6	-10.8	-26.3	-.3	128.5	18.1	44.4	.1	-92.3	-56.0
.65	-89.9	-16.3	-26.6	-.5	147.2	27.2	44.5	.1	-92.8	-57.3
.7	-102.7	-21.8	-27.0	-.7	165.9	36.3	44.7	.1	-93.3	-59.1
.75	-116.0	-27.4	-27.5	-1.0	185.0	45.4	44.9	0	-94.2	-61.2
.8	-130.1	-33.2	-28.2	-1.2	204.6	54.6	45.3	0	-95.4	-63.7
.85	-145.0	-39.2	-29.1	-1.6	224.2	63.9	45.6	-.1	-96.4	-66.6
.9	-160.7	-45.4	-30.1	-2.0	244.1	73.2	46.0	-.1	-97.7	-69.9
.95	-177.3	-51.8	-31.3	-2.4	264.2	82.6	46.5	-.1	-99.0	-73.7
1.0	-195.2	-58.5	-32.8	-2.9	284.6	92.2	47.0	-.1	-100.2	-78.2
$\frac{3}{12}$	.6	27.4	-27.5	1.0	-.2	-45.4	44.9	0	-90.6	-54.2
$\frac{7}{12}$	-73.5	-9.0	-26.3	-.3	122.0	15.0	44.3	0	-92.0	-55.5
$\frac{11}{12}$	-166.5	-47.2	-30.7	-2.2	251.0	76.3	46.1	-.1	-98.4	-72.1

$\beta_B = 165^\circ$	$\lambda = 75^\circ$	$t/l = 1.5$								
$\frac{x}{l}$	$10^3 g_{\gamma 0}$	$10^3 g_{\gamma 1}$	$10^3 g_{\gamma 2}$	$10^3 g_{\gamma 3}$	$10^3 f_{\gamma 0}$	$10^3 f_{\gamma 1}$	$10^3 f_{\gamma 2}$	$10^3 f_{\gamma 3}$	$10^3 g_{q0}$	$10^3 f_{q0}$
0	109.8	118.2	-74.1	13.3	-165.0	-167.6	86.8	-0.6	-170.2	-126.6
.05	87.1	102.9	-68.1	10.9	-132.0	-150.2	85.6	-.8	-168.4	-118.7
.1	65.2	88.9	-63.1	9.0	-98.9	-132.8	84.5	-1.0	-166.7	-112.6
.15	44.0	75.9	-59.1	7.3	-66.2	-115.7	83.3	-1.0	-165.2	-107.8
.2	23.2	63.6	-55.8	5.9	-33.5	-98.8	82.3	-1.0	-164.1	-104.0
.25	2.6	52.1	-53.2	4.6	-.6	-82.1	81.5	-.8	-163.6	-101.6
.3	-17.7	41.0	-51.1	3.4	32.2	-65.4	80.7	-.6	-163.0	-99.7
.35	-37.7	30.4	-49.6	2.4	64.8	-49.0	80.2	-.5	-162.8	-98.5
.4	-58.2	20.1	-48.3	1.5	97.9	-32.6	79.7	-.3	-163.1	-98.4
.45	-79.2	10.0	-47.9	.7	131.1	-16.3	79.6	-.1	-163.7	-99.2
.5	-100.8	0	-47.6	0	164.2	0	79.5	0	-164.2	-100.8
.55	-123.9	-10.0	-47.9	-.7	197.8	16.3	79.6	.1	-165.2	-103.9
.6	-148.1	-20.1	-48.3	-1.5	232.1	32.6	79.7	.3	-166.9	-107.9
.65	-173.7	-30.4	-49.6	-2.4	266.8	49.0	80.2	.5	-168.8	-112.9
.7	-201.4	-41.0	-51.1	-3.4	302.0	65.4	80.7	.6	-171.2	-119.4
.75	-231.2	-52.1	-53.2	-4.6	337.7	82.1	81.5	.8	-173.5	-127.0
.8	-263.3	-63.6	-55.8	-5.9	373.3	98.8	82.4	1.0	-175.7	-136.1
.85	-298.9	-75.9	-59.1	-7.3	409.9	115.7	83.3	1.0	-178.5	-147.1
.9	-339.1	-88.9	-63.1	-9.0	446.7	132.8	84.5	1.0	-181.1	-161.3
.95	-384.0	-102.9	-68.1	-10.9	483.2	150.2	85.6	.8	-182.8	-178.2
1.0	-433.6	-118.2	-74.1	-13.3	519.4	167.6	86.8	.6	-184.2	-197.2
$\frac{3}{12}$	2.6	52.1	-53.2	4.6	-.6	-82.1	81.5	-.8	-163.6	-101.6
$\frac{7}{12}$	-139.0	-16.8	-48.2	-1.2	220.5	27.3	79.7	.2	-165.9	-105.4
$\frac{11}{12}$	-354.0	-93.5	-65.0	-9.6	459.0	138.5	84.8	.9	-182.0	-167.0

TABLE 17.- Continued

CASCADE DOWNWASH TABLES FOR BLADE ANGLES OF $\beta_s = 90^o$ TO 165^o

(CORRESPONDING TO STAGGER ANGLES OF $\lambda = 0^o$ TO 75^o)

AND PITCH RATIO OF $\frac{t}{l} = 2$ TO 0.5

$\beta_s = 165^o$ $\lambda = 75^o$ $t/l = 1.25$										
$\frac{x}{l}$	$10^3 g_{\gamma 0}$	$10^3 g_{\gamma 1}$	$10^3 g_{\gamma 2}$	$10^3 g_{\gamma 3}$	$10^3 f_{\gamma 0}$	$10^3 f_{\gamma 1}$	$10^3 f_{\gamma 2}$	$10^3 f_{\gamma 3}$	$10^3 g_{q0}$	$10^3 f_{q0}$
0	175.5	195.9	-135.2	34.5	-239.2	-242.6	123.4	4.0	-246.0	-216.3
.05	138.3	167.8	-120.5	28.6	-192.0	-218.6	124.5	.5	-245.2	-197.3
.1	103.1	142.6	-108.3	23.3	-144.7	-193.9	123.9	-1.5	-243.1	-182.1
.15	70.0	120.0	-98.4	18.9	-97.0	-169.1	122.5	-2.2	-241.2	-170.0
.2	38.0	99.4	-90.1	14.7	-49.1	-144.2	120.8	-2.4	-239.3	-160.8
.25	6.8	80.4	-83.7	11.2	-1.6	-119.7	119.3	-2.1	-237.8	-154.0
.3	-23.8	62.9	-78.9	8.5	46.0	-95.4	117.9	-1.8	-236.8	-149.6
.35	-54.6	46.4	-75.3	6.0	93.7	-71.4	116.8	-1.4	-236.5	-147.4
.4	-85.9	30.5	-72.8	3.9	141.9	-47.4	115.9	-.9	-236.7	-146.9
.45	-118.5	15.1	-71.3	1.9	189.9	-23.7	115.5	-.4	-237.3	-148.7
.5	-153.0	0	-70.8	0	239.0	0	115.1	0	-239.0	-153.0
.55	-189.8	-15.1	-71.3	-1.9	289.0	23.7	115.5	.4	-241.6	159.6
.6	-229.6	-30.5	-72.8	-3.9	340.4	47.4	115.9	.9	-245.6	-168.6
.65	-273.0	-46.4	-75.3	-6.0	390.9	71.4	116.8	1.4	-248.1	-180.2
.7	-320.7	-62.9	-78.9	-8.5	442.3	95.4	117.9	1.8	-251.5	-194.9
.75	-375.5	-80.4	-83.7	-11.2	494.8	119.7	119.3	2.1	-255.4	-214.7
.8	-438.6	-99.4	-90.1	-14.7	547.1	144.2	120.8	2.4	-258.7	-239.8
.85	-507.5	-120.0	-98.4	-18.9	597.9	169.1	122.5	2.2	-259.7	-267.5
.9	-585.6	-142.6	-108.3	-23.3	644.5	193.9	123.9	1.5	-256.7	-300.4
.95	-677.1	-167.8	-120.5	-28.6	683.3	218.6	124.5	-.5	-246.1	-341.5
1.0	-781.9	-195.9	-135.2	-34.5	709.1	242.6	123.4	-4.0	-223.9	-390.1
$\frac{3}{12}$	6.8	80.4	-83.7	11.2	-1.6	-119.7	119.3	-2.1	-237.8	-154.0
$\frac{7}{12}$	-214.0	-25.5	-72.3	-3.3	323.0	39.9	115.6	.8	-243.2	-163.0
$\frac{11}{12}$	-615.0	-150.8	-112.2	-25.0	660.0	201.9	124.1	1.0	-256.2	-313.4

$\beta_s = 165^o$ $\lambda = 75^o$ $t/l = 1.0$										
$\frac{x}{l}$	$10^3 g_{\gamma 0}$	$10^3 g_{\gamma 1}$	$10^3 g_{\gamma 2}$	$10^3 g_{\gamma 3}$	$10^3 f_{\gamma 0}$	$10^3 f_{\gamma 1}$	$10^3 f_{\gamma 2}$	$10^3 f_{\gamma 3}$	$10^3 g_{q0}$	$10^3 f_{q0}$
0	329.5	386.8	-296.7	88.9	-352.5	-338.1	123.4	76.1	-323.7	-444.1
.05	259.7	328.0	-263.8	84.4	-290.0	-320.6	155.1	45.2	-351.2	-396.3
.1	194.4	273.9	-230.8	73.4	-222.3	-294.4	174.5	22.9	-366.5	-353.4
.15	133.1	225.2	-200.7	59.7	-151.5	-263.0	185.4	7.9	-374.5	-317.3
.2	75.7	182.4	-175.8	46.8	-78.3	-227.4	189.2	-.1	-376.5	-289.1
.25	21.2	144.7	-156.0	35.4	-4.2	-190.1	189.4	-3.5	-376.0	-268.2
.3	-31.8	111.3	-141.4	26.6	71.2	-151.8	187.6	-4.4	-374.8	-254.4
.35	-85.2	80.9	-130.3	18.6	146.8	-113.7	185.7	-3.8	-374.2	-247.0
.4	-140.8	52.6	-122.7	11.7	223.8	-75.6	183.7	-2.8	-375.0	-246.0
.45	-199.4	26.0	-118.6	5.7	302.1	-37.8	182.9	-1.5	-377.7	-251.4
.5	-263.1	0	-117.1	0	381.2	0	182.3	0	-381.2	-263.1
.55	-333.2	-26.0	-118.6	-5.7	461.4	37.8	182.9	1.5	-385.8	-281.2
.6	-413.9	-52.6	-122.7	-11.7	542.2	75.6	183.7	2.8	-391.0	-308.7
.65	-508.3	-80.9	-130.3	-18.6	623.4	113.7	185.7	3.8	-396.0	-346.5
.7	-614.1	-111.3	-141.4	-26.6	700.4	151.8	187.6	4.4	-396.8	-391.5
.75	-740.6	-144.7	-156.0	-35.4	766.9	190.1	189.4	3.5	-386.7	-451.2
.8	-891.7	-182.4	-175.8	-46.8	812.7	227.4	189.2	.1	-357.9	-526.9
.85	-1,059.7	-225.2	-200.7	-59.7	825.2	263.0	185.4	-7.9	-299.2	-609.3
.9	-1,235.5	-273.9	-230.8	-73.4	798.8	294.4	174.5	-22.9	-210.0	-687.7
.95	-1,400.2	-328.0	-263.8	-84.4	726.8	320.6	155.1	-45.2	-85.6	-744.2
1.0	-1,533.3	-386.8	-296.7	-88.9	616.3	338.1	123.4	-76.1	59.9	-759.7
$\frac{3}{12}$	21.2	144.7	-156.0	35.4	-4.2	-190.1	189.4	-3.5	-376.0	-268.2
$\frac{7}{12}$	-384.0	-43.7	-121.0	-9.6	515.0	63.1	183.3	2.5	-388.8	-296.6
$\frac{11}{12}$	-1,295.0	-291.2	-241.3	-77.4	778.0	304.5	169.0	-29.2	-169.0	-712.6

TABLE 17.- Concluded

CASCADE DOWNWASH TABLES FOR BLADE ANGLES OF $\beta_s = 90^\circ$ TO 165°

(CORRESPONDING TO STAGGER ANGLES OF $\lambda = 0^\circ$ TO 75°)

AND PITCH RATIO OF $\frac{t}{l}$ = 2 TO 0.5

$\beta_s = 165^\circ$ $\lambda = 75^\circ$ $t/l = 0.75$										
$\frac{x}{l}$	$10^3 g_{\gamma 0}$	$10^3 g_{\gamma 1}$	$10^3 g_{\gamma 2}$	$10^3 g_{\gamma 3}$	$10^3 f_{\gamma 0}$	$10^3 f_{\gamma 1}$	$10^3 f_{\gamma 2}$	$10^3 f_{\gamma 3}$	$10^3 g_{q0}$	$10^3 f_{q0}$
0	657.2	739.8	-446.4	-75.2	-455.8	-327.5	-109.4	279	-199.2	-822.4
.05	543.9	672.7	-474.9	4.1	-380.0	-343.9	-27.5	273	-307.8	-801.5
.1	430.7	598.9	-484.5	74.3	-295.8	-351.2	58.0	241	-406.6	-767.1
.15	316.6	517.7	-470.9	121.8	-203.2	-349.4	143.2	187	-495.6	-718.8
.2	202.0	432.2	-438.3	143.3	-99.5	-333.3	216.4	126	-567.1	-662.4
.25	86.2	345.3	-391.2	136.2	13.7	-302.6	272.5	70	-618.9	-604.4
.3	-31.7	262.1	-340.5	111.1	137.7	-257.4	308.0	29	-652.5	-555.9
.35	-152.9	186.5	-296.8	80.0	271.2	-200.7	326.1	6	-672.6	-525.9
.4	-280.1	119.0	-264.8	49.9	409.8	-136.5	332.0	-2	-682.8	-518.1
.45	-422.5	58.0	-246.5	24.3	552.8	-68.9	332.9	-3	-690.6	-538.5
.5	-588.4	0	-240.6	0	695.9	0	332.6	0	-695.9	-588.4
.55	-783.0	-58.0	-246.5	-24.3	825.5	68.9	332.9	3	-687.7	-667.0
.6	-1,023.3	-119.0	-264.8	-49.9	919.8	136.5	332.0	2	-646.8	-785.3
.65	-1,300.2	-186.5	-296.8	-80.0	945.8	200.7	326.1	-6	-544.4	-927.2
.7	-1,577.6	-262.1	-340.5	-111.1	882.6	257.4	308.0	-29	-367.8	-1,053.4
.75	-1,805.8	-345.3	-391.2	-136.2	741.2	302.6	272.5	-70	-136.0	-1,115.2
.8	-1,936.9	-432.2	-438.3	-143.3	558.5	333.3	216.4	-126	108.1	-1,072.5
.85	-1,986.0	-517.7	-470.9	-121.8	374.8	349.4	143.2	-187	324.0	-950.6
.9	-1,982.6	-598.9	-484.5	-74.3	233.6	351.2	58.0	-241	468.8	-784.8
.95	-1,950.9	-672.7	-474.9	-4.1	144.7	343.9	-27.5	-273	543.1	-605.5
1.0	-1,917.5	-739.8	-446.4	75.2	88.5	327.5	-109.4	-279	566.5	-437.9
$\frac{3}{12}$	86.2	345.3	-391.2	136.2	13.7	-302.6	272.5	70	-618.9	-604.4
$\frac{7}{12}$	-932.0	-98.0	-257.5	-41.2	889.0	114.8	332.4	3	-659.4	-736.0
$\frac{11}{12}$	-1,978.0	-624.0	-483.0	-50.8	200.0	349.9	29.0	-254	499.8	-730.0

$\beta_s = 165^\circ$ $\lambda = 75^\circ$ $t/l = 0.5$										
$\frac{x}{l}$	$10^3 g_{\gamma 0}$	$10^3 g_{\gamma 1}$	$10^3 g_{\gamma 2}$	$10^3 g_{\gamma 3}$	$10^3 f_{\gamma 0}$	$10^3 f_{\gamma 1}$	$10^3 f_{\gamma 2}$	$10^3 f_{\gamma 3}$	$10^3 g_{\gamma 0}$	$10^3 f_{\gamma 0}$
0	1,313	1,265	-367.7	-367.9	-583.9	-259.7	-294.7	42.8	64.5	-1,216
.05	1,099	1,182	-448.5	-370.6	-445.2	-280.3	-251.5	148.9	-115.4	-1,266
.1	884	1,092	-527.6	-337.5	-285.6	-288.5	-196.2	256.3	-291.4	-1,301
.15	671	1,001	-604.7	-272.4	-108.4	-289.7	-120.6	349.2	-471.0	-1,331
.2	442	901	-674.7	-177.6	88.1	-281.0	-28.7	418.5	-650.1	-1,360
.25	190	796	-736.5	-68.3	303.5	-265.7	86.1	446.0	-834.9	-1,402
.3	-112	676	-780.7	39.8	537.5	-239.8	215.7	433.9	-1,017.1	-1,464
.35	-483	543	-811.8	122.5	777.6	-201.8	357.3	371.4	-1,181.2	-1,569
.4	-973	386	-820.1	153.6	963.5	-148.8	497.4	272.1	-1,261.1	-1,746
.45	-1,560	204	-821.2	109.6	985.7	-79.9	609.1	142.8	-1,145.5	-1,969
.5	-2,078	0	-817.9	0	785.6	0	654.1	0	-785.6	-2,078
.55	-2,358	-204	-821.2	-109.6	476.5	79.9	609.1	-142.8	-316.7	-1,949
.6	-2,429	-386	-820.1	-153.6	245.8	148.8	497.4	-272.1	51.8	-1,656
.65	-2,427	-543	-811.8	-122.5	138.6	201.8	357.3	-371.4	265.0	-1,340
.7	-2,418	-676	-780.7	-39.8	113.5	239.8	215.7	-433.9	366.1	-1,066
.75	-2,444	-796	-736.5	68.3	125.0	265.7	86.1	-446.0	406.4	-853
.8	-2,502	-901	-674.7	177.6	163.3	281.0	-28.7	-418.5	398.7	-700
.85	-2,598	-1,001	-604.7	272.4	201.6	289.7	-120.6	-349.2	377.8	-597
.9	-2,715	-1,092	-527.6	337.5	203.0	288.5	-196.2	-256.3	374.0	-531
.95	-2,839	-1,182	-448.5	370.6	166.6	280.3	-251.5	-148.9	394.0	-474
1.0	-2,940	-1,265	-367.7	367.9	90.9	259.7	-294.7	-42.8	428.5	-410
$\frac{3}{12}$	190	796	-736.5	-68.3	303.5	-265.7	86.1	446.0	-834.9	-1,402
$\frac{7}{12}$	-2,415	-331	821.0	-147.5	318.0	128.1	542.5	-231.0	-61.8	-1,753
$\frac{11}{12}$	-2,755	-1,122	-502.0	353.0	194.0	287.0	-217.5	-220.5	380.0	-511

TABLE 18

TABLES OF THE RESULTING DOWNWASH FUNCTIONS ACCORDING TO EQUATION (65) FOR THE THREE CONTROL POINTS

β_s, deg	λ, deg	$\frac{x}{l}$	t/l = 2.0 $10^3f^*_{\gamma 0}$	$10^3f^*_{\gamma 1}$	$10^3f^*_{\gamma 2}$	$10^3f^*_{\gamma 3}$	$10^3g^*_{q0}$	t/l = 1.5 $10^3f^*_{\gamma 0}$	$10^3f^*_{\gamma 1}$	$10^3f^*_{\gamma 2}$	$10^3f^*_{\gamma 3}$	$10^3g^*_{q0}$	t/l = 1.25 $10^3f^*_{\gamma 0}$	$10^3f^*_{\gamma 1}$	$10^3f^*_{\gamma 2}$	$10^3f^*_{\gamma 3}$	$10^3g^*_{q0}$
90	0	$\frac{3}{12}$	-1,001	549	-548	-1,002	2,100	-1,004	585	-582	-1,005	2,174	-1,007	619	-615	-1,009	2,244
		$\frac{7}{12}$	-1,131	-183	-994	483	765	-1,226	-195	-1,030	483	836	-1,320	-207	-1,065	485	905
		$\frac{11}{12}$	-1,250	-914	343	188	-578	-1,418	-971	313	193	-524	-1,573	-1,025	286	198	-477
105 or 75	±15	$\frac{3}{12}$	-1,001	543	-542	-1,001	2,087	-1,002	576	-574	-1,003	2,153	-1,004	607	-604	-1,006	2,218
		$\frac{7}{12}$	-1,116	-181	-987	482	754	-1,203	-192	-1,020	483	819	-1,286	-203	-1,052	484	881
		$\frac{11}{12}$	-1,224	-905	348	187	-585	-1,382	-957	319	191	-532	-1,526	-1,007	293	195	-488
120 or 60	±30	$\frac{3}{12}$	-1,000	526	-526	-1,000	2,052	-1,000	548	-548	-1,000	2,097	-1,000	570	-570	-999	2,140
		$\frac{7}{12}$	-1,070	-175	-970	482	720	-1,129	-183	-991	482	764	-1,190	-190	-1,013	481	809
		$\frac{11}{12}$	-1,146	-878	362	185	-610	-1,267	-915	340	185	-563	-1,386	-952	317	185	-518
135 or 45	±45	$\frac{3}{12}$	-1,000	502	-503	-999	2,004	-998	506	-508	-996	2,011	-994	512	-516	991	2,020
		$\frac{7}{12}$	-1,005	-167	-946	481	671	-1,017	-168	-948	480	681	-1,035	-170	-952	479	695
		$\frac{11}{12}$	-1,026	-838	384	183	-651	-1,080	-848	374	178	-617	-1,154	-863	358	172	-573
150 or 30	±60	$\frac{3}{12}$	-1,000	476	-476	-999	1,951	-997	460	461	-1,000	1,917	-995	445	449	-992	1,886
		$\frac{7}{12}$	-935	-159	-920	-481	618	-893	-153	-903	480	587	-854	-148	-886	479	558
		$\frac{11}{12}$	-882	-794	411	183	-706	-828	-770	421	178	-713	-817	-752	423	168	-688
165 or 15	±75	$\frac{3}{12}$	-1,000	455	-455	-1,000	1,909	-1,001	418	-419	-1,001	1,836	-1,002	380	-381	-1,002	1,762
		$\frac{7}{12}$	-878	-152	-900	482	575	-780	-139	-865	482	501	-677	-127	-829	482	424
		$\frac{11}{12}$	-749	-757	435	185	-765	-1,541	-695	-474	186	-849	-340	-631	513	186	-923

β_s, deg	γ, deg	$\frac{x}{l}$	t/l = 1.0 $10^3f^*_{\gamma 0}$	$10^3f^*_{\gamma 1}$	$10^3f^*_{\gamma 2}$	$10^3f^*_{\gamma 3}$	$10^3g^*_{q0}$	t/l = 0.75 $10^3f^*_{\gamma 0}$	$10^3f^*_{\gamma 1}$	$10^3f^*_{\gamma 2}$	$10^3f^*_{\gamma 3}$	$10^3g^*_{q0}$	t/l = 0.5 $10^3f^*_{\gamma 0}$	$10^3f^*_{\gamma 1}$	$10^3f^*_{\gamma 2}$	$10^3f^*_{\gamma 3}$	$10^3g^*_{q0}$
90	0	$\frac{3}{12}$	-1,008	682	-670	-1,019	2,372	-1,035	794	-776	-1,045	2,623	-1,118	1,059	-1,011	-1,133	3,236
		$\frac{7}{12}$	-1,476	-228	-1,129	489	1,021	-1,778	-269	-1,257	500	1,241	-2,457	-362	-1,567	539	1,734
		$\frac{11}{12}$	-1,830	-1,122	242	210	-415	-2,271	-1,292	171	240	-314	-3,232	-1,680	36	319	-149
105 or 75	±15	$\frac{3}{12}$	-1,009	662	-665	-1,013	2,332	-1,025	770	-756	-1,033	2,564	-1,091	1,023	-983	-1,110	3,138
		$\frac{7}{12}$	-1,432	-222	-1,110	486	989	-1,718	-260	-1,227	494	1,199	-2,372	-350	-1,518	-528	1,673
		$\frac{11}{12}$	-1,766	-1,093	252	205	-419	-2,205	-1,258	178	231	-312	-3,132	-1,638	42	305	-145
120 or 60	±30	$\frac{3}{12}$	-997	611	-610	-998	2,219	-999	697	-695	-1,000	2,393	-1,013	918	895	-1,042	2,853
		$\frac{7}{12}$	-1,298	-203	-1,051	480	893	-1,537	-234	-1,138	479	1,070	-2,122	-313	-1,379	492	1,497
		$\frac{11}{12}$	-1,592	-1,018	276	188	-445	-1,977	-1,155	203	2,016	-334	-2,806	-1,485	65	267	-165
135 or 45	±45	$\frac{3}{12}$	-986	530	-537	980	2,046	-961	581	-594	-957	2,123	-904	745	-756	-934	2,394
		$\frac{7}{12}$	-1,084	-175	-963	474	735	-1,234	-191	-998	461	853	-1,716	-250	-1,149	433	1,217
		$\frac{11}{12}$	-1,308	-899	324	161	-491	-1,634	-990	-249	148	-347	-2,300	-1,238	101	196	-177
150 or 30	±60	$\frac{3}{12}$	-984	425	-435	-975	1,835	-944	419	-450	-914	-1,782	-776	512	-581	-783	1,800
		$\frac{7}{12}$	-799	-139	-857	474	522	-792	-130	-815	-454	532	-1,196	-165	-830	355	867
		$\frac{11}{12}$	-902	-738	404	136	-575	-1,186	-768	316	76	-349	-1,651	-918	141	98	-186
165 or 15	±75	$\frac{3}{12}$	-1,004	310	-311	-1,004	1,624	-986	197	-228	-930	1,381	-697	234	-414	-554	1,165
		$\frac{7}{12}$	-485	-104	-761	484	278	-111	-52	-612	484	7	-682	-39	-402	251	605
		$\frac{11}{12}$	-222	-529	558	156	-836	-800	-483	418	-69	-167	-806	-546	171	-35	-287

$\frac{x}{l}$	β_s arbitrary t/l = ∞ $10^3f_{\gamma 0}$	$10^3f_{\gamma 1}$	$10^3f_{\gamma 2}$	$10^3f_{\gamma 3}$	10^3g_{q0}
$\frac{3}{12}$	-1,000	500	-500	-1,000	2,000
$\frac{7}{12}$	-1,000	-167	-944	482	667
$\frac{11}{12}$	-1,000	-833	389	185	-667

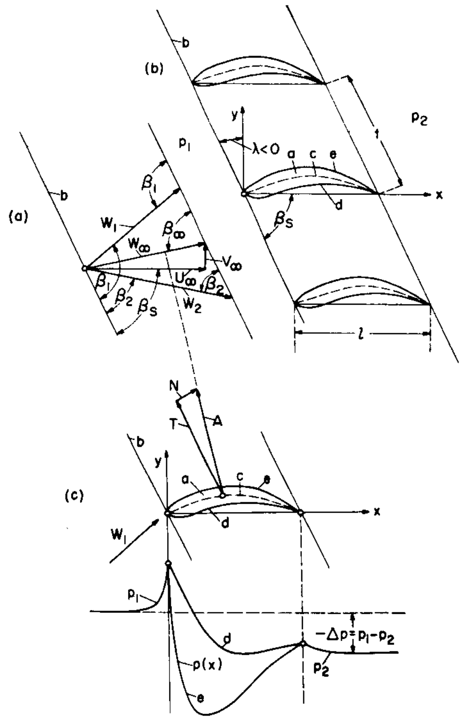

(a) Velocity diagram.

(b) Cascade.

(c) Blade with pressure distribution.

Figures 1(a) to (c)

Main symbols on the blade cascade: a blade of the cascade; b cascade front or direction of cascade front; c mean camber line; d pressure side; e suction side; l length of blade chord; t spacing; λ angle of stagger (negative, since shown as a turbine cascade); $\beta_S = 90^o + \lambda$ blade angle; x coordinate in the direction of l; y coordinate perpendicular to the direction of l; p_1 static pressure far in front of the cascade; p_2 static pressure far behind the cascade; p(x) static pressure along the blade contour; β_1 inflow angle; β_2 outflow angle; β_∞ angle of the translational velocity W_∞ with respect to b; U_∞ component of W_∞ in the x-direction; V_∞ component of W_∞ in the y-direction; W_1 inflow velocity far in front of the cascade; W_2 outflow velocity far behind the cascade; A lift (resultant force on a blade in frictionless flow) with the components; T parallel to b; and N perpendicular to b.

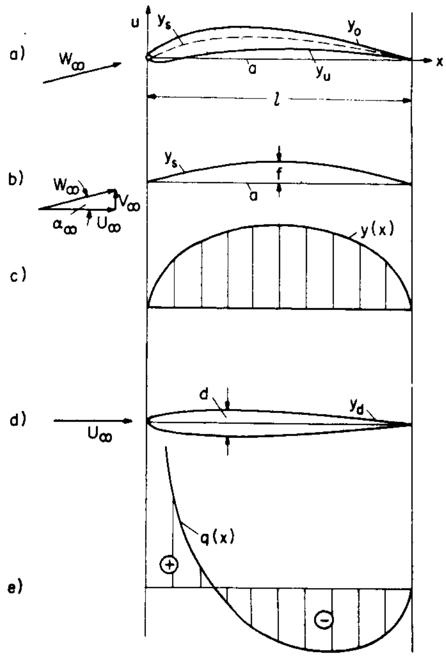

(a) Blade profile.

(b) Mean camber line.

(c) Representation of the mean camber line by a vortex distribution.

(d) Uncambered profile (thickness distribution).

(e) Representation of the thickness distribution by a source distribution.

Figures 2(a) to (e)

Subdivision of a profile into mean camber line and thickness distribution according to equations (1) and (2). x, y, l, W_∞, U_∞, and V_∞ as in figures 1(a) to 1(c); a blade chord; y_s coordinate of the mean camber line; y_o coordinate of the upper side of the blade; y_u coordinate of the lower side of the blade; y_d coordinate of the uncambered profile (thickness distribution) in the y-direction; d maximum thickness of the uncambered profile; f maximum displacement of the mean camber line (camber); α_∞ angle between W_∞ and a; $\gamma(x)$ vortex distribution (circulation per unit length); and $q(x)$ source distribution (plus sign for sources, minus sign for sinks).

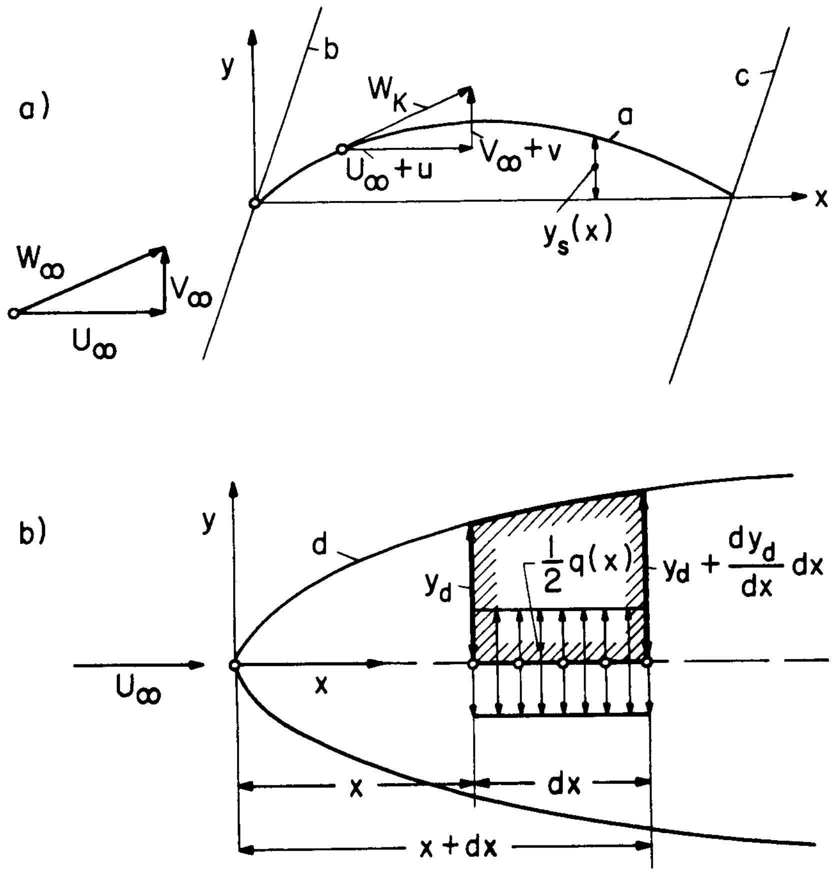

(a) Mean camber line profile (first condition).

(b) Uncambered profile (thickness distribution, second condition).

Figures 3(a) and (b)

On the derivation of the kinematic flow conditions. x, y, U_∞, V_∞, W_∞ as in figure 1; a mean camber line with the ordinate $y_s(x)$; b cascade front; c cascade-outflow plane; d uncambered profile with the ordinate $y_d(x)$; and q(x) source distribution.

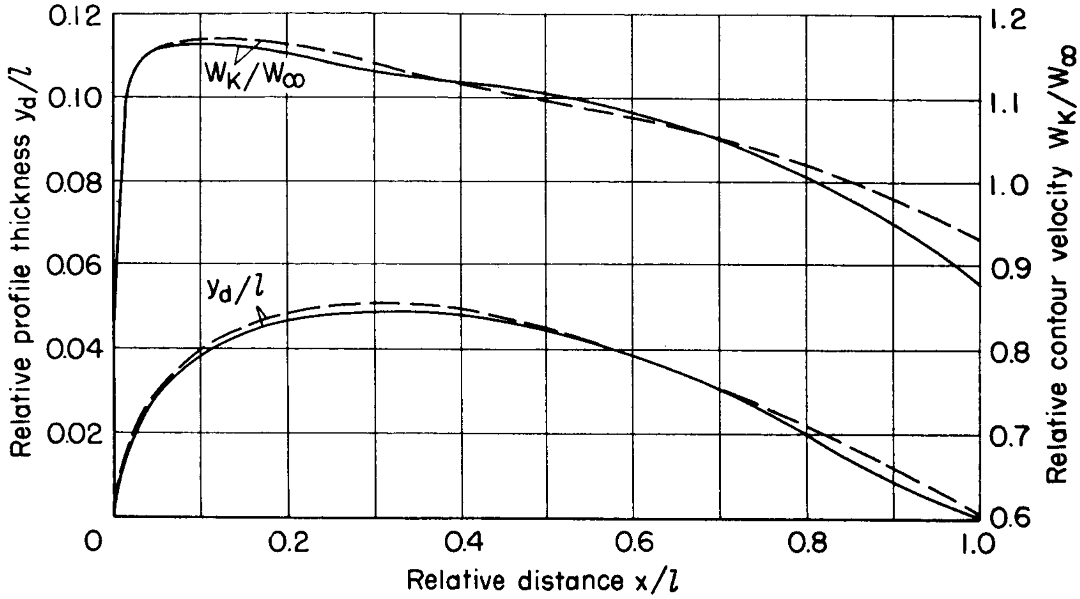

Figure 4. - Thickness distribution and contour-velocity distribution for symmetrical approach flow for the NACA 0010 profile as a single profile. (Solid curves for approximation according to equation (40) and to equations (37) and (38), dashed curves for actual variations.)

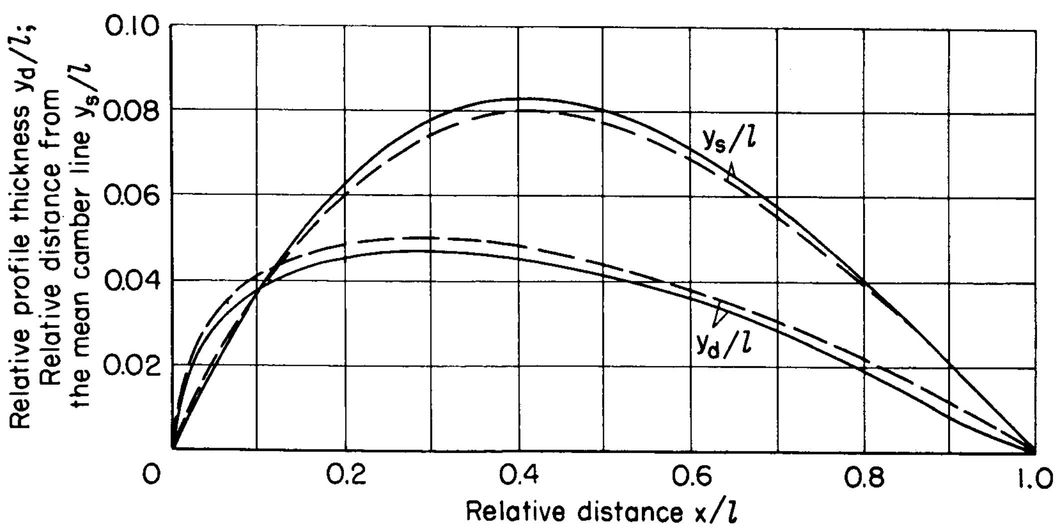

Figure 5. - Thickness and camber distribution for the NACA 8410 profile. Solid curves for approximation, dashed curves for actual variations.

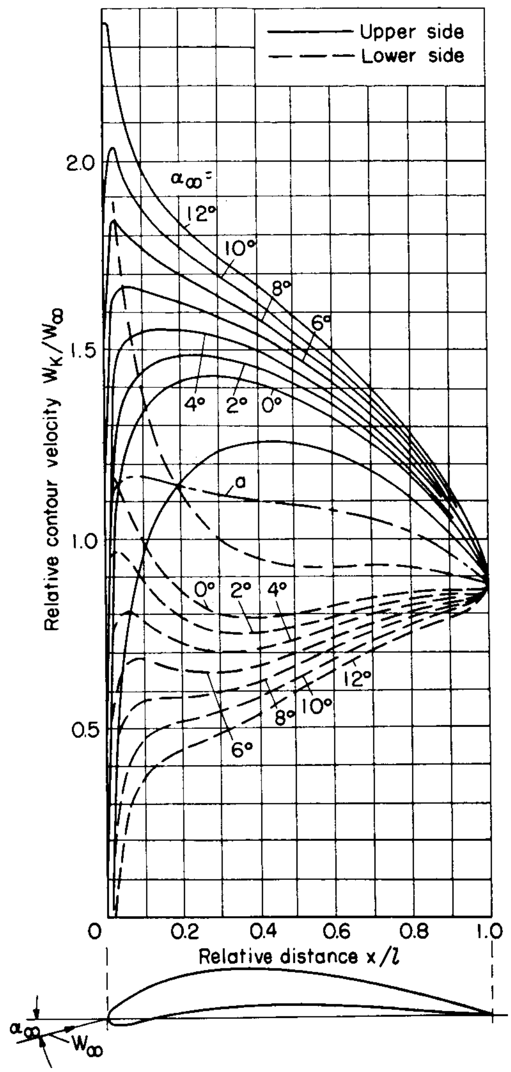

Figure 6. - Distribution of the contour velocity for the NACA 8410 profile at various angles of attack α_∞. Curve a corresponds to the coordinated symmetrical profile for symmetrical approach flow. W_∞ approach-flow velocity; lift coefficient c_A and angle-of-attack parameter $K = \tan \alpha_\infty = V_\infty/U_\infty$ according to:

α_∞	-7.3° (zero lift)	0°	2° (shock-free inflow)	4°	6°	8°	10°	12°
c_A	0	0.80	1.01	1.24	1.46	1.67	1.88	2.10
K	-0.130	0	0.034	0.040	0.105	0.141	0.177	0.213

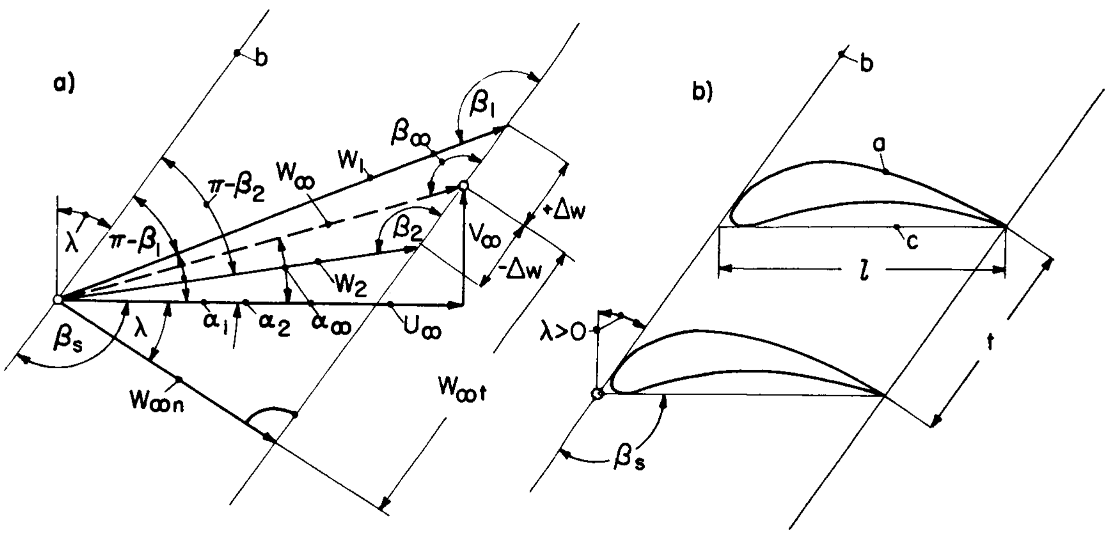

(a) Velocity diagram.

(b) Cascade.

Figures 7(a) and (b)

Velocity diagram for the staggered two-dimensional cascade. a, b, l, t, and λ are positive since drawn as a compressor cascade. β_s, β_1, β_2, β_∞, W_∞, U_∞, V_∞, W_1, and W_2 are the same as in figure 1. Furthermore, c is chord; α_1 is angle between c and W_1; α_2 is angle between c and W_2; $W_{\infty n}$ is component of W_∞ normal to b; $W_{\infty t}$ is component of W_∞ tangential to b; and $\pm\Delta w$ is induced velocity parallel to b far in front of the cascade and far behind it, respectively.

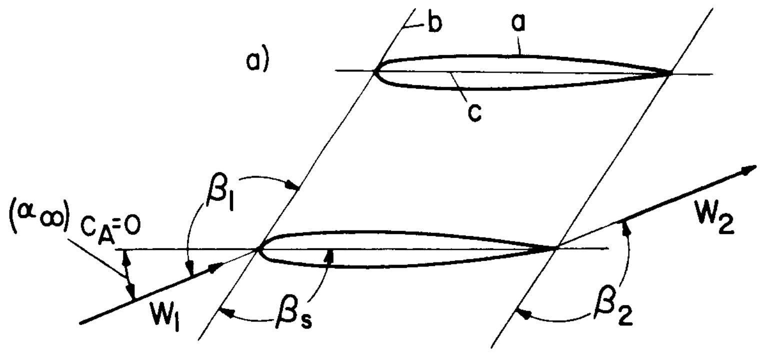

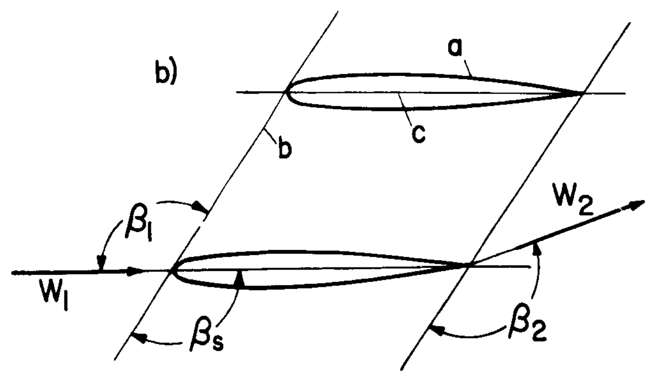

(a) Cascade free from deflection (with W_1 parallel to W_2, $\beta_1 > \beta_s$, and pertaining angle of attack $(\alpha_\infty)_{c_A=0}$ according to equation (95)).

(b) Cascade with inflow parallel to the chord (deflection toward the cascade front).

Figures 8(a) and (b)

Staggered cascade of symmetrical profiles. a profile; b cascade front; c chord; W_1 inflow velocity; W_2 outflow velocity; β_1 inflow angle; β_2 outflow angle; and β_s blade angle (angle between c and b).

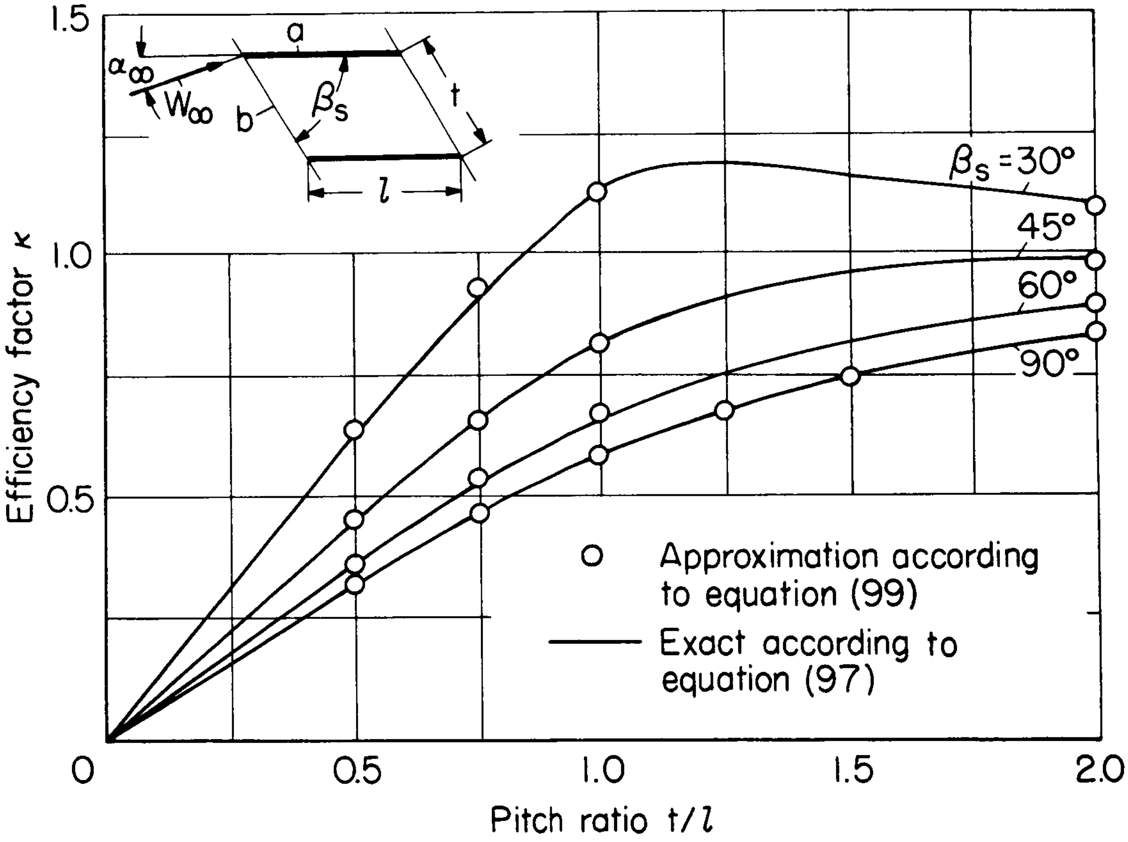

Figure 9.- Dependence of the efficiency factor κ for the lift increase, according to equation (97), on the pitch ratio t/l for the flat-plate cascade. a flat plate; b cascade front; l length of blade chord; t spacing; β_s angle between chord and b; W_∞ translational velocity; and α_∞ angle of attack.

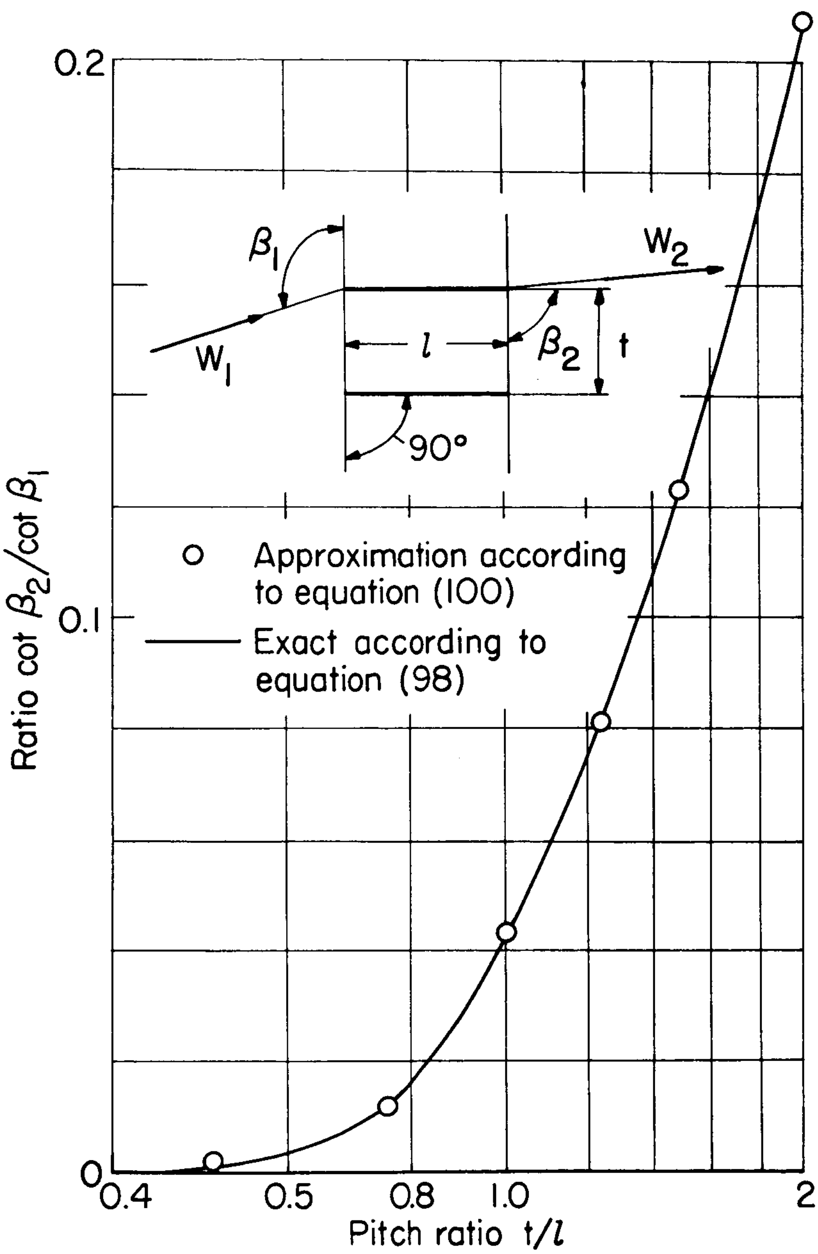

Figure 10.- Dependence of the ratio $\cot\beta_2/\cot\beta_1$ on the pitch ratio for the unstaggered plate cascade. (Symbols as in figures 1(a) to (c).)

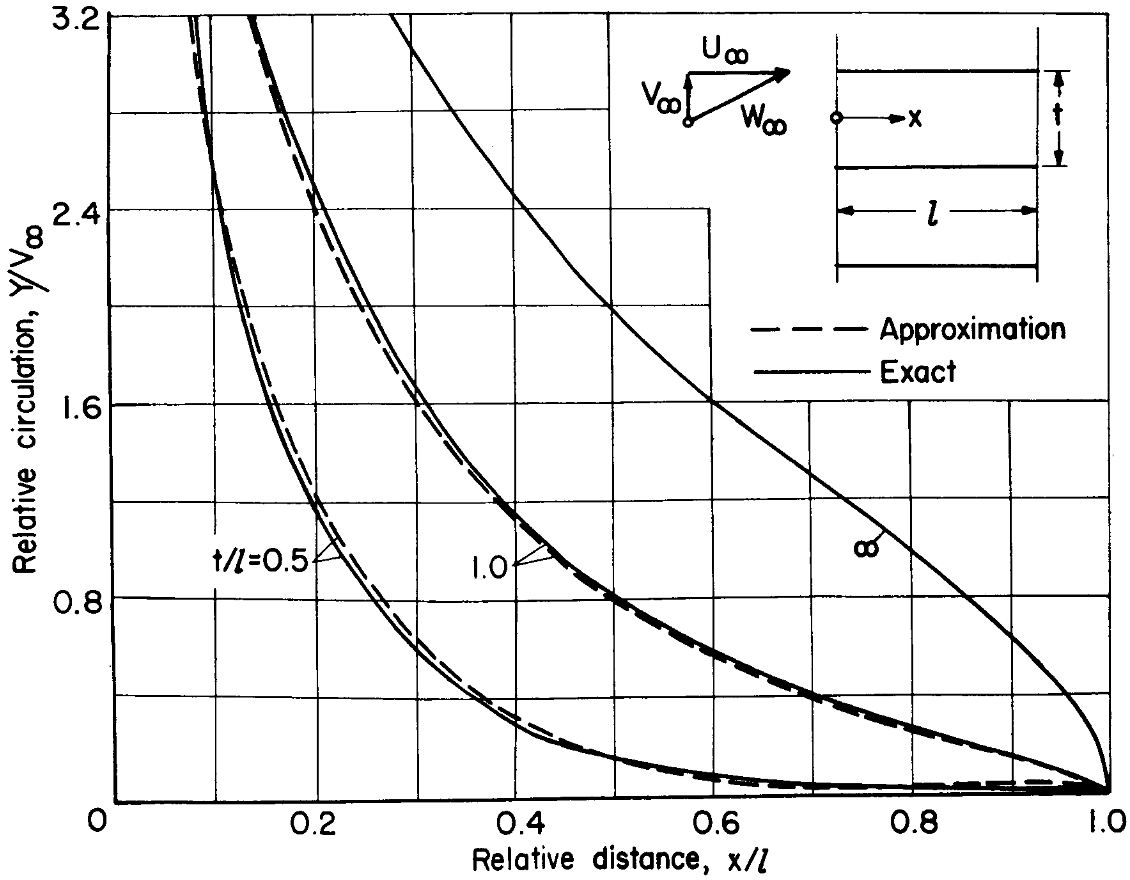

Figure 11.- Circulation distribution over the length of the plate chord for the unstaggered plate cascade. (Symbols as in figures 1(a) to (c); for $t/l = \infty$, approximate and exact solutions coincide.)

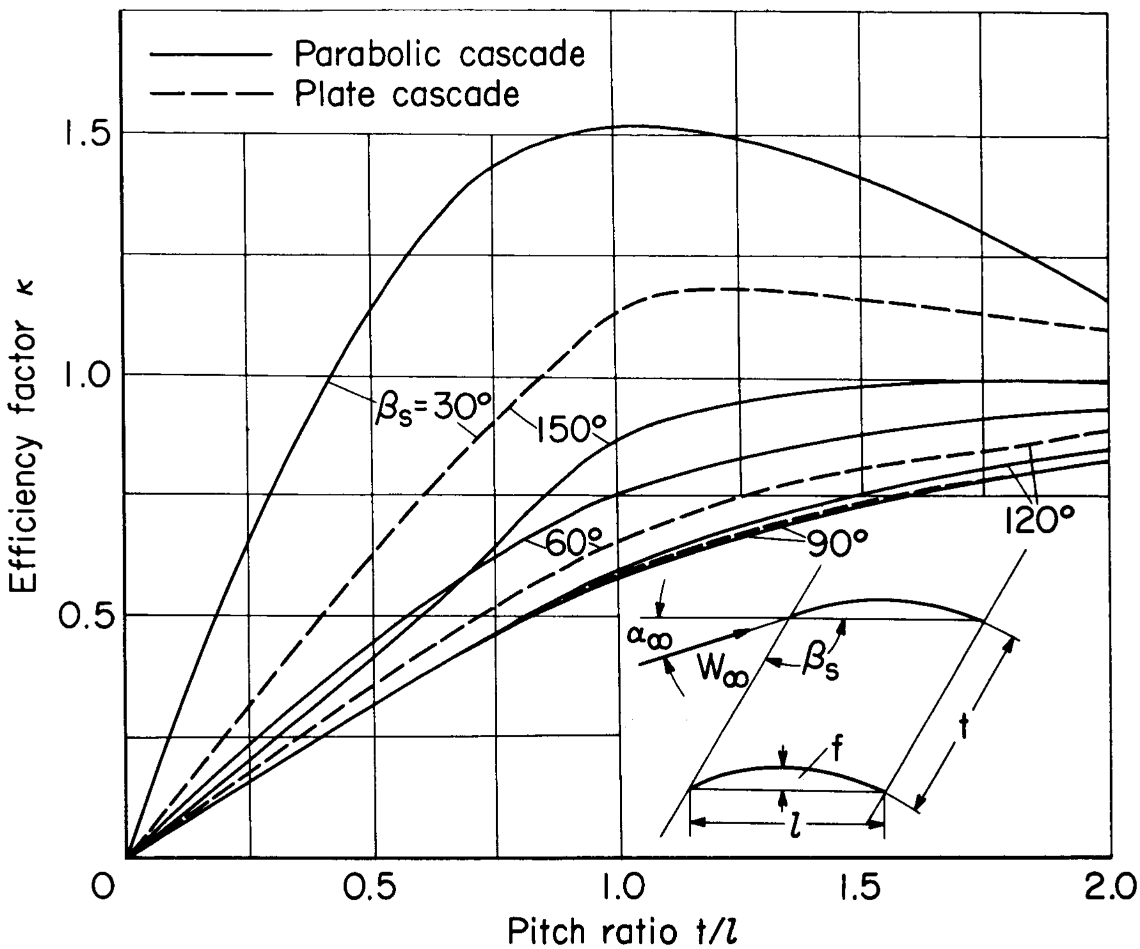

Figure 12.- Dependence of the efficiency factor κ for the lift increase according to equation (97) on the pitch ratio t/l for parabolic cascades of the camber ratio $\frac{f}{l} = 0.1$ compared to the results for plate cascades. (Symbols as in figure 2(b); for plate cascades, the same variation results for $\beta_s = 30^{\circ}$ and 150°, and for 60° and 120°, respectively.)

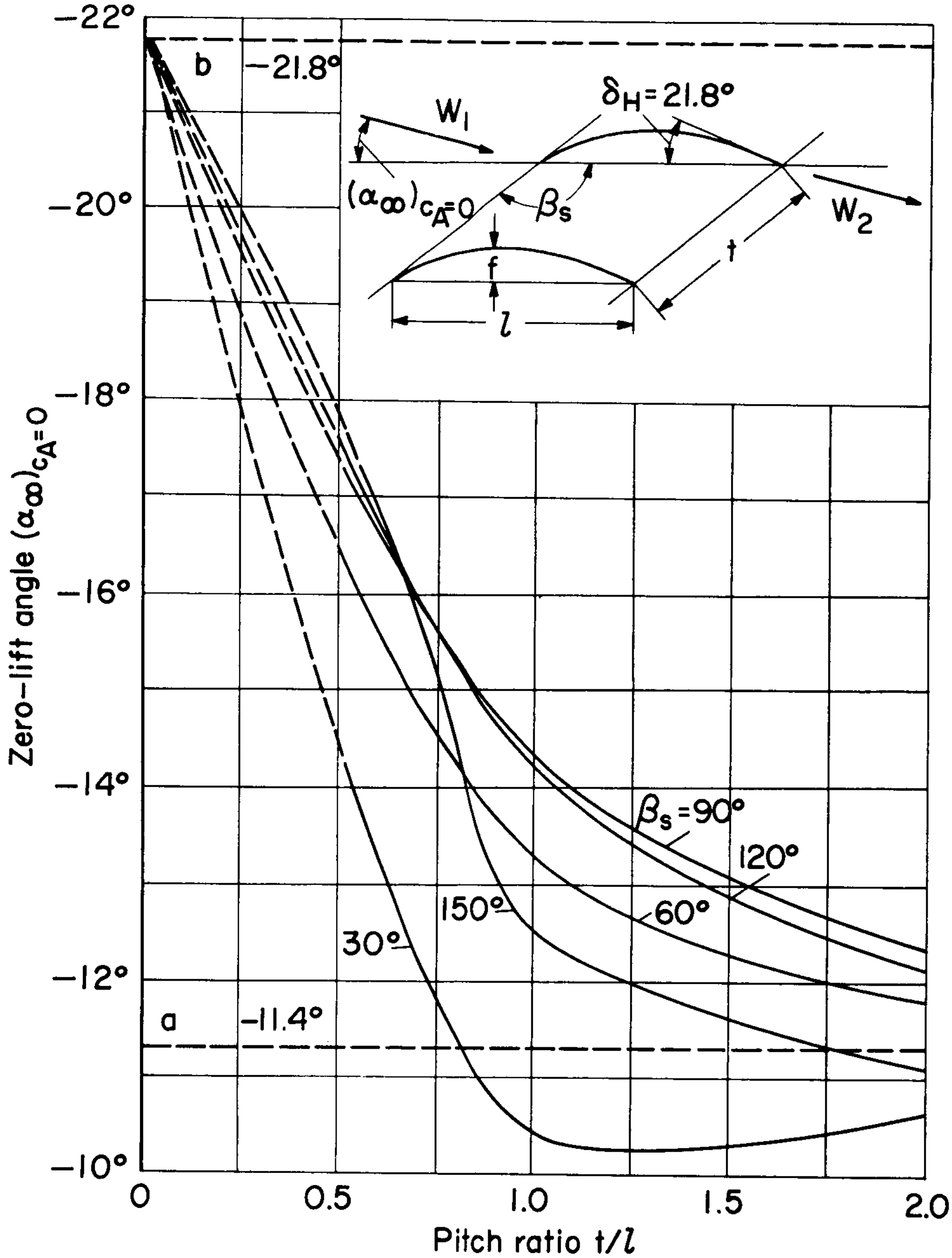

Figure 13.- Dependence of the zero-lift angle on the pitch ratio for parabolic cascades with the camber ratio $\frac{f}{l} = 0.1$, for various blade angles β_S. a value of the single blade; b value for blade-congruent flow; other symbols as in figure 2(b).

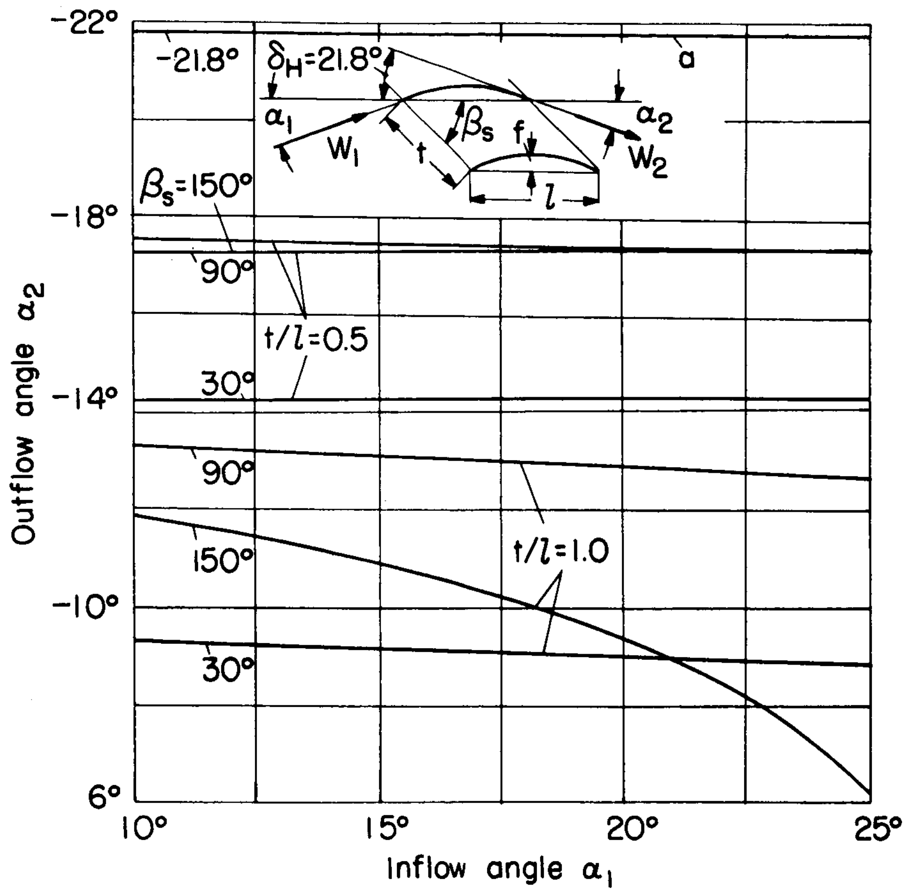

Figure 14.- Dependence of the outflow angle α_2 on the inflow angle α_1 for parabolic cascades with the camber ratio $\frac{f}{l} = 0.1$ for various blade angles β_s and pitch ratios t/l. a value for blade-congruent flow; δ_H trailing-edge angle; other symbols as in figures 7(a) and (b).

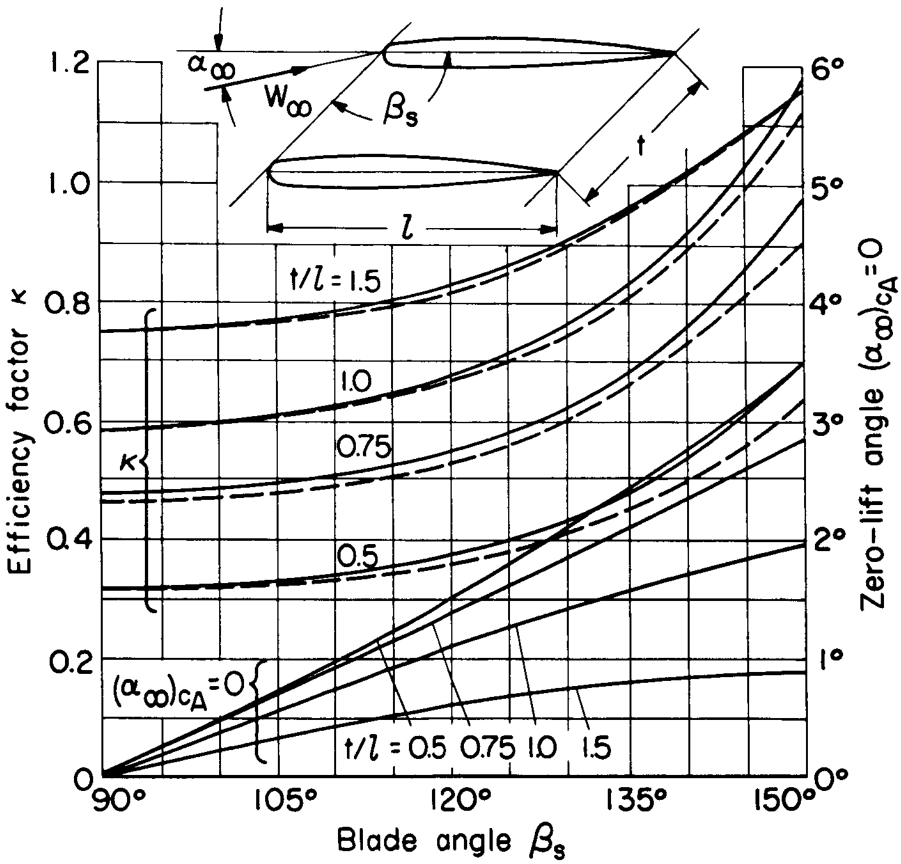

Figure 15.- Dependence of the efficiency factor κ for the lift increase according to equation (97) and of the zero-lift angle $(\alpha_\infty)_{c_A=0}$ on the blade angle β_S for various pitch ratios t/l for cascades of blades with NACA 0010 profiles. (Symbols as in figure 2(b); solid curves for NACA 0010 profile, dashed curves for plate cascades, for comparison.)

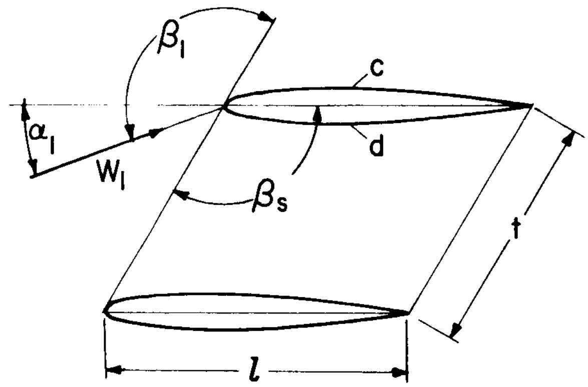

Explanatory sketch to figures 16 to 24

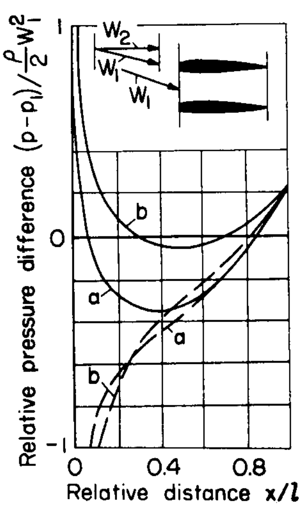

Figure 16.- $\beta_S = 90^{\circ}$; $\alpha_1 = -15^{\circ}$.

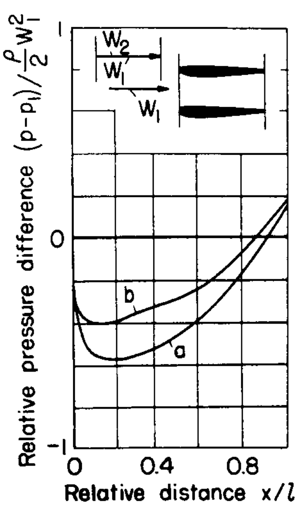

Figure 17.- $\beta_S = 90^{\circ}$; $\alpha_1 = 0^{\circ}$.

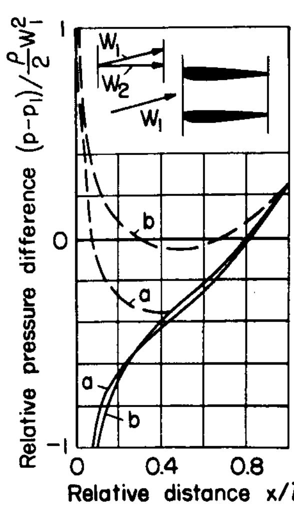

Figure 18.- $\beta_S = 90^{\circ}$; $\alpha_1 = 15^{\circ}$.

Figures 16 to 24

Pressure distributions on the blade contours for cascades of blades with NACA 0010 profiles. Curve a for pitch ratio $\frac{t}{l} = 0.5$; curve b for pitch ratio $\frac{t}{l} = 1.0$; solid curves for the upper side c of profile; and dashed curves for the lower side d of profile. (The cascade arrangements sketched apply for $\frac{t}{l} = 0.5$; the velocity diagrams apply for both pitch ratios.)

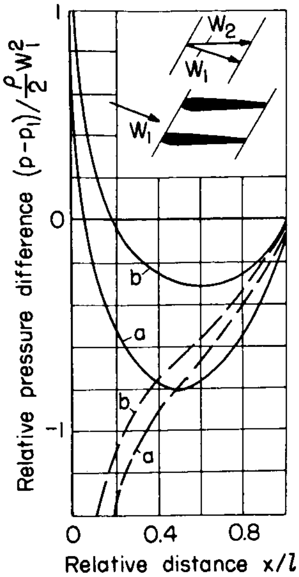

Figure 19.- $\beta_S = 120^\circ$; $\alpha_1 = -15^\circ$.

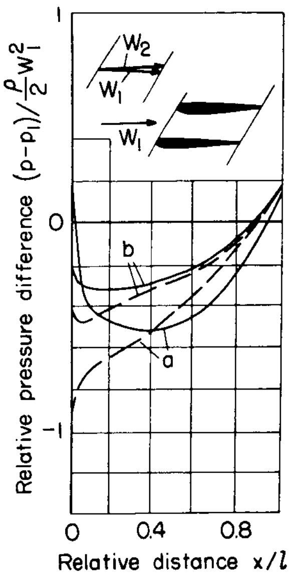

Figure 20.- $\beta_S = 120^\circ$; $\alpha_1 = 0^\circ$.

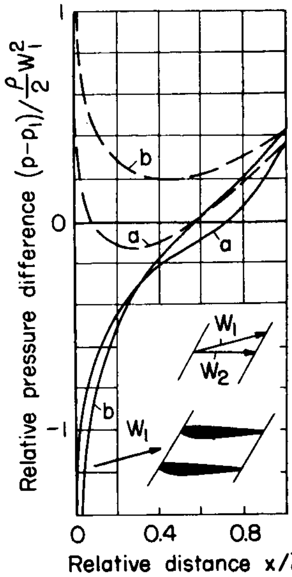

Figure 21.- $\beta_S = 120^\circ$; $\alpha_1 = 15^\circ$.

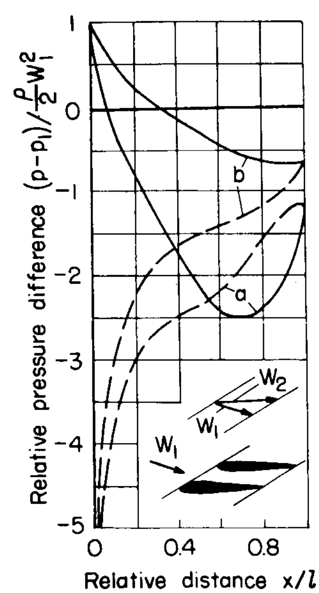

Figure 22.- $\beta_S = 150^\circ$; $\alpha_1 = -15^\circ$.

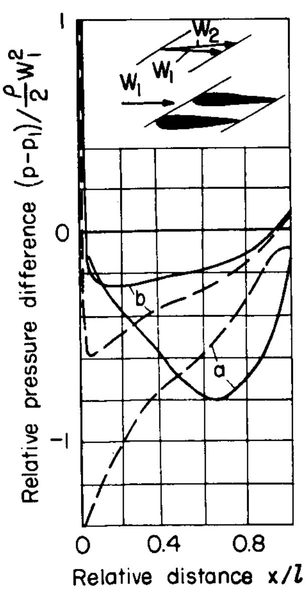

Figure 23.- $\beta_S = 150^\circ$; $\alpha_1 = 0^\circ$.

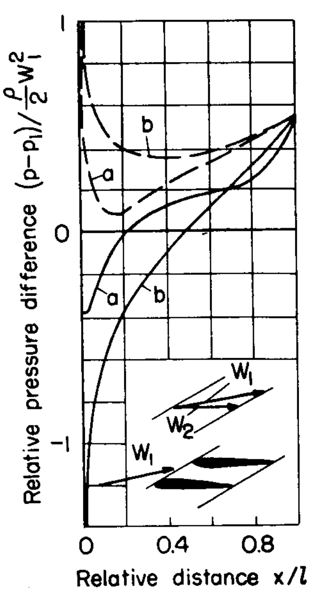

Figure 24.- $\beta_S = 150^\circ$; $\alpha_1 = 10^\circ$.

(See preceding page for further information.)

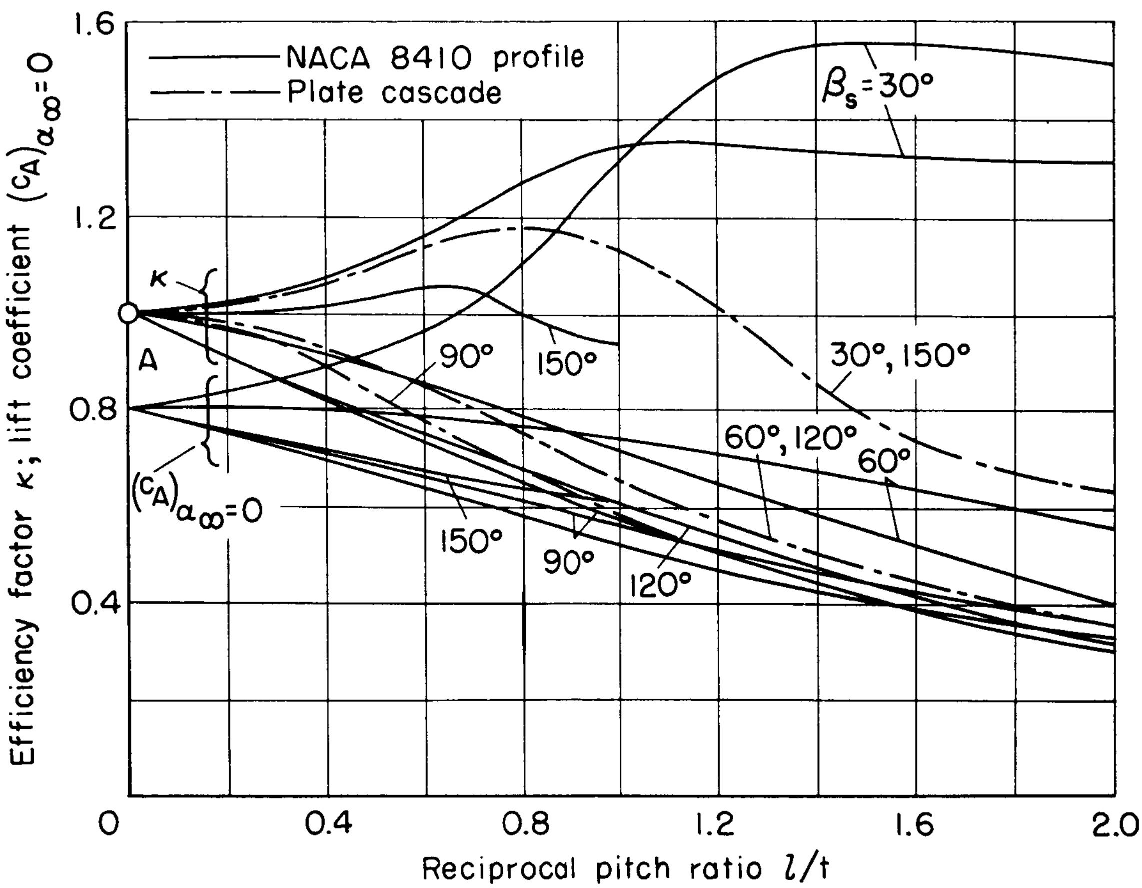

Figure 25.- Variation of the efficiency factor κ (lift increase relative to the value of the single blade), according to equation (97), and of the lift coefficient $(c_A)_{\alpha_\infty=0}$ against the reciprocal pitch ratio l/t for various blade angles $\beta_s = 90^\circ + \lambda$ for cascades of blades with NACA 8410 profiles. (For comparison, the variation of κ was plotted also for plate cascades. A is the point corresponding to the single blade.)

Figures 26 to 30

Angle exaggeration δ for cascades of blades with NACA 8410 profiles. (Compare also figures 1(a) and 7(a).) Inflow angle $\beta_1 = \beta_S + \alpha_1$ (angle between W_1 and b); angle exaggeration $\delta = \beta_2 - \beta_H = \alpha_2 + 12.9^\circ$ (angle between the outflow velocity W_2 and the tangent c to the mean camber line at the trailing edge) with $\beta_2 = \beta_S - 12.9^\circ + \delta$ as the outflow angle (angle between W_2 and b); β_H as the trailing-edge angle (angle between c and b); and with angle of attack α_2 as the angle between W_2 and a.

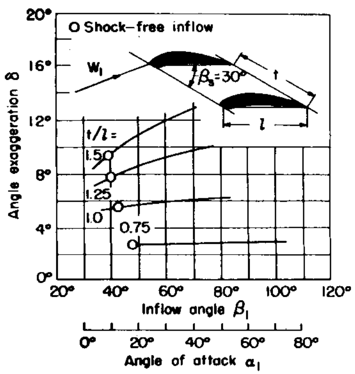

Figure 26. - Variation for $\beta_S = 30^\circ$.

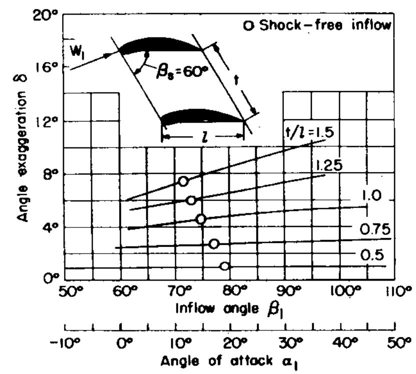

Figure 27. - Variation for $\beta_S = 60^\circ$.

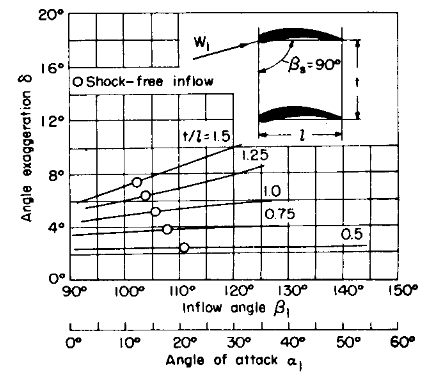

Figure 28. - Variation for $\beta_S = 90^\circ$.

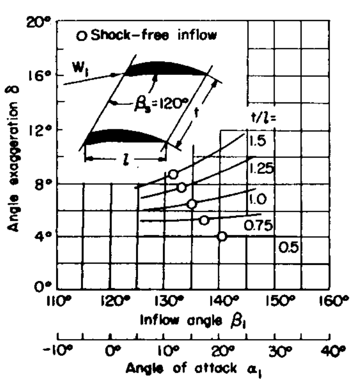

Figure 29. - Variation for $\beta_S = 120^\circ$.

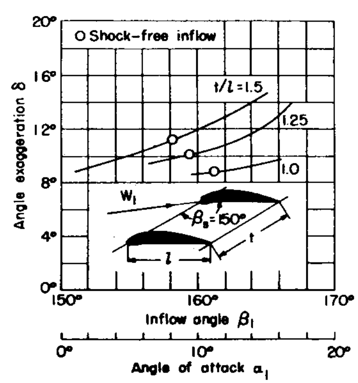

Figure 30. - Variation for $\beta_S = 150^\circ$.

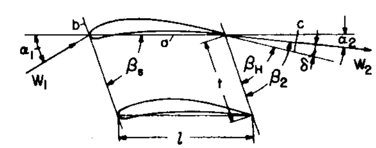

Explanatory sketch to figures 26 to 30

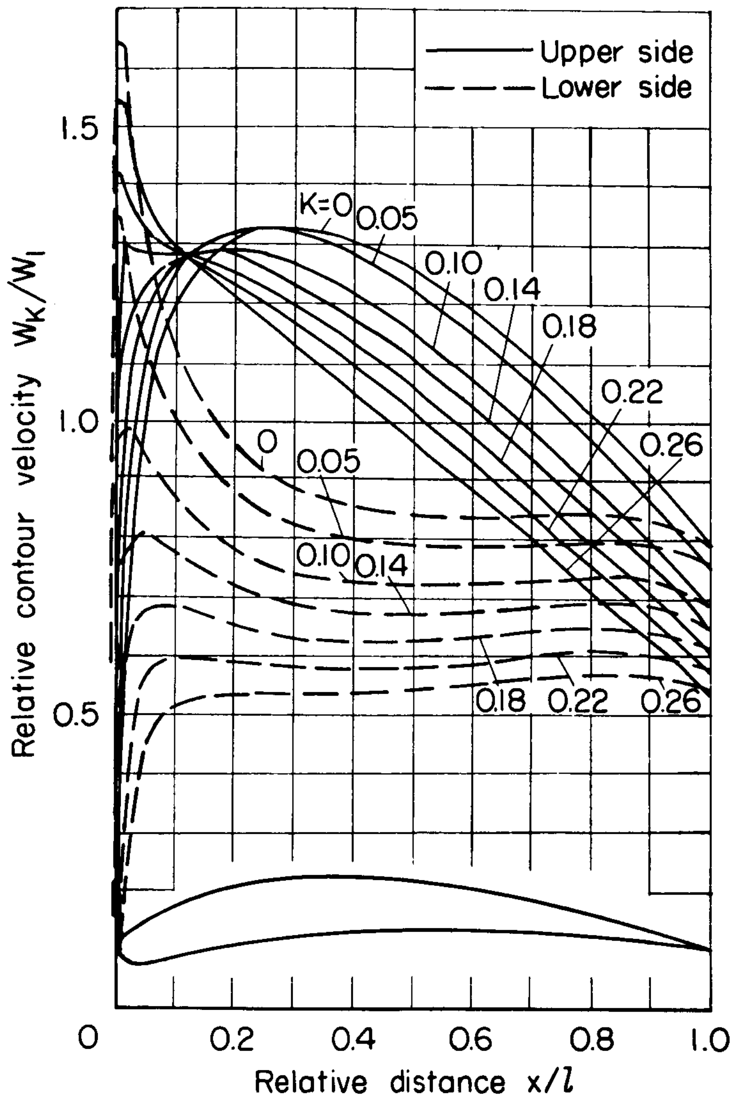

Figure 31.- Velocity distribution on the blade contour for the calculation example treated later in section 7.2 (compare table 15). NACA 8410 blade profile, pitch ratio $\frac{t}{l} = 0.75$, blade angle $\beta_s = 120^\circ$; values of $K = \tan \alpha_\infty$ for angle of attack α_∞ according to:

K	0	0.05	0.10	0.14	0.18	0.22	0.26
α_∞	0°	2.9°	5.7°	8.0°	10.2°	12.4°	14.6°

Angle of attack for shock-free inflow $\alpha_{\infty st} = 6.7^\circ$.

Figures 32 to 43

Pressure distribution on the blade contour for cascades of blades with NACA 8410 profiles, for a blade angle $\beta_S = 30^{\circ}$. (Solid curves for upper side, dashed curves for lower side of the profile; x, l, p, p_1, ρ, and W_1 as in figures 16 to 24.)

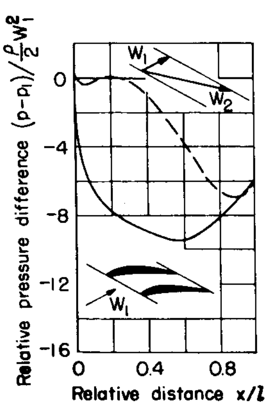

Figure 32.- $\alpha_1 = 30^{\circ}$; $\frac{t}{l} = 0.5$.

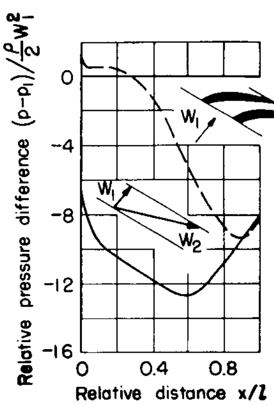

Figure 33.- $\alpha_1 = 50^{\circ}$; $\frac{t}{l} = 0.5$.

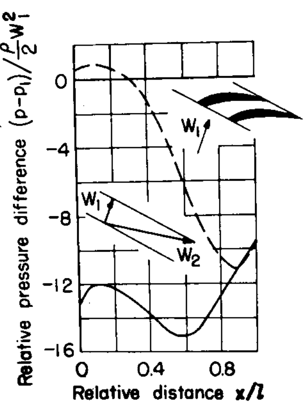

Figure 34.- $\alpha_1 = 70^{\circ}$; $\frac{t}{l} = 0.5$.

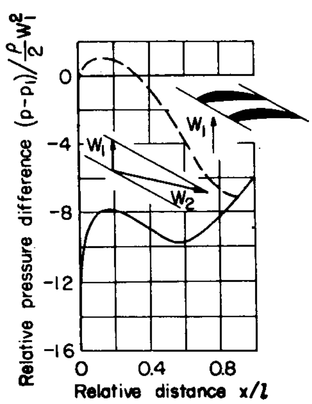

Figure 35.- $\alpha_1 = 90^{\circ}$; $\frac{t}{l} = 0.5$.

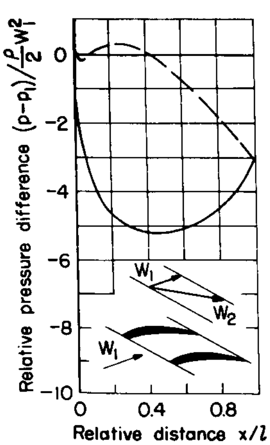

Figure 36.- $\alpha_1 = 20^{\circ}$; $\frac{t}{l} = 0.75$.

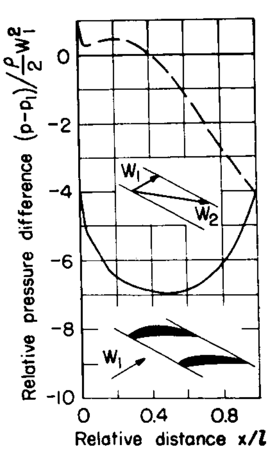

Figure 37.- $\alpha_1 = 30^{\circ}$; $\frac{t}{l} = 0.75$.

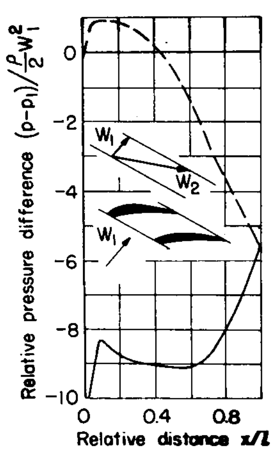

Figure 38.- $\alpha_1 = 50^{\circ}$; $\frac{t}{l} = 0.75$.

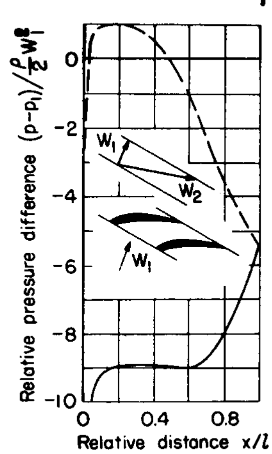

Figure 39.- $\alpha_1 = 70^{\circ}$; $\frac{t}{l} = 0.75$.

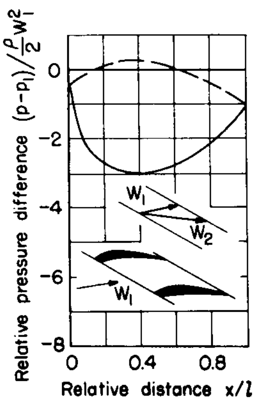

Figure 40.- $\alpha_1 = 10^o$; $\frac{t}{l} = 1.0$.

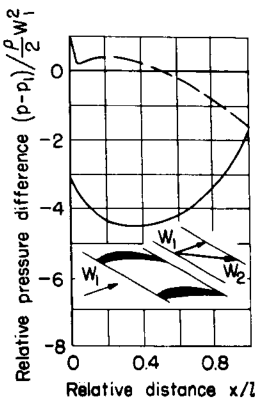

Figure 41.- $\alpha_1 = 20^o$; $\frac{t}{l} = 1.0$.

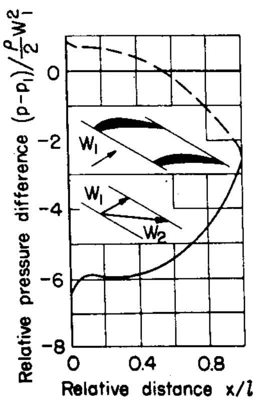

Figure 42.- $\alpha_1 = 30^o$; $\frac{t}{l} = 1.0$.

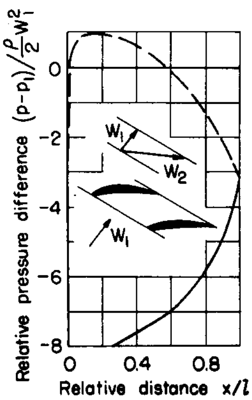

Figure 43.- $\alpha_1 = 50^o$; $\frac{t}{l} = 1.0$.

(See preceding page for further information.)

417

Figures 44 to 58

Pressure distribution on the blade contour for cascades of blades with NACA 8410 profiles, for a blade angle $\beta_s = 60^{\circ}$. (Solid curves for upper side, dashed curves for lower side of profile; x, l, p, p_1, ρ, and W_1 as in figures 16 to 24.)

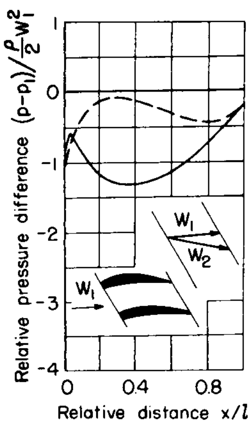

Figure 44.- $\alpha_1 = 5^{\circ}$; $\frac{t}{l} = 0.5$.

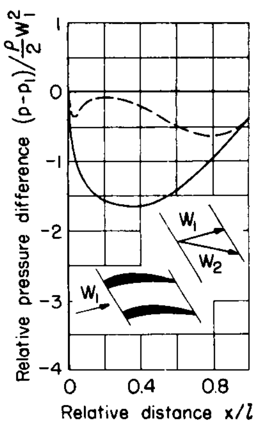

Figure 45.- $\alpha_1 = 15^{\circ}$; $\frac{t}{l} = 0.5$.

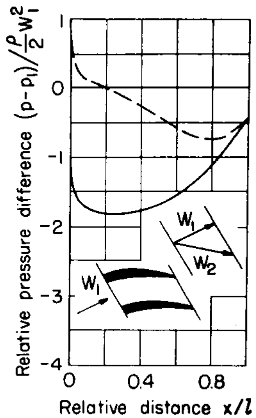

Figure 46.- $\alpha_1 = 25^{\circ}$; $\frac{t}{l} = 0.5$.

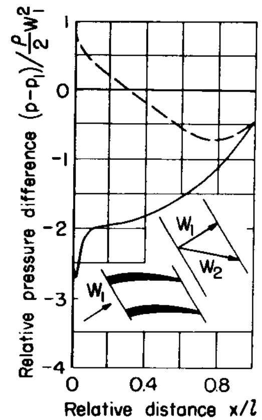

Figure 47.- $\alpha_1 = 35^{\circ}$; $\frac{t}{l} = 0.5$.

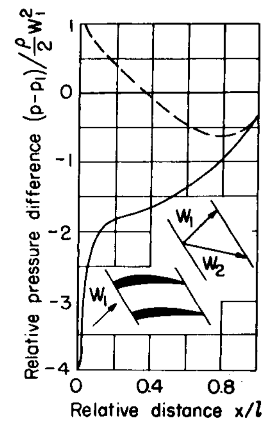

Figure 48.- $\alpha_1 = 45^{\circ}$; $\frac{t}{l} = 0.5$.

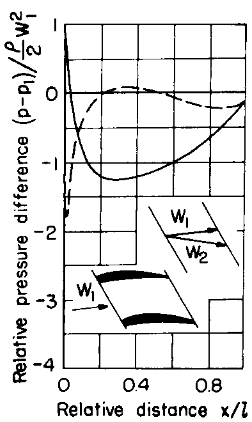

Figure 49.- $\alpha_1 = 5^{\circ}$; $\frac{t}{l} = 0.75$.

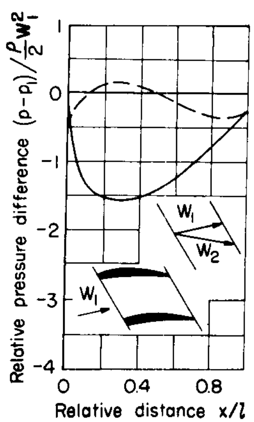

Figure 50.- $\alpha_1 = 15^{\circ}$; $\frac{t}{l} = 0.75$.

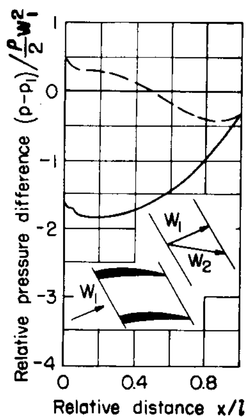

Figure 51.- $\alpha_1 = 25^{\circ}$; $\frac{t}{l} = 0.75$.

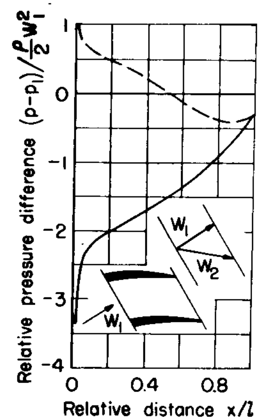

Figure 52.- $\alpha_1 = 35^{\circ}$; $\frac{t}{l} = 0.75$.

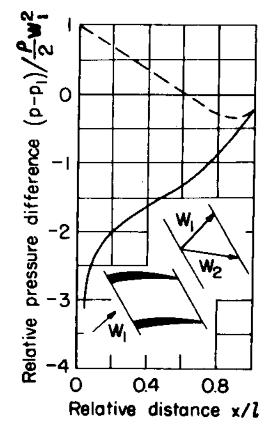

Figure 53.- $\alpha_1 = 45^{\circ}$; $\frac{t}{l} = 0.75$.

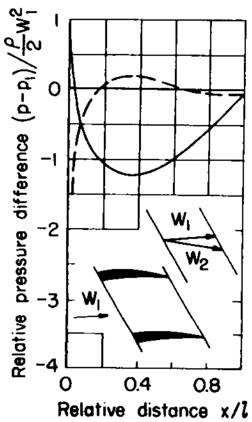

Figure 54.- $\alpha_1 = 5^o$;
$\frac{t}{l} = 1.0$.

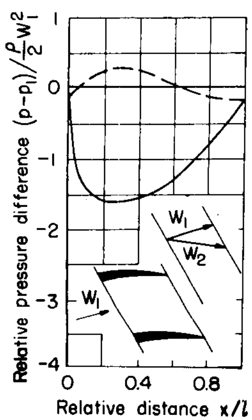

Figure 55.- $\alpha_1 = 15^o$;
$\frac{t}{l} = 1.0$.

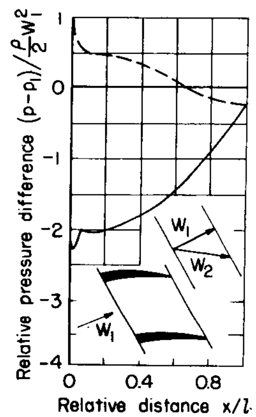

Figure 56.- $\alpha_1 = 25^o$;
$\frac{t}{l} = 1.0$.

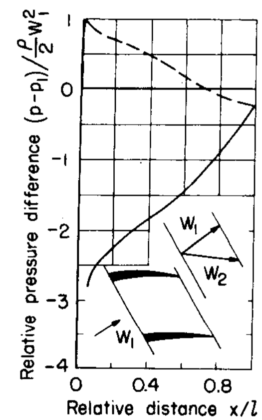

Figure 57.- $\alpha_1 = 35^o$;
$\frac{t}{l} = 1.0$.

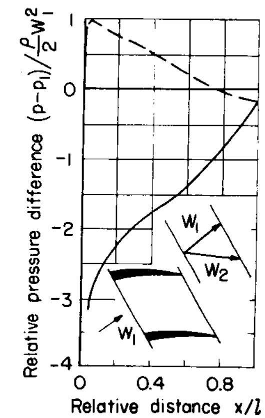

Figure 58.- $\alpha_1 = 40^o$;
$\frac{t}{l} = 1.0$.

(See preceding page for further information.)

Figures 59 to 72

Pressure distribution on the blade contour for cascades of blades with NACA 8410 profiles, for a blade angle $\beta_S = 90^\circ$. (Solid curves for upper side, dashed curves for lower side of profile; x, l, p, p_1, ρ, and W_1 as in figures 16 to 24.)

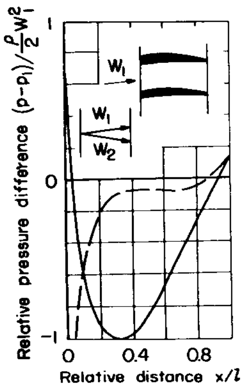

Figure 59.- $\alpha_1 = 5^\circ$; $\frac{t}{l} = 0.5$.

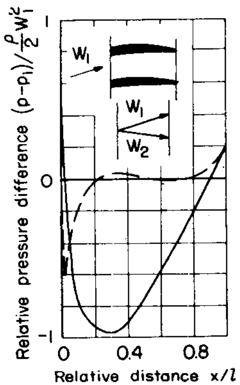

Figure 60.- $\alpha_1 = 15^\circ$; $\frac{t}{l} = 0.5$.

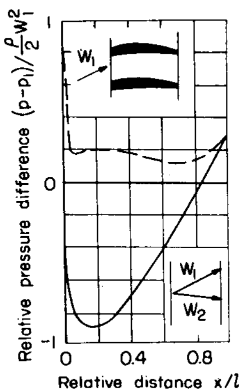

Figure 61.- $\alpha_1 = 25^\circ$; $\frac{t}{l} = 0.5$.

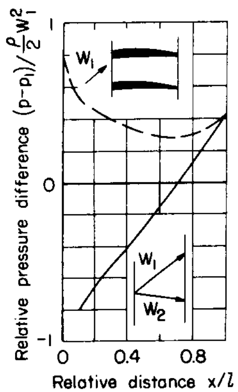

Figure 62.- $\alpha_1 = 35^\circ$; $\frac{t}{l} = 0.5$.

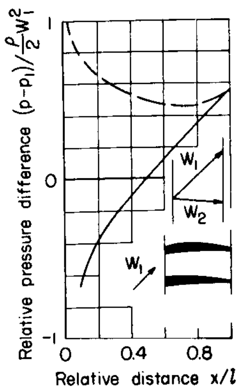

Figure 63.- $\alpha_1 = 45^\circ$; $\frac{t}{l} = 0.5$.

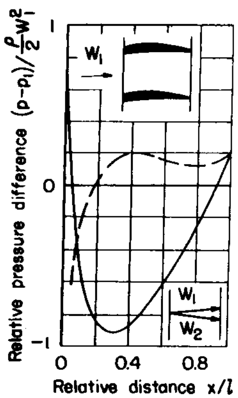

Figure 64.- $\alpha_1 = 5^\circ$; $\frac{t}{l} = 0.75$.

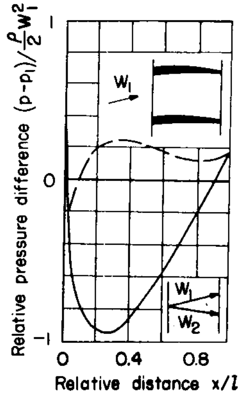

Figure 65.- $\alpha_1 = 15^\circ$; $\frac{t}{l} = 0.75$.

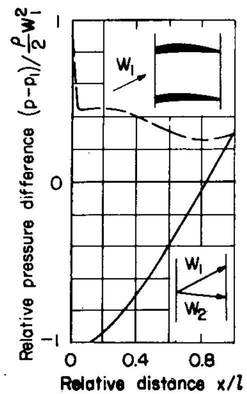

Figure 66.- $\alpha_1 = 25^\circ$; $\frac{t}{l} = 0.75$.

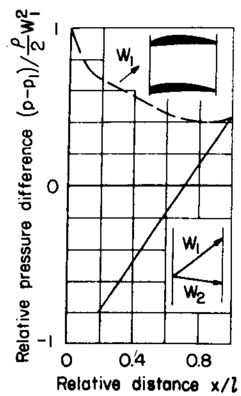

Figure 67.- $\alpha_1 = 35^\circ$; $\frac{t}{l} = 0.75$.

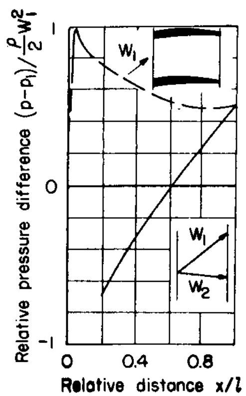

Figure 68.- $\alpha_1 = 40^\circ$; $\frac{t}{l} = 0.75$.

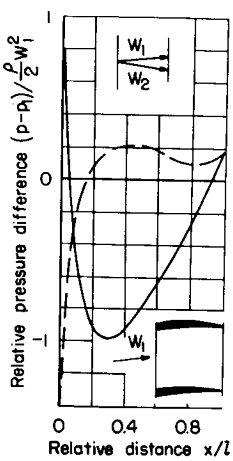

Figure 69.- $\alpha_1 = 5^O$; $\frac{t}{l} = 1.0$.

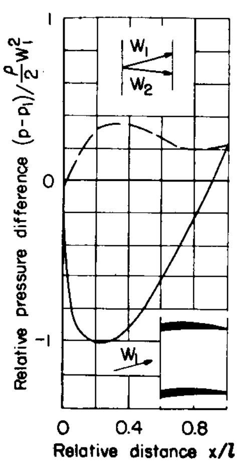

Figure 70.- $\alpha_1 = 15^O$; $\frac{t}{l} = 1.0$.

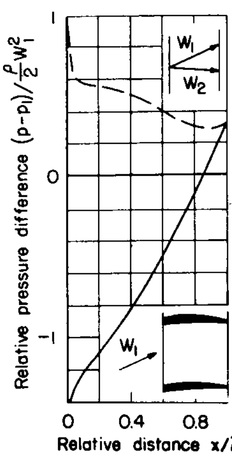

Figure 71.- $\alpha_1 = 25^O$; $\frac{t}{l} = 1.0$.

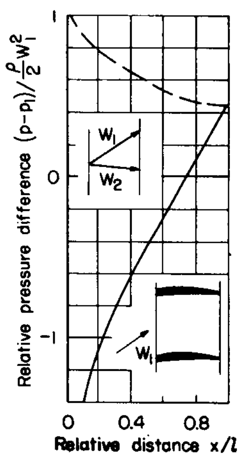

Figure 72.- $\alpha_1 = 35^O$; $\frac{t}{l} = 1.0$.

(See preceding page for further information.)

Figures 73 to 85

Pressure distribution on the blade contour for cascades of blades with NACA 8410 profiles, for a blade angle $\beta_s = 120^o$. (Solid curves for upper side, dashed curves for lower side of profile; x, l, p, p_1, ρ, and W_1 as in figures 16 to 24.)

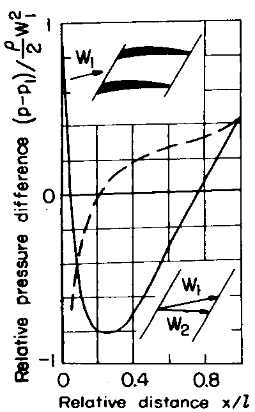

Figure 73.- $\alpha_1 = 10^o$; $\frac{t}{l} = 0.5$.

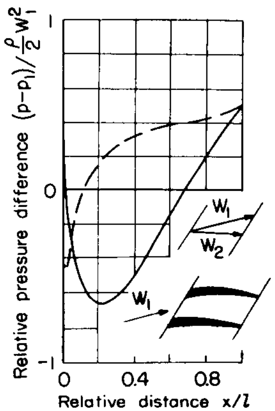

Figure 74.- $\alpha_1 = 15^o$; $\frac{t}{l} = 0.5$.

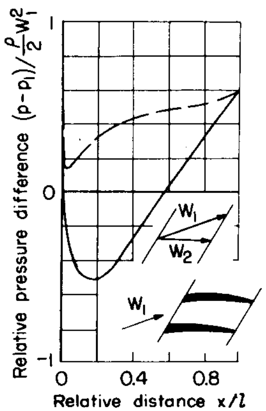

Figure 75.- $\alpha_1 = 20^o$; $\frac{t}{l} = 0.5$.

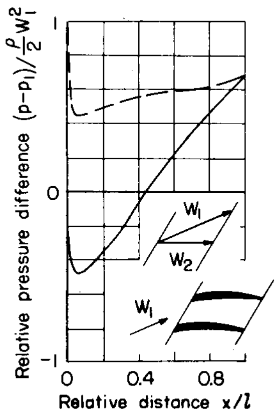

Figure 76.- $\alpha_1 = 25^o$; $\frac{t}{l} = 0.5$.

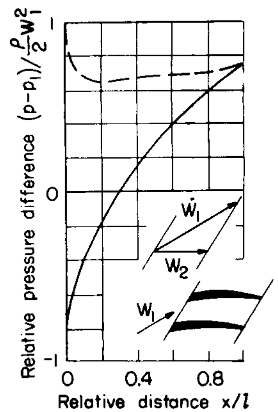

Figure 77.- $\alpha_1 = 30^o$; $\frac{t}{l} = 0.5$.

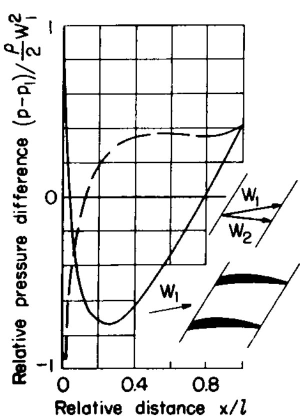

Figure 78.- $\alpha_1 = 10^o$; $\frac{t}{l} = 0.75$.

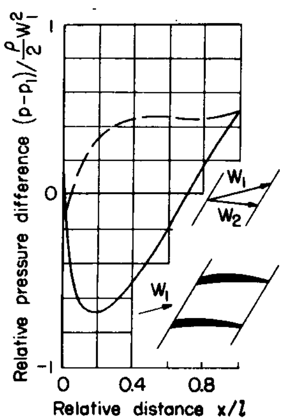

Figure 79.- $\alpha_1 = 15^o$; $\frac{t}{l} = 0.75$.

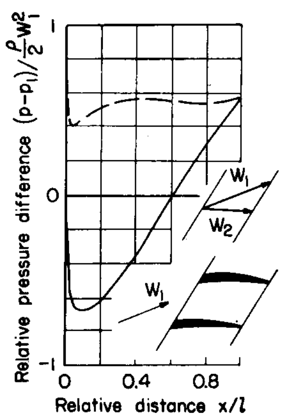

Figure 80.- $\alpha_1 = 20^o$; $\frac{t}{l} = 0.75$.

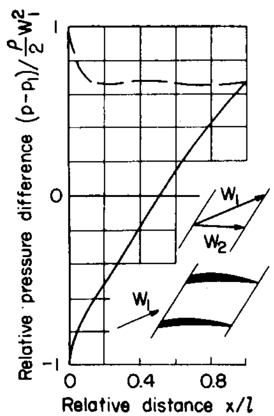

Figure 81.- $\alpha_1 = 25^o$; $\frac{t}{l} = 0.75$.

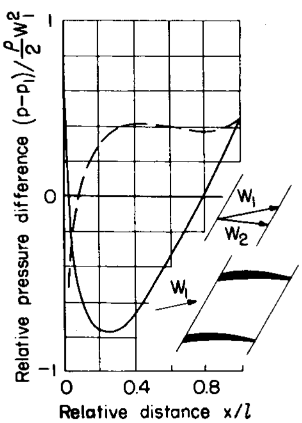

Figure 82.- $\alpha_1 = 10^\circ$; $\frac{t}{l} = 1.0$.

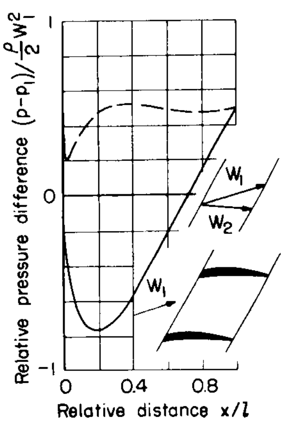

Figure 83.- $\alpha_1 = 15^\circ$; $\frac{t}{l} = 1.0$.

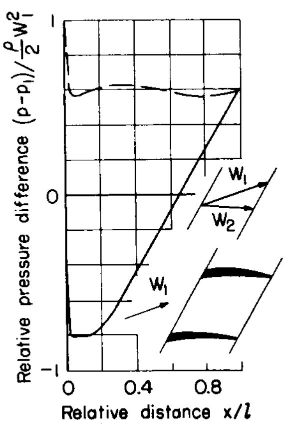

Figure 84.- $\alpha_1 = 20^\circ$; $\frac{t}{l} = 1.0$.

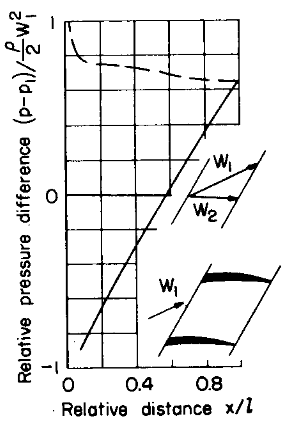

Figure 85.- $\alpha_1 = 25^\circ$; $\frac{t}{l} = 1.0$.

(See preceding page for further information.)

Figures 86 to 98

Pressure distribution on the blade contour for cascades of blades with NACA 8410 profiles, for a blade angle $\beta_S = 150^{\circ}$. (Solid curves for upper side, dashed curves for lower side of profile; x, l, p, p_1, ρ, and W_1 as in figures 16 to 24.)

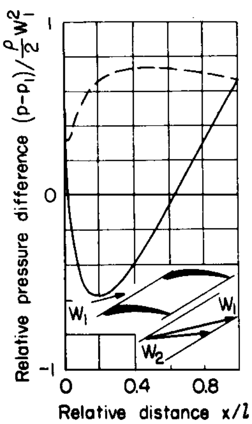

Figure 86.- $\alpha_1 = 11^{\circ}$; $\frac{t}{l} = 1.0.$

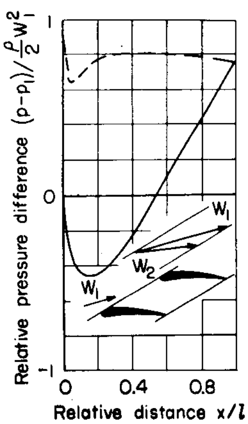

Figure 87.- $\alpha_1 = 14^{\circ}$; $\frac{t}{l} = 1.0.$

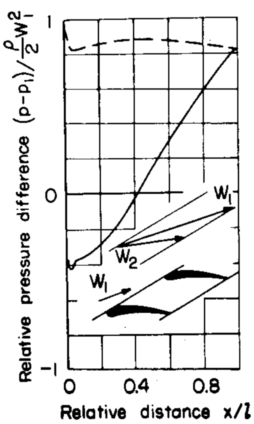

Figure 88.- $\alpha_1 = 17^{\circ}$; $\frac{t}{l} = 1.0.$

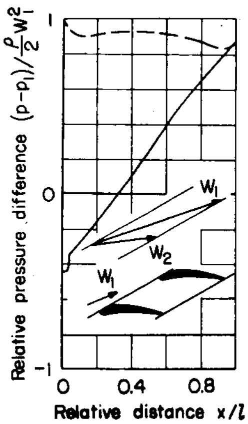

Figure 89.- $\alpha_1 = 19^{\circ}$; $\frac{t}{l} = 1.0.$

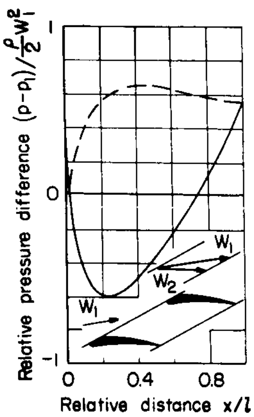

Figure 90.- $\alpha_1 = 8^{\circ}$; $\frac{t}{l} = 1.25.$

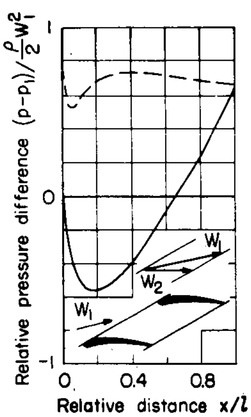

Figure 91.- $\alpha_1 = 11^{\circ}$; $\frac{t}{l} = 1.25.$

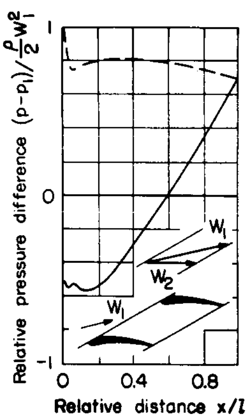

Figure 92.- $\alpha_1 = 14^{\circ}$; $\frac{t}{l} = 1.25.$

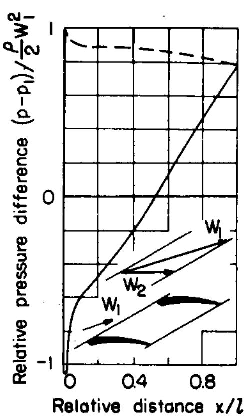

Figure 93.- $\alpha_1 = 17^{\circ}$; $\frac{t}{l} = 1.25.$

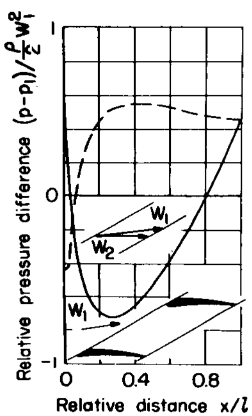

Figure 94. - $\alpha_1 = 5^\circ$; $\frac{t}{l} = 1.5$.

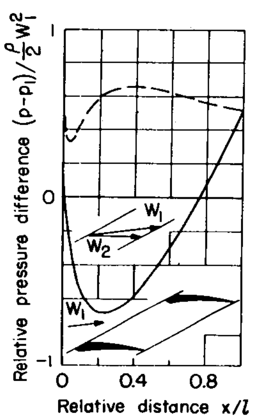

Figure 95. - $\alpha_1 = 8^\circ$; $\frac{t}{l} = 1.5$.

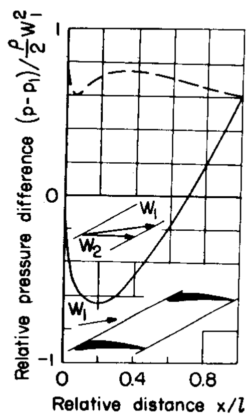

Figure 96. - $\alpha_1 = 11^\circ$; $\frac{t}{l} = 1.5$.

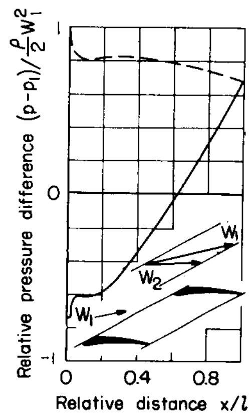

Figure 97. - $\alpha_1 = 14^\circ$; $\frac{t}{l} = 1.5$.

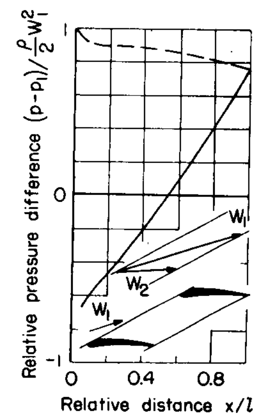

Figure 98. - $\alpha_1 = 17^\circ$; $\frac{t}{l} = 1.5$.

(See preceding page for further information.)

Figures 99 to 104

Comparison of measured and calculated pressure distributions on the blade contour for cascades of blades with NACA 8410 profiles, for a pitch ratio $\frac{t}{l} = 1.0$. Measurements for a Reynolds number $W_2 \frac{l}{\nu} \approx 6 \times 10^5$; solid curves calculated for upper side of profile a, dashed curves for lower side of profile b, curves with open circles for measured variation on upper side of profile, curves with filled-in circles for measured variation on lower side of profile, point for beginning of the separation denoted by A.

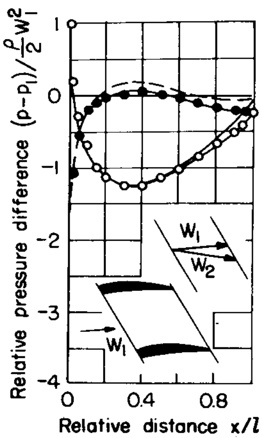

Figure 99. - $\alpha_1 = 5^\circ$; $\beta_s = 60^\circ$.

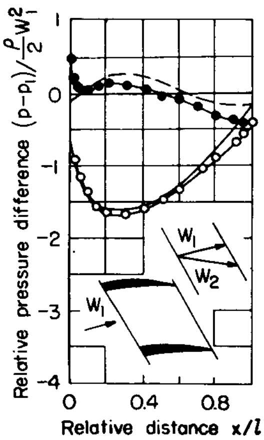

Figure 100. - $\alpha_1 = 15^\circ$; $\beta_s = 60^\circ$.

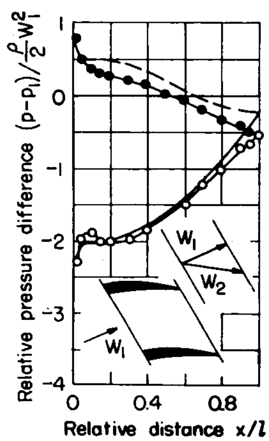

Figure 101. - $\alpha_1 = 25^\circ$; $\beta_s = 60^\circ$.

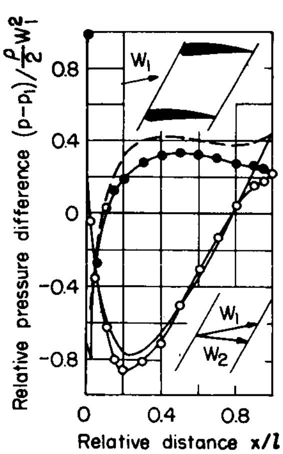

Figure 102. - $\alpha_1 = 10^\circ$; $\beta_s = 120^\circ$.

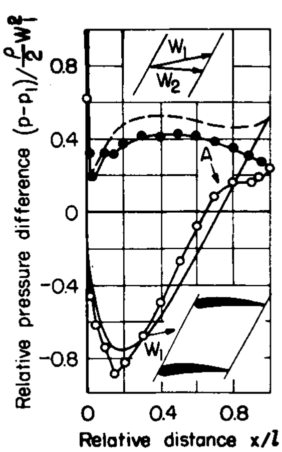

Figure 103. - $\alpha_1 = 15^\circ$; $\beta_s = 120^\circ$.

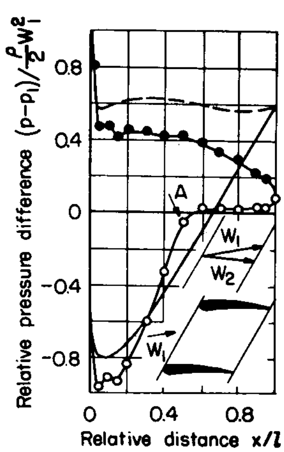

Figure 104. - $\alpha_1 = 20^\circ$; $\beta_s = 120^\circ$.

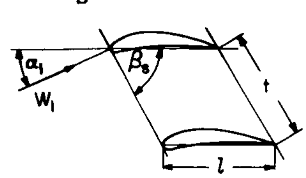

Explanatory sketch to figures 99 to 104

Figures 105 to 112

Comparison of measured and calculated pressure distributions on the blade contour for cascades of blades with NACA 8410 profiles, for various pitch ratios t/l, blade angles β_s, and angles of attack α_1. (Symbols and explanations as in figures 99 to p04; measurements at a Reynolds number $W_2 \frac{l}{\nu} \approx 6 \times 10^5$.)

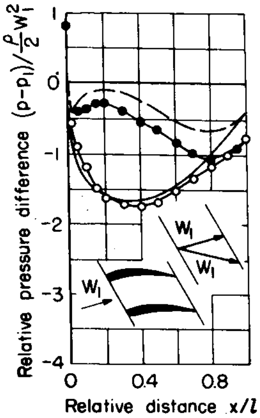

Figure 105. - $\frac{t}{l} = 0.5$; $\beta_s = 60^0$; $\alpha_1 = 15^0$.

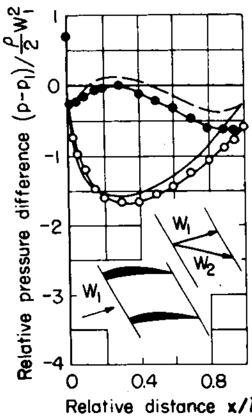

Figure 106. - $\frac{t}{l} = 0.75$; $\beta_s = 60^0$; $\alpha_1 = 15^0$.

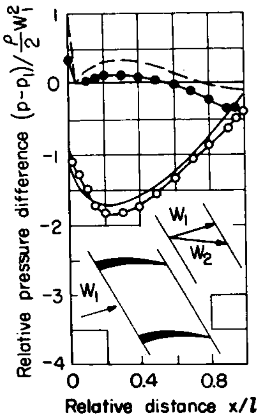

Figure 107. - $\frac{t}{l} = 1.25$; $\beta_s = 60^0$; $\alpha_1 = 15^0$.

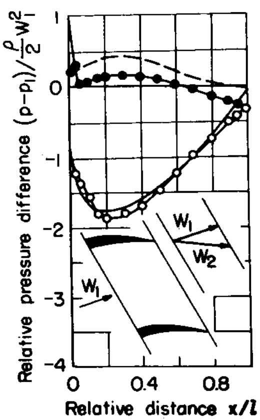

Figure 108. - $\frac{t}{l} = 1.5$; $\beta_s = 60^0$; $\alpha_1 = 15^0$.

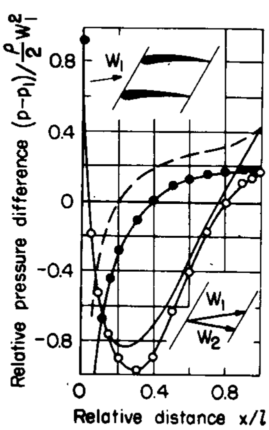

Figure 109. - $\frac{t}{l} = 0.5$; $\beta_s = 120^0$; $\alpha_1 = 10^0$.

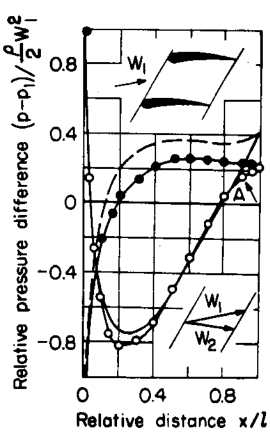

Figure 110. - $\frac{t}{l} = 0.75$; $\beta_s = 120^0$; $\alpha_1 = 10^0$.

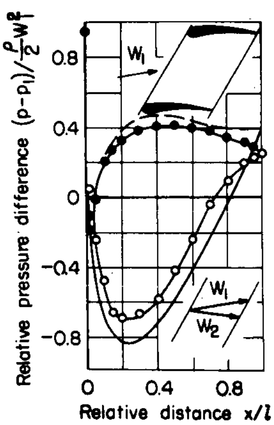

Figure 111. - $\frac{t}{l} = 1.25$; $\beta_s = 120^0$; $\alpha_1 = 10^0$.

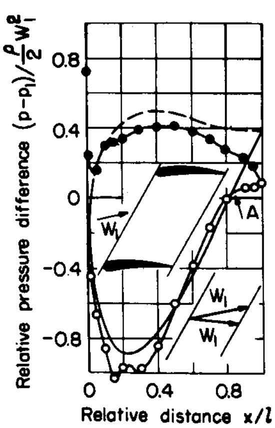

Figure 112. - $\frac{t}{l} = 1.5$; $\beta_s = 120^0$; $\alpha_1 = 10^0$.

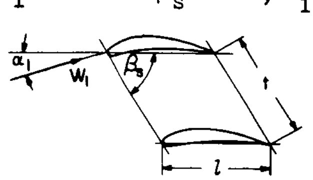

Explanatory sketch to figures 105 to 112